ANISOTROPY EFFECTS IN SUPERCONDUCTIVE TUNNELLING

ANISOTROPY EFFECTS IN SUPERCONDUCTIVE TUNNELLING

by

DAVID GEORGE WALMSLEY, B.Sc., M.Sc.

A Thesis

Submitted to the Faculty of Graduate Studies

in Partial Fulfilment of the Requirements

for the Degree

Doctor of Philosophy

McMaster University

November 1965

DOCTOR OF PHILOSOPHY (1965)
(Physics)

McMASTER UNIVERSITY
Hamilton, Ontario

TITLE: Anisotropy Effects in Superconductive Tunnelling

AUTHOR: David George Walmsley, B.Sc. (Queen's University of Belfast)
M.Sc. (McMaster University)

SUPERVISOR: Professor C. K. Campbell

NUMBER OF PAGES: vii, 141

SCOPE AND CONTENTS:

The application of the microscopic theory of superconductivity to the results of experiments on quantum-mechanical electron tunnelling between superconductors is discussed. A cryostat and associated electrical circuitry, constructed for tunnelling experiments, are described. There is a discussion of sample fabrication techniques which have received much attention, and have been extended, during the course of this work. Finally, results obtained on the metals aluminium, indium, tin, and lead are illustrated, and interpreted with particular emphasis on superconductor energy gap anisotropy.

PREFACE

This thesis is based on a programme carried out over the past three years on the topic of electron tunnelling between superconductors. It seeks to establish that energy gap anisotropy is responsible for much imprecision in the data normally collected from tunnelling experiments. How this problem can be drastically reduced is readily understood in terms of presently-known theory. Experimental results have been obtained in the light of these considerations with much better definition than is usually reported. Quantitative measurements have been carried out on the anisotropy of the energy gap in indium, tin, and lead, under conditions where it is most evident; the measurements are not complete.

Over one thousand samples have been prepared in the course of the work, most of them in attempts to develop new tunnel barrier fabrication techniques. Experience suggests that once a barrier formation technique has been found, for a given system, it may usually be controlled to give reproducible results.

Throughout this programme Dr. C. K. Campbell, as supervisor, has been a friend and selfless helper. His tolerant guidance has been deeply appreciated.

It is pleasant to be able to record gratitude to other workers in the same research field, particularly Dr. Milan Fiske and Dr. John Rowell, for their generosity in sharing information and discussing results prior to publication.

This project was financed through a grant-in-aid from the National Research Council of Canada to Dr. Campbell and the author was supported by a National Research Council Studentship; for both he wishes to express his gratitude.

In the later stages of the programme Mr. W. Scott has kindly assumed responsibility for the necessary helium liquefaction. Appreciation far outweighs any feeling of lost experience on the part of the author.

Mr. R. C. Dynes kindly lent his results shown in Figure (4-8c) for this thesis and allowed the author extensive use of his harmonic detection circuitry.

Mr. R. H. Hum helped generously in the preparation of this thesis.

Finally the author derives much pleasure in recollecting the encouragement and friendship, during the past three years, of Miss H. Edmonstone whose least contribution has been the typing of this thesis.

D. G. W.

TABLE OF CONTENTS

CHAPTER 1. HISTORICAL REVIEW

1.1. INTRODUCTION

Since 1911, when Kamerlingh Onnes[1] observed the apparently complete disappearance of electrical resistance in mercury at $4.2^{o}K$, there has been sustained interest in the superconductive state. Over twenty metallic elements, several hundred intermetallic compounds and alloys[2] and a few semiconductors[3,4] are now known to exhibit the phenomenon.

In this Chapter the first aim is to outline a few of the milestones along the way towards the present understanding of superconductors. The phenomenological theories, some of the crucial experimental results which pointed the way to the microscopic theory, and the theoretical background against which superconductivity finally found a molecular interpretation are very briefly outlined. The limitation on the original form of the theory and some extensions that have since been effected are then mentioned.

Throughout this thesis we shall restrict our interest mainly to Type I (or soft) superconductors.

1.2. PHENOMENOLOGY

Once Meissner and Ochsenfeld[5] had established in 1933 that a superconductor expels all magnetic flux from its interior when cooled through the normal-to-superconducting transition, or in other words that a superconductor is a perfect diamagnet as well as being a perfect

conductor, it was an obvious step to incorporate the reversibility of the transition into a consistent thermodynamic treatment. The Gorter-Casimir[6] two-fluid model resulted. It assumes that in the superconducting state a temperature-dependent fraction of the conduction electrons has condensed into a state of zero entropy. Such a picture is consistent with the observed disappearance of all thermoelectric effects. Gorter and Casimir assumed that the two fluids are spatially interpenetrating. The theory accounts for the parabolic law relating the critical magnetic field H_c at finite temperatures, T, to its limiting value at $T = 0^{\circ}K$, viz.

$$H_c = H_o \left(1 - \left(\frac{T}{T_c}\right)^2\right) , \qquad (1\text{-}1)$$

where T_c is the superconducting transition temperature. Shown to be thermodynamically equivalent was the statement that the specific heat, C_{es}, of the electrons in a superconductor obeys a T^3 law thus:

$$C_{es} = \frac{3\gamma T^3}{T_c^2} , \qquad (1\text{-}2)$$

where γ is the coefficient of the linear term γT in the specific heat of electrons of the normal metal.

Both these relations are good approximations to the observed behaviour in real superconductors. It is significant that a law of corresponding states seems to exist, thus making it possible to use reduced co-ordinates such as H_c/H_o and T/T_c.

A complementary electrodynamic description was developed shortly afterwards by F. and H. London[7]. In it the normal fluid is treated as in classical electrodynamics, but, for the superfluid component, there are incorporated the concepts of infinite conductivity and perfect

diamagnetism. The resulting picture of a superconductor is a diamagnet with persistent shielding currents in a layer over the surface of the specimen. In the London theory the penetration depth of an applied magnetic field varies with temperature according to the law

$$\frac{\lambda(T)}{\lambda(0)} = \frac{1}{\left[1 - \left(\frac{T}{T_c}\right)^4\right]^{1/2}} \quad . \tag{1-3}$$

$\lambda(0)$ is the penetration depth at $T = 0^{o}K$ and is typically 10^{-6} cm.

The foregoing phenomenological description of superconductors gives, of course, no insight into the microscopic effects responsible for this new physical state of matter.

1.3. SOME FURTHER EXPERIMENTS

In 1950-51 Maxwell[8] and Reynolds et al.[9] found that the critical temperature of mercury isotopes depends on the mass of the atoms, M, so that

$$T_c M^{\alpha} = \text{constant} \quad , \tag{1-4}$$

with the coefficient "α" having a value of approximately 0.5. Similar behaviour was subsequently found in other non-transition metals. The obvious conclusion, then, is that the lattice must be involved in the mechanism responsible for superconductivity in these elements.

Another body of experimental results was simultaneously being built up, which suggested that the superconducting state exhibits an energy gap. Specific heat measurements deviating from a T^3 law were observed[10] and can be better fitted to an exponential law typical of an energy gap.

Absorption of electromagnetic radiation revealed no difference between the normal and superconducting states down to 10^{14} c/s. At lower frequencies, up to 10^{10} c/s, the observed absorption was negligible. This suggested a gap corresponding to a frequency in the interval between these values.

1.4. DEVELOPMENT OF MICROSCOPIC THEORY

In 1935 F. London introduced the concept of "stiff" wave functions to explain the diamagnetism of superconductors. He envisaged the superconducting state as an ordering in momentum-space, as opposed to the more familiar configuration-space ordering encountered in the freezing process of matter. Previously, the uniqueness of the ground state of the system had been in question because the different electric current distributions within a superconductor, in the presence of different externally applied magnetic fields, suggested a large number of different equilibrium states. Such difficulties disappear if the local mean value of the momentum vector of the superconducting electron, viz.

$$\vec{p}_s = m^* \vec{v}_s + e^* \vec{A} \qquad (1\text{-}5)$$

(m^* is effective mass of superconducting electron, e^* is effective charge on superconducting electron, $\vec{A}$ is magnetic vector potential), is used to characterize the ground state. Then, for any externally applied magnetic field determined by $\vec{A}$, it is possible to have a complementary current distribution, determined by $\vec{v}_s$, which will keep $\vec{p}_s$ (or more strictly its local mean value) constant at all points within the specimen. A unique ground state is thereby hypothesized and the Meissner-Ochsenfeld

observation is a logical consequence, since the external fields and thermodynamic history of the specimen are not then relevant to determining $\vec{p}_s$.

The constancy of the local mean value of the momentum tends to establish long-range order by way of the uncertainty principle. In turn this leads to a sharp transition at the critical temperature.

With the isotope results available, the probable specific microscopic mechanism responsible for superconductivity was eventually identified as being an attraction between pairs of electrons arising through overscreened electron-phonon interaction. This followed closely on the discovery by Cooper[11] that a pair of electrons interacting via a momentum-dependent potential above a filled Fermi sea of non-interacting electrons would form a bound pair provided the potential were attractive, even though arbitrarily weak, in the region of the Fermi surface. The final theory[12], which involves macroscopic occupation of coherent pair states, will be further treated in the next Chapter.

Earlier, before the isotope effect was observed, Fröhlich[13] had suggested that superconductivity arises from electron-phonon interaction, not necessarily involving pair states, and his theory showed good correlation between predicted and observed occurrence of superconductivity in the non-transition elements. In detail, he encountered mathematical difficulties because of the perturbation approach used. It is now known that the electron-phonon coupling constant enters the proper theory in a non-analytic form, and the ground state is therefore not obtainable by finite order perturbative methods.

Parenthetically, we might note that Landau[14] showed in 1956 how to deal with an interacting Fermi gas by describing excitations from

the ground state in terms of quasi-particles. Each of these has a definite momentum and may be regarded as a particle in a self-consistent field of surrounding particles, i.e. a sort of localized co-operative motion is involved. Few enough quasi-particles are excited at low temperatures, and the exclusion principle exercises so much restriction on available states for scattering, that the lifetimes of these quasi-particles are long and the excitations are therefore well defined. Interactions between quasi-particles may often be completely neglected but Cooper's result follows implicitly from taking these into account.

Landau's[15] consolidation of his original concepts and subsequent work by Bohm and Pines[16] have done much to elucidate the behaviour of the interacting electron gas. Their attention to the ground state, and the spectra of elementary excitations therefrom, has served as a background against which Bardeen, Cooper and Schrieffer[12] (henceforth BCS) described the superconducting state.

The most celebrated result of the BCS theory is the existence of an energy gap for quasi-particle excitations from the superconducting ground state. The technique of electron tunnelling between superconductors introduced by Giaever[17] is a simple and convenient experimental method of measurement of the gap, within the considerable limitations of tunnel barrier preparation techniques.

In the original BCS work attention was limited to an idealized model of a superconductor, a reasonable first step since, as we noted earlier, superconductors obey closely a law of corresponding states and can be described in terms of reduced co-ordinates. Subsequently, a more sophisticated description of a superconductor has become possible through the use of field theoretic techniques and, in particular, the method of

Green's functions which enables one to take into account damping effects in strongly coupled systems and retardation. One specialized calculation exists[18] for the case of lead, where even some (simplified) phononic band structure was built into the formulation of the problem, to correlate with observed anomalies in the structure of tunnelling curves for this metal.

CHAPTER 2. THEORY

2.1. ELECTRON-PHONON AND SCREENED COULOMB INTERACTION; BOUND PAIRS

An electron moving through a lattice causes a localized polarization of the ionic structure which may be described as a cloud of virtual phonons. Emission and reabsorption of these virtual phonons is a dynamic process taking place all the time in a normal metal; it introduces the need for renormalization of the electron mass and gives rise to the concept of a quasi-particle. Fröhlich realised that the self energy involved in these processes is proportional to the square of the phonon energy and thus inversely proportional to the isotopic mass. Such a result is in accord with the isotope effect but the energy involved in the specific processes considered by Fröhlich is much greater than the condensation energy of a superconductor.

The BCS theory takes into account a process involving pairs of electrons which interact through exchange of a virtual phonon. Diagramatically the process may be represented thus:

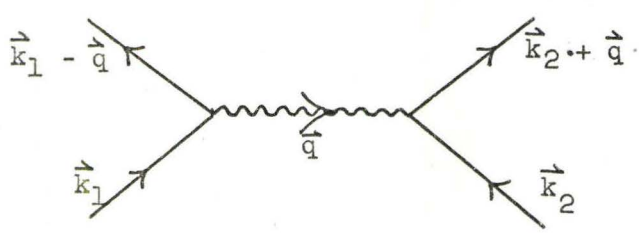

where an electron of wave vector $\vec{k}_1$ scatters to a state $\vec{k}_1 - \vec{q}$ emitting a virtual phonon of wave vector $\vec{q}$. This phonon in turn is absorbed by a second electron initially in state $\vec{k}_2$ which is scattered into state

$\vec{k}_2 + \vec{q}$. It is important to note that, although wave vector is conserved at the two vertices in the diagram, there need not be energy conservation in the separate events provided the phonon lifetime be small. Since the initial and final states of the electrons are well defined, there must be energy conservation in the overall process.

If the phonon energy ($\hbar\omega_{\vec{q}}$) exceeds the electron energy change ($|\epsilon_{\vec{k}_1} - \vec{q} - \epsilon_{\vec{k}_2}|$), the interaction is attractive, because, from second order perturbation theory, the matrix element for the transition is

$$\left\langle \vec{k}_1 - \vec{q},\ \vec{k}_2 + \vec{q} \left| V \right| \vec{k}_1,\ \vec{k}_2 \right\rangle = \frac{M_{\vec{k}_1,\ \vec{k}_1 - \vec{q}}\ M^{*}_{\vec{k}_2,\ \vec{k}_2 + \vec{q}}}{\epsilon_{\vec{k}_1} - (\epsilon_{\vec{k}_1 - \vec{q}} + \hbar\omega_{\vec{q}})}\ , \qquad (2\text{-}1)$$

where $M_{\vec{k},\ \vec{k} \pm \vec{q}}$ is the matrix element of the electron-phonon interaction. The converse event, represented by the diagram

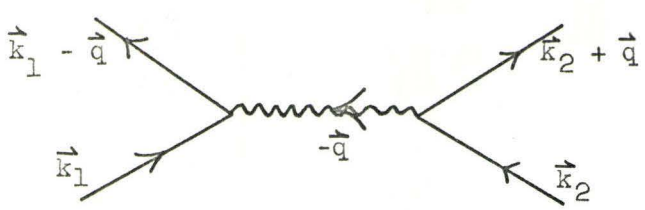

(where the electron with wave vector $\vec{k}_2$ emits a phonon of wave vector $-\vec{q}$ which is in turn absorbed by the electron in $\vec{k}_1$), must also be considered and contributes

$$\left\langle \vec{k}_2 + \vec{q},\ \vec{k}_1 - \vec{q} \left| V \right| \vec{k}_2,\ \vec{k}_1 \right\rangle = \frac{M_{\vec{k}_2,\ \vec{k}_2 + \vec{q}}\ M^{*}_{\vec{k}_1,\ \vec{k}_1 - \vec{q}}}{\epsilon_{\vec{k}_2} - (\epsilon_{\vec{k}_2 + \vec{q}} + \hbar\omega_{\vec{q}})}\ . \qquad (2\text{-}2)$$

Combining the processes under the assumption that the electron-phonon matrix elements are the same in the range of interest, we obtain

$$\left\langle \vec{k}_1 - \vec{q},\ \vec{k}_2 + \vec{q} \left| V \right| \vec{k}_1,\ \vec{k}_2 \right\rangle = \frac{\left| M_{\vec{k}_1,\ \vec{k}_1 - \vec{q}} \right|^2\ 2\hbar\omega_{\vec{q}}}{(\epsilon_{\vec{k}_1} - \epsilon_{\vec{k}_1 - \vec{q}})^2 - (\hbar\omega_{\vec{q}})^2}\ . \qquad (2\text{-}3)$$

For the energy range $|\epsilon_{\vec{k}_1} - \epsilon_{\vec{k}_1 - \vec{q}}| < \hbar\omega_{\vec{q}}$ this interaction is attractive, as claimed above. By confining our attention to states near the Fermi surface, where $|\epsilon_{\vec{k}_1}|, |\epsilon_{\vec{k}_1 - \vec{q}}|$, ... etc. $\leqslant \hbar\omega_D$, the expression simplifies to

$$- \frac{2|M_{\vec{k}_1, \vec{k}_1 - \vec{q}}|^2}{\hbar\omega_{\vec{q}}} \quad .$$

In addition to the electron-phonon coupling between pairs of electrons, account must also be taken of screened Coulomb repulsion. An unscreened interaction of the form $- \frac{e^2}{4\pi\epsilon_o r}$ is expressed in the momentum representation as

$$\frac{e^2}{\epsilon_o} \sum_{\vec{k}} \frac{1}{k^2} e^{i\vec{k}\cdot\vec{r}} \quad ,$$

and the expectation value, when box normalized, is $\frac{e^2}{\epsilon_o k^2}$. Screening is often expressed in terms of a parameter λ to give an expression

$$\frac{e^2}{\epsilon_o(k^2 + \lambda^2)} \, .$$

The total interaction will then give a matrix element

$$- V_{\vec{k}_1, \vec{k}_1 - \vec{q}} = - \frac{2|M_{\vec{k}, \vec{k} - \vec{q}}|^2}{\hbar\omega_{\vec{q}}} + \frac{e^2}{\epsilon_o(k^2 + \lambda^2)} \, . \qquad (2\text{-}4)$$

If -V is negative, a bound pair results. Cooper's far-reaching contribution was to show the validity of the assertion for arbitrarily weak interaction strength. Around the Fermi surface the interaction, though weak, is exceedingly intense.

2.2. SUPERCONDUCTORS

(a) The Ground State

In actual superconductors the bound pairs are not well separated entities, a concept that had eluded Schafroth, Blatt and Butler[19] in their attempts to formulate a theory of superconductivity. As BCS point out, the number of electrons within kT_c of the Fermi energy E_F, and therefore presumably involved in the interactions, is proportional to kT_c/E_F or about 1 in 10^4 of the conduction electrons in a metal, corresponding to a density of 10^{18} per cc. Furthermore, the average local value of momentum is well-defined according to London's concepts. Since the group velocity $\vec{v}_F$ of an electron at the Fermi surface obeys

$$\vec{v}_F = \left.\frac{\partial E}{\partial \vec{p}}\right|_{E_F} \quad \text{or} \quad \Delta E = \vec{v}_F \cdot \Delta\vec{p} \ ,$$

where E is the energy and $\vec{p}$ the momentum of the electron, and since we are concerned with an energy range $\Delta E \doteq kT_c$, it can be concluded that the momentum uncertainty is given by the relation (only magnitudes interest us)

$$\Delta p = \frac{kT_c}{v_F} \ ,$$

and this definition on the momentum of the particle leads to a spatial extension of the wave functions given by,

$$\Delta x \doteq \frac{\hbar}{\Delta p} = \frac{\hbar v_F}{kT_c} = \frac{E_F}{kT_c} \cdot \frac{1}{k_F} \doteq \frac{1}{10^{-4}.10^8} \text{ cm} = 10^{-4} \text{ cm.} \quad (2\text{-}5)$$

We now see that there will probably be $10^{18} \times (10^{-4})^3$ superconducting electrons with their wave packets centred in this region. (Suitable factors of 2, to account for pairs, can be inserted above with no qualitative effects.) Tremendous configurational degeneracy of the pairs

therefore prevails and must be taken into account when formulating a ground state for the superconductor.

The picture that evolves is a sea of pairs continually scattering from one pair state to another. The number of degeneracies is maximized, with a resulting energy minimum for the state, if we choose pairs with the same value of total momentum. It is just a simple problem of geometry[20] to show that the greatest possible stability is achieved if the pairs are chosen to have zero total momentum (if there is no net current flow). Exchange tends to reduce the pairing interaction energy, so that electrons of opposite spin as well as opposite momentum afford the best solution.

These concepts can be put on a formal basis with the use of second quantization notation. Let us suppose that the creation and destruction operators for electrons in Bloch states of a metal are $C^{+}_{\vec{k}\sigma}$ and $C_{\vec{k}\sigma}$ respectively where $\vec{k}$ is the wave vector of the state and σ is the spin index. The product $C^{+}_{\vec{k}\sigma}\, C_{\vec{k}\sigma}$ then denotes the probability $n_{\vec{k}\sigma}$ that the state in question is filled. The operators obey the Fermion anti-commutation rules:

$$\left[C_{\vec{k}\sigma},\ C^{+}_{\vec{k}'\sigma'}\right]_{+} = \delta_{\vec{k}\vec{k}'}\,\delta_{\sigma\sigma'} \quad .$$

$$\left[C_{\vec{k}\sigma},\ C_{\vec{k}'\sigma'}\right]_{+} = \left[C^{+}_{\vec{k}\sigma},\ C^{+}_{\vec{k}'\sigma'}\right]_{+} = 0 \quad . \tag{2-6}$$

It is, furthermore, convenient to introduce the corresponding operators for Cooper pair states,

$$b^{+}_{\vec{k}\uparrow} = C^{+}_{\vec{k}}\ C^{+}_{-\vec{k}\downarrow}$$

$$b_{\vec{k}} = C_{\vec{k}\uparrow}\, C_{-\vec{k}\downarrow}\ , \tag{2-7}$$

where we now acknowledge the limitations on the wave vector and spin of the pair electrons. The appropriate commutation relations are:

$$\left[b_{\vec{k}},\ b^{+}_{\vec{k}'}\right]_{-} = (1 - n_{\vec{k}\uparrow} - n_{-\vec{k}\downarrow})\ \delta_{\vec{k}\vec{k}'} \tag{2-8a}$$

$$\left[b_{\vec{k}},\ b_{\vec{k}'}\right]_{-} = 0 \tag{2-8b}$$

$$\left[b_{\vec{k}},\ b_{\vec{k}'}\right]_{+} = 2b_{\vec{k}}b_{\vec{k}'}(1 - \delta_{\vec{k}\vec{k}'}) \tag{2-8c}$$

These pairon operators behave like Boson operators in (2-8b) but in the other two relations the influence of the Pauli principle on the individual electrons is evident.

The reduced Hamiltonian, H, for the system in this notation is

$$H = \sum_{\vec{k}} 2\epsilon_{\vec{k}} b^{+}_{\vec{k}} b_{\vec{k}} - \sum_{\vec{k}\vec{k}'} V_{\vec{k}\vec{k}'}\ b^{+}_{\vec{k}'} b_{\vec{k}}\ , \tag{2-9}$$

where $\epsilon_{\vec{k}}$ is the energy of the normal state quasi-particles (or electrons) as measured from the Fermi energy and the indices $\vec{k}$, $\vec{k}'$ correspond to pairs of electrons in states $\left[(\vec{k}_1)\uparrow,\ (-\vec{k}_1)\downarrow\right]$ and $\left[(\vec{k}_1 - \vec{q})\uparrow,\ -(\vec{k}_1 - \vec{q})\downarrow\right]$ in the notation of equation (2-4).

The wave function for the ground state of the system is represented by

$$\Psi = \prod_{k} \left[u_{\vec{k}} + v_{\vec{k}}\ b^{+}_{\vec{k}}\right] \Phi_o\ , \tag{2-10}$$

that is, it is a product of all the constituent configurations with suitable amplitude coefficients $u_{\vec{k}}$, $v_{\vec{k}}$ introduced to describe the relative occupation of each state. Since $v_{\vec{k}}$ is the coefficient of $b^{+}_{\vec{k}}$ it represents the amplitude to which the pair state $\vec{k}$ is filled and $u_{\vec{k}}$ is the complementary amplitude that it is vacant ($u_{\vec{k}}^2 + v_{\vec{k}}^2 = 1$ for all $\vec{k}$). Φ_o is the vacuum state.

The wave function Ψ represents a system where the number of pairs is not unique, but in fact for a large system such as an electron gas in a metal the number has a sufficiently peaked probability at a definite value that no difficulty arises. A well known analogue is the description of a gas through the Grand Canonical Ensemble[21].

It is convenient to represent the wave function Ψ in two orthogonal sub-spaces (Hilbert spaces) as

$$\Psi = v_{\vec{k}}\phi_1 + u_{\vec{k}}\phi_0 \quad , \tag{2-11}$$

where ϕ_1 represents the occupied sub-space and ϕ_0 the vacant sub-space if considering single pair states; for considerations involving two different pair states the extended decomposition

$$\Psi = v_{\vec{k}}v_{\vec{k}'}\phi_{11} + v_{\vec{k}}u_{\vec{k}'}\phi_{10} + u_{\vec{k}}v_{\vec{k}'}\phi_{01} + u_{\vec{k}}u_{\vec{k}'}\phi_{00} \tag{2-12}$$

is helpful. In ϕ_{11} both $\vec{k}$ and $\vec{k}'$ are occupied, etc.

Now we can see that the expectation value for the reduced Hamiltonian in the ground state is:

$$W = \langle \Psi | H | \Psi \rangle$$

$$= \sum_{\vec{k}} \langle v_{\vec{k}}\phi_1 + u_{\vec{k}}\phi_0 \,|\, 2\epsilon_{\vec{k}} b_{\vec{k}}^{+} b_{\vec{k}} \,|\, v_{\vec{k}}\phi_1 + u_{\vec{k}}\phi_0 \rangle \quad . \tag{2-13}$$

$$- \sum_{\vec{k}\vec{k}'} \langle v_{\vec{k}}v_{\vec{k}'}\phi_{11} + v_{\vec{k}}u_{\vec{k}'}\phi_{10} + u_{\vec{k}}v_{\vec{k}'}\phi_{01} + u_{\vec{k}}u_{\vec{k}'}\phi_{00} \,|\, V_{\vec{k}\vec{k}'} b_{\vec{k}}^{+} b_{\vec{k}} \,|\, v_{\vec{k}}v_{\vec{k}'}\phi_{11} + \cdots \rangle .$$

$$\text{Hence } W = \sum_{\vec{k}} 2\epsilon_{\vec{k}} v_{\vec{k}}^2 - \sum_{\vec{k}\vec{k}'} V_{\vec{k}\vec{k}'}\, u_{\vec{k}}v_{\vec{k}}u_{\vec{k}'}v_{\vec{k}'} \quad . \tag{2-14}$$

Minimizing W with respect to variations in $v_{\vec{k}}^2$ determines the ground state; this occurs when

$$v_{\vec{k}}^2 = \frac{1}{2}\left[1 - \frac{\epsilon_{\vec{k}}}{(\epsilon_{\vec{k}}^2 + \Delta_{\vec{k}}^2)^{1/2}}\right] , \qquad (2\text{-}15)$$

where $\Delta_{\vec{k}}$ is the so-called energy gap parameter.

$$\text{Here,} \qquad \Delta_{\vec{k}} = \sum_{\vec{k}'} V_{\vec{k}\vec{k}'}\, u_{\vec{k}'}\, v_{\vec{k}'} , \qquad (2\text{-}16)$$

and therefore too,

$$\Delta_{\vec{k}} = \sum_{\vec{k}'} \frac{V_{\vec{k}\vec{k}'}\, \Delta_{\vec{k}'}}{2(\epsilon_{\vec{k}'}^2 + \Delta_{\vec{k}'}^2)^{1/2}} = \sum_{\vec{k}'} \frac{V_{\vec{k}\vec{k}'}\Delta_{\vec{k}'}}{2E_{\vec{k}'}} , \qquad (2\text{-}17)$$

$$\text{where } E_{\vec{k}} = \left[\epsilon_{\vec{k}}^2 + \Delta_{\vec{k}}^2\right]^{1/2} . \qquad (2\text{-}18)$$

We shall see that $E_{\vec{k}}$ is the energy for quasi-particle creation from the superconducting ground state; it differs from that for a normal metal through the presence of the gap parameter $\Delta_{\vec{k}}$.

Under the assumption that the gap is a constant independent of $\vec{k}$ within a certain range and zero otherwise, viz.

$$\begin{aligned} \Delta_{\vec{k}} &= \Delta = \text{constant} && |\epsilon_{\vec{k}}| \leqslant k_B\Theta_D \\ &= 0 && |\epsilon_{\vec{k}}| > k_B\Theta_D, \end{aligned} \qquad (2\text{-}19)$$

where $k_B\Theta_D$ is a cut-off energy (k_B is Boltzmann's constant), the condensation energy is then

$$W_N - W_S = N(0)\Theta_D\left[(\Theta_D^2 + \Delta^2)^{1/2} - \Theta_D\right] , \qquad (2\text{-}20)$$

or, if $\Delta << \Theta_D$, it is

$$W_N - W_S = \frac{1}{2} N(0)\Delta^2 , \qquad (2\text{-}21)$$

where W_N, W_S are the energy eigenvalues for the reduced Hamiltonian in

the normal and superconducting states respectively and N(0) is the density of states of electrons of one spin at the Fermi surface. We have now established that a superconducting state will occur if the gap parameter, $\Delta_{\vec{k}}$, has a non-zero, real value.

(b) Quasi-Particle Excitations from the Ground State (BCS Method)

Suppose an electron in state $\vec{k}\uparrow$ is added to the system just considered. Then the pair state $(\vec{k}\uparrow, -\vec{k}\downarrow)$ is blocked from participating in the pairing interaction and the energy of the interacting pairs is increased by (see (2-14)):

$$-2\epsilon_{\vec{k}} v_{\vec{k}}^2 + 2\left[\sum_{\vec{k}'} V_{\vec{k}\vec{k}'} u_{\vec{k}'} v_{\vec{k}'}\right] u_{\vec{k}} v_{\vec{k}} \,. \tag{2-22}$$

The single particle energy of the injected electron must be added also to give a total energy increase of

$$\epsilon_{\vec{k}}\left[1 - 2 v_{\vec{k}}^2\right] + 2\Delta_{\vec{k}} u_{\vec{k}} v_{\vec{k}} = \frac{\epsilon_{\vec{k}}^2}{E_{\vec{k}}} + \frac{\Delta_{\vec{k}}^2}{E_{\vec{k}}} = E_{\vec{k}} \tag{2-23}$$

where we have used (2-15), (2-16) and (2-18). The increase in energy of the system is thus $E_{\vec{k}}$, which we identified earlier as the quasi-particle creation energy. For an isolated superconductor the excitations, which are Fermions, must appear or disappear in pairs.

(c) Bogoliubov-Valatin Transformation

The original wave function for the ground state of the system (2-10) regarded states $\vec{k}$ as being filled with probability amplitude $v_{\vec{k}}$ and empty with probability amplitude $u_{\vec{k}}$ (where $u_{\vec{k}}^2 + v_{\vec{k}}^2 = 1$). It is therefore likely that quasi-particle excitations will result from application of the creation operators

$$\gamma^{+}_{\vec{k}\uparrow} = u_{\vec{k}}\, C^{+}_{\vec{k}\uparrow} - v_{\vec{k}}\, C_{-\vec{k}\downarrow}$$
$$\gamma^{+}_{-\vec{k}\downarrow} = u_{\vec{k}}\, C^{+}_{-\vec{k}\downarrow} + v_{\vec{k}}\, C_{\vec{k}\uparrow} \qquad (2\text{-}24)$$

This is commonly referred to as the B-V (Bogoliubov-Valatin) canonical transformation. The relevant commutation relations are:

$$\left[\gamma_{\vec{k}\sigma},\ \gamma^{+}_{\vec{k}'\sigma'}\right]_{+} = \delta_{\vec{k}\vec{k}'}\,\delta_{\sigma\sigma'}$$
$$\left[\gamma_{\vec{k}\sigma},\ \gamma_{\vec{k}'\sigma'}\right]_{+} = \left[\gamma^{+}_{\vec{k}\sigma},\ \gamma^{+}_{\vec{k}'\sigma'}\right]_{+} = 0 \quad . \qquad (2\text{-}25)$$

This preservation of the Fermion character (cf. (2-6)) justifies the term canonical. Again we may determine the quasi-particle excitation energy by evaluating

$$W^{\gamma}_{\vec{k}\uparrow} = \left\langle \Psi^{\gamma}_{\vec{k}\uparrow} \middle| H \middle| \Psi^{\gamma}_{\vec{k}\downarrow} \right\rangle, \qquad (2\text{-}26)$$

where $\Psi^{\gamma}_{\vec{k}\uparrow} = \gamma^{+}_{\vec{k}\uparrow}\,\Psi = C^{+}_{\vec{k}\uparrow} \prod_{\vec{k}\neq\vec{k}'} (u_{\vec{k}'} + v_{\vec{k}'}\, b^{+}_{\vec{k}'})\,\Psi_{o}$, (2-27)

to find $W^{\gamma}_{\vec{k}\uparrow} = W_S + E_{\vec{k}}$, (2-28)

Similarly $W^{\gamma}_{-\vec{k}\downarrow} = W_S + E_{\vec{k}}$. (2-29)

In obtaining (2-23) no statement was made as to whether $|\vec{k}|$ was greater or less than the Fermi wave vector magnitude $|\vec{k}_F|$. The same result holds true without restriction and in fact is unaltered if a state $-\vec{k}$ is considered. We have therefore got consistency between the methods of BCS and B-V as is seen by comparing (2-23) with (2-28) and (2-29).

The merit of the B-V transformation is that it gives some physical insight as to how the quasi-particle originates. If we consider the $\gamma^{+}_{\vec{k}\uparrow}$ operator, we see that it operates as a normal creation operator on the $\vec{k}\uparrow$ member of the pair state $\vec{k}$ with an amplitude corresponding to the emptiness of that state ($u_{\vec{k}}$), and as a normal destruction operator on the state $-\vec{k}\downarrow$ with an amplitude corresponding to the occupation of that state ($v_{\vec{k}}$). A quasi-particle with wave vector $\vec{k}$ and spin up is thus created. The spin-down particle is completely removed from the system. Similarly the $\gamma^{+}_{-\vec{k}\downarrow}$ operator creates a quasi-particle with wave vector $-\vec{k}$ and spin down and the spin-up occupation is reduced to zero.

We note that

$$\gamma^{+}_{\vec{k}\uparrow}\,\Psi = C^{+}_{\vec{k}\uparrow} \prod_{\vec{k}\neq\vec{k}'} (u_{\vec{k}'} + v_{\vec{k}'}\, b^{+}_{\vec{k}'})\,\Psi_o \qquad (2\text{-}30a)$$

$$\text{but}\quad \gamma^{+}_{-\vec{k}\downarrow}\gamma^{+}_{\vec{k}\uparrow}\Psi = (v_{\vec{k}} - u_{\vec{k}}\, b^{+}_{\vec{k}}) \prod_{\vec{k}\neq\vec{k}'} (u_{\vec{k}'} + v_{\vec{k}'}\, b^{+}_{\vec{k}'})\,\Psi_o \qquad (2\text{-}30b)$$

$$\neq C^{+}_{\vec{k}\uparrow}C^{+}_{-\vec{k}\downarrow} \prod_{\vec{k}\neq\vec{k}'} (u_{\vec{k}'} + v_{\vec{k}'}\, b^{+}_{\vec{k}'})\,\Psi_o \qquad (2\text{-}30c)$$

The application of $\gamma^{+}_{\vec{k}\uparrow}$ is equivalent to placing a quasi-particle definitely in the state $\vec{k}\uparrow$ and multiple applications will place several quasi-particles similarly, provided paired states such as $\vec{k}\uparrow$ and $-\vec{k}\downarrow$ are not involved. If a pair were to be created in these states its members would indulge in the superconducting interaction and partially condense again — it would in general not be in a state orthogonal to the ground state. Orthogonality is procured through the use of γ operators. The

pair occupation created by these operators is in anti-coherence with the occupation of the pair when no excitation is present. Instead of a term $u_{\vec{k}} + v_{\vec{k}} b^{+}_{\vec{k}}$, there is a term $v_{\vec{k}} - u_{\vec{k}} b^{+}_{\vec{k}}$ in the wave function. The negative sign is relevant to the anti-coherence concept. Fortunately, from the viewpoint of computations, the same energy is involved for exciting two quasi-particles whether they are in pair states or not.

(d) Energy Gap at $T = 0^{\circ}K$, $\Delta(0)$

To obtain a simple expression for the energy gap at $T = 0^{\circ}K$ we make the following assumptions:

$$(1)\quad -V_{\vec{k}\vec{k}'} = -V \text{ for } |\epsilon_{\vec{k}}|, |\epsilon_{\vec{k}'}| < k_B\Theta_D$$
$$= 0 \text{ elsewhere,} \qquad (2\text{-}31)$$

(2) A constant density of states $N(0)$ exists at the Fermi surface over a range of at least $k_B\Theta_D$ on either side. Then, from equation (2-17), we have

$$\Delta(0) = V \int_{-k_B\Theta_D}^{k_B\Theta_D} \frac{\Delta(0)\, N(0) d\epsilon}{2(\epsilon^2 + \Delta(0)^2)^{1/2}} \qquad (2\text{-}32)$$

$$\text{or} \quad \frac{1}{N(0)V} = \int_{0}^{k_B\Theta_D} \frac{d\epsilon}{(\epsilon^2 + \Delta(0)^2)^{1/2}} \qquad (2\text{-}33)$$

Integration gives

$$\Delta(0) = \frac{k_B\Theta_D}{\sinh\left(\frac{1}{N(0)V}\right)} \simeq 2\, k_B\Theta_D \exp\left(-\frac{1}{N(0)V}\right). \qquad (2\text{-}34)$$

The latter form is valid in the weak coupling limit, $N(0)V \ll 1$.

(e) Temperature Dependence of the Energy Gap, $\Delta(T)$

At finite temperatures some of the pair states are broken up to form quasi-particles with a resulting decrease in the energy gap parameter. If the probability of quasi-particle excitation to energy $E_{\vec{k}}$ at temperature T is $g_{\vec{k}} = g_{\vec{k}}(E_{\vec{k}}, T)$ then the Helmholtz free energy expression to be minimized is

$$F = 2\sum_{\vec{k}}\left\{\epsilon_{\vec{k}}\left[(1-2g_{\vec{k}})v_{\vec{k}}^{2} + g_{\vec{k}}\right]\right\} - \sum_{\vec{k}\vec{k}'} V_{\vec{k}\vec{k}'}\, u_{\vec{k}}v_{\vec{k}}u_{\vec{k}'}v_{\vec{k}'}(1-2g_{\vec{k}})(1-2g_{\vec{k}'})$$

$$+ 2k_B T \sum_{\vec{k}}\left[g_{\vec{k}} \ln g_{\vec{k}} + (1-g_{\vec{k}}) \ln (1-g_{\vec{k}})\right] . \qquad (2\text{-}35)$$

Both $v_{\vec{k}}$ and $g_{\vec{k}}$ are now variational parameters. The equilibrium condition exists when

$$g_{\vec{k}} = \left[\exp\left(\frac{E_{\vec{k}}}{k_B T}\right) + 1\right]^{-1} , \qquad (2\text{-}36a)$$

$$v_{\vec{k}}^{2} = \frac{1}{2}\left[1 - \frac{\epsilon_{\vec{k}}}{E_{\vec{k}}}\right] , \qquad (2\text{-}36b)$$

$$E_{\vec{k}} = \left(\epsilon_{\vec{k}}^{2} + \Delta_{\vec{k}}(T)^{2}\right)^{1/2} , \qquad (2\text{-}36c)$$

$$\Delta_{\vec{k}}(T) = \sum_{\vec{k}'} V_{\vec{k}\vec{k}'}\, v_{\vec{k}'}u_{\vec{k}'}(1-g_{\vec{k}'}) = \sum_{\vec{k}'} \frac{V_{\vec{k}\vec{k}'}\Delta_{\vec{k}'}(T)}{2E_{\vec{k}'}} \tanh\left(\frac{E_{\vec{k}'}}{2k_B T}\right) . \qquad (2\text{-}36d)$$

Under the simplified conditions of the previous section, we obtain

$$\frac{1}{N(0)V} = \int_{0}^{k_B\Theta_D} \frac{\tanh\left(\frac{E}{2k_B T}\right)}{2E}\, d\epsilon , \qquad (2\text{-}37)$$

where $E = \left[\epsilon^2 + \Delta(T)^2\right]^{1/2}$. This must be solved numerically to determine $\Delta(T)$, the energy gap parameter, as a function of temperature[22]. The energy gap parameter vanishes at the critical temperature T_c which is found from (2-37) by putting $\Delta(T_c) = 0$. Then the following relation holds:

$$\frac{1}{N(0)V} = \int_0^{k\Theta_D} \frac{d\epsilon}{\epsilon} \tanh\left(\frac{\epsilon}{2k_B T_c}\right) : \qquad (2\text{-}38)$$

In the weak coupling limit this leads to

$$kT_c = 1.14\, k_B \Theta_D \exp\left(-\frac{1}{N(0)V}\right) . \qquad (2\text{-}39)$$

We have here the explanation of the isotope effect since $k\Theta_D \propto M^{-1/2}$ and $N(0)V$ should not be isotope-dependent. Hence

$$T_c M^{\alpha} = \text{constant}, \qquad (1\text{-}4)$$

where $\alpha = -0.5$.

The temperature dependence of the energy gap $\Delta(T)$ is illustrated in Figure (2-1).

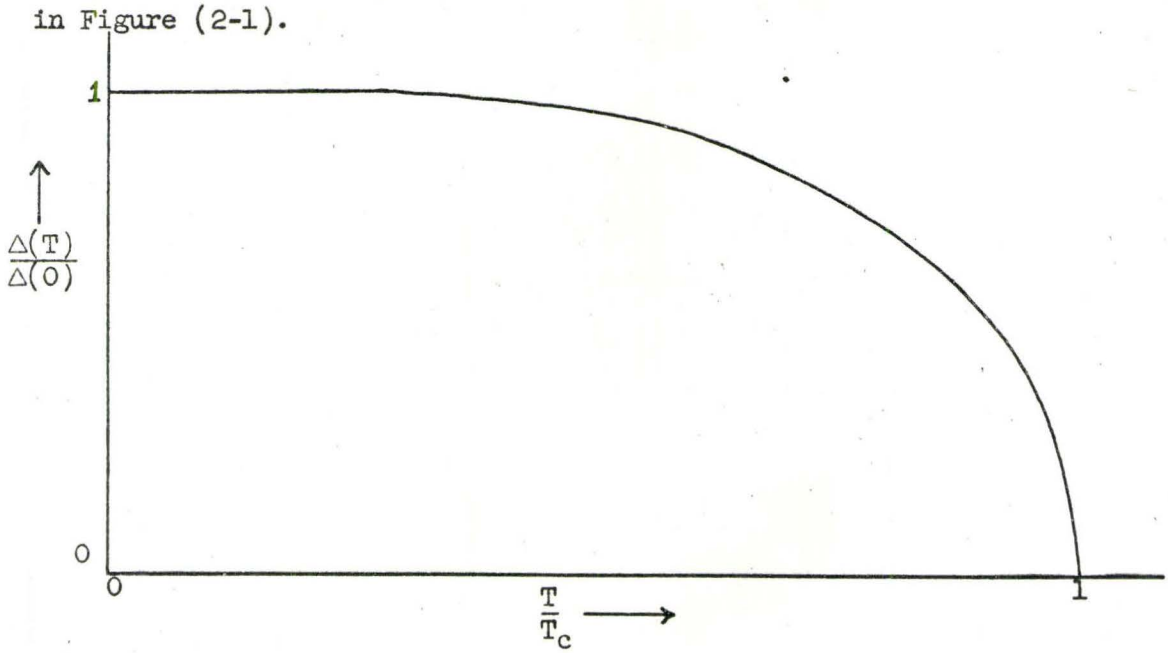

FIGURE (2-1)

A rather useful result is found by combining (2-39) and (2-34):

$$2\,\Delta(0) \;=\; 3.52\,k_B T_c\,. \tag{2-40}$$

(f) Density-of-States of Excited Quasi-Particles

We assume that (a) we can label the electrons in a normal metal by their wave vector $\vec{k}$ and they occupy Bloch states $\epsilon_{\vec{k}}$, (b) these electrons condense in the presence of the superconducting interaction to occupy (partially, according to the value of $v_{\vec{k}}^2$) pairs, characterized by $(\vec{k}\uparrow\ ;\ -\vec{k}\downarrow)$ and (c) in the presence of an excitation one of these states is no longer available for pair occupation because a single quasi-particle completely occupies one member of the pair state.

Excitation thus results in an electron-hole pair being produced. An energy of $2E_{\vec{k}}$ is required. There is a 1:1 correspondence between electrons that occupy the Bloch states $\epsilon_{\vec{k}}$ in the normal metal and the excitations whose energy is

$$E_{\vec{k}} \;=\; (\epsilon_{\vec{k}}^2 + \Delta^2)^{1/2}\,. \tag{2-41}$$

Therefore the following conservation-of-states equality must hold

$$N_N\,(\epsilon_{\vec{k}})\,d\epsilon_{\vec{k}} \;=\; N_S\,(E_{\vec{k}})\,dE_{\vec{k}} \tag{2-42}$$

where it is understood that the intervals $dE_{\vec{k}}$ and $d\epsilon_{\vec{k}}$ are interrelated by (2-41). Hence

$$N_S\,(E_{\vec{k}}) \;=\; N_N\,(\epsilon_{\vec{k}})\,\frac{d\epsilon_{\vec{k}}}{dE_{\vec{k}}} \;=\; \frac{E_{\vec{k}}\,N_N(\epsilon_{\vec{k}})}{\epsilon_{\vec{k}} + \Delta\frac{d\Delta}{d\epsilon}}\,. \tag{2-43}$$

For a constant gap material we have, defining $n_S(E)$,

$$n_S(E) = \frac{N_S(E_{\vec{k}})}{N_N(\epsilon_{\vec{k}})} = \frac{E}{(E^2 - \Delta^2)^{1/2}} \quad \text{if } E \geq \Delta \tag{2-44a}$$

$$= 0 \quad \text{if } E < \Delta . \tag{2-44b}$$

A peaking of $E_{\vec{k}}$ states occurs at the gap edge and is illustrated in Figure (2-2).

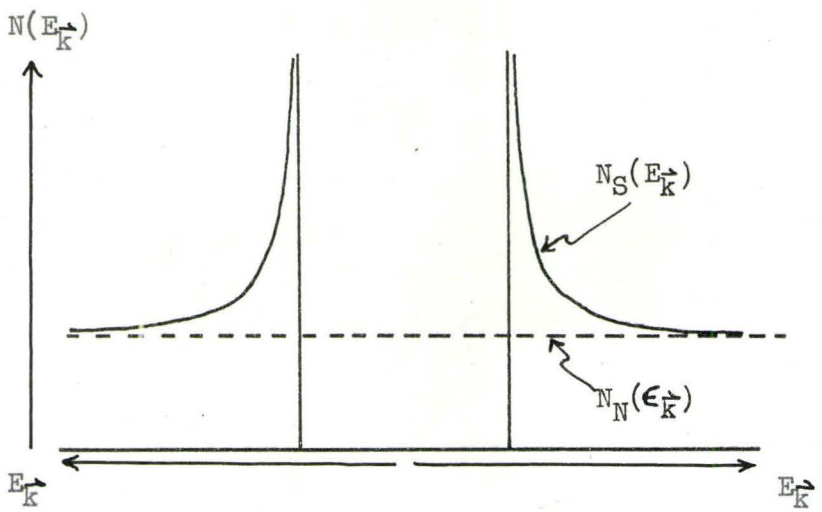

FIGURE (2-2)

In real metals the interaction between electrons through phonon exchange is not instantaneous. To cope with this problem of retardation and lifetime effects it is necessary to apply more sophisticated techniques. Schrieffer et al.[18] have employed Green's function methods within a formulation where the superconducting states, and not the Bloch states of the normal metal, are used to determine the effective superconducting electron-electron interaction. They find that the "effective tunnelling density-of-states" is given by

$$N_T(E) = N_N(\epsilon)\ \mathrm{Re}\left\{\frac{E}{\left[E^2 - \bar{\Delta}(E)^2\right]^{1/2}}\right\} . \qquad (2\text{-}44c)$$

Now there are no derivative terms involving Δ as occurred in (2-43). However, $\bar{\Delta}$ is complex, reflecting the damping effects due to real phonon emission. In strong coupling superconductors, where the quasi-particle concept is no longer valid, this result still holds true.

2.3. ELECTRON TUNNELLING BETWEEN SUPERCONDUCTORS

(a) Tunnelling Probability

Potential barrier penetration by quantum-mechanical tunnelling is a non-classical result that is well supported by experimental evidence. Nuclear α-decay, cold cathode field emission and interband transitions in semiconductors are but a few examples. Recently[23], it has even been suggested that proton tunnelling may be responsible for biological mutations and the occurrence of tumours.

We are interested here in the tunnelling of electrons from one metal film to another through an insulating oxide layer about 10 to 100 Å thick. The probability, T^2, of barrier penetration may be determined from elementary wave mechanics to be of the form

$$T^2 = \exp -\frac{2}{\hbar}\int_a^b \left(2m(\phi(x) - E_x)\right)^{1/2} dx , \qquad (2\text{-}45)$$

where a WKB or similar approximation is applied to a geometry of the form shown in Figure (2-3).

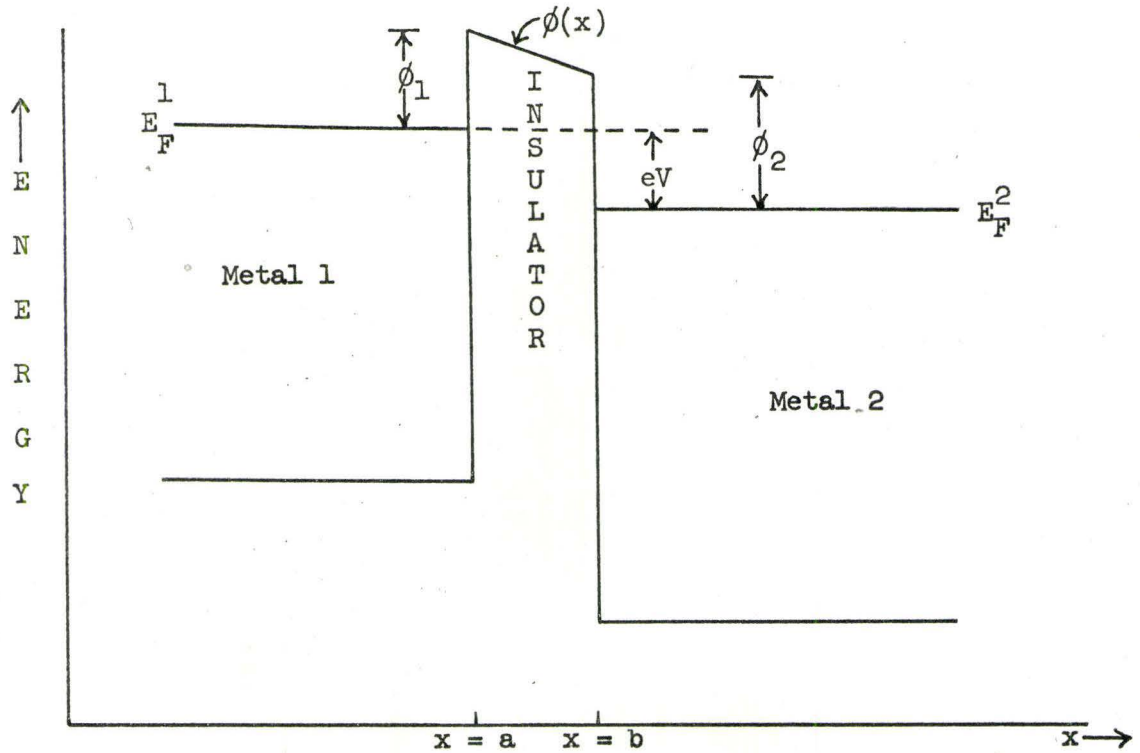

FIGURE (2-3)

In this Figure,

$\phi(x)$ is the potential barrier height as a function of position, x

ϕ_1, ϕ_2 are the metal-to-oxide work functions of metals 1 and 2

E_F^1, E_F^2 are the Fermi energies of metals 1 and 2

E_x is the kinetic energy associated with the x component of the electron velocity

V is the potential applied across the barrier

e, m are the electron charge and mass.

In practice, much uncertainty exists concerning the proper values to substitute in (2-45). Indeed the desire for a better understanding of the relevant factors has inspired a wide research field in the subject. How are metal-to-oxide work functions related to metal-to-vacuum work

functions? Does a semiconductor transition region between the insulator and metal exist and, if so, to what extent will it give electron current flow between the metals? These questions are only partially answered as yet[24].

From (2-45) we may deduce that the tunnelling probability, T^2, should be constant if the trapezoidal barrier cross-section is not significantly altered by applying a small potential, V. On the other hand, if V is large it may so distort the barrier as to give a triangular cross-section and under these conditions the exponent will decrease quickly with applied potential: there will then be an exponential increase in the tunnelling probability. The latter condition prevails when V approaches the value of the work function of the metal, i.e. at about 1 volt. When superconductors are being investigated by the tunnel effect, the applied potentials are usually not in excess of 50 mV so that T^2 is fairly constant in the region of interest.

(b) Densities-of-States and Current Flow

In addition to the tunnelling probability, the density-of-states of available electrons and their occupation will be most important in determining the tunnel current that flows between two metals under the influence of an applied potential.

Taking into consideration the current flow in both directions we should expect the net value, for an applied potential V, to be

$$I = \frac{C}{e} \int_{-\infty}^{\infty} dE n_1(E)\, n_2(E + eV) \left[f(E) - f(E + eV) \right] \quad , \qquad (2\text{-}46)$$

where $$C = \frac{2\pi}{\hbar} |T|^2 \; N_{1N}(0)\, N_{2N}(0) \quad . \qquad (2\text{-}47)$$

The symbols $n_1(E)$, $n_2(E)$ refer to the relative density-of-states in the metals as compared with normal states as defined in (2-44): when the

metals are in the normal state these assume a value of unity. The transfer of electrons by tunnelling is being regarded here as a quantum transition and $|T|^2$ is the square of the associated matrix element[25]. $N_{1N}(0)$ and $N_{2N}(0)$ are the densities-of-states of electrons in the normal metals at the Fermi surface and f is the Fermi distribution function.

Evaluation of (2-46) at different temperatures has to be done numerically. We illustrate the results of computations by Shapiro et al.[26,27] with two of their published figures in (2-4a) and (2-4b).

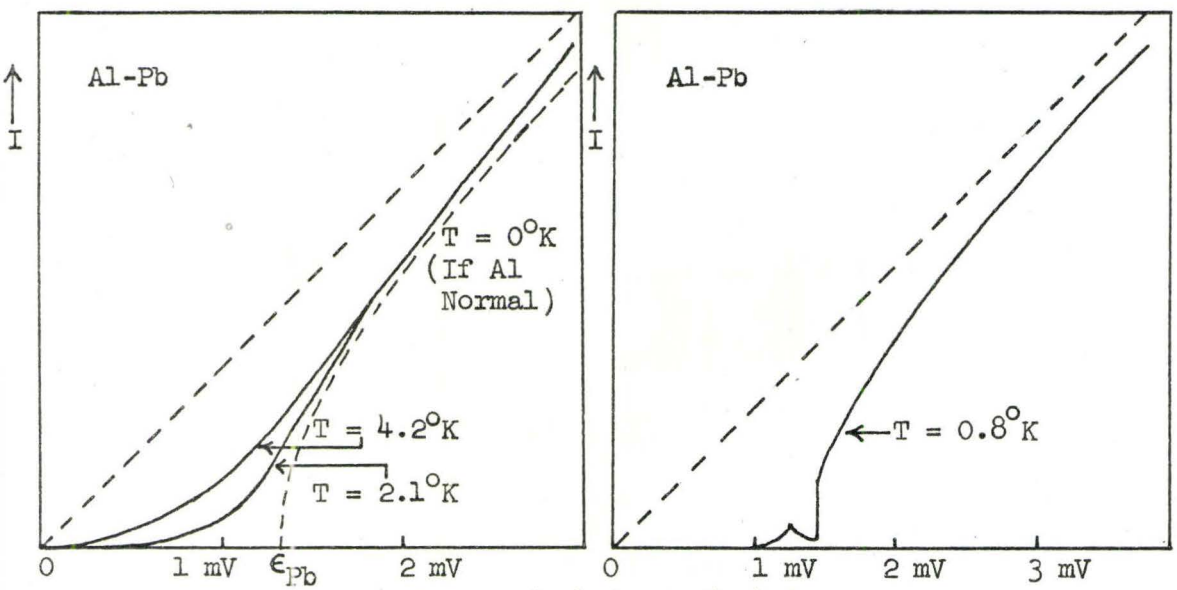

FIGURES (2-4a) AND (2-4b)

They used the density-of-states expression (2-44) in (2-46). The conclusions may be simply stated as follows.

(i) N-N Case

When both metals are normal, the current-voltage (I-V) characteristic is linear at all temperatures of interest. Here $I_{NN} = CV$, i.e. C is the conductance.

(ii) N-S Case

When one metal is superconducting no current flows at $T = 0^{\circ}K$ until the applied potential, V, reaches a value determined by

$$eV = \Delta \ , \qquad (2\text{-}48)$$

where Δ is the energy gap of the superconducting metal; then there is a relatively abrupt current increase which tends, at higher biases, to the value associated with N-N curves. At non-zero temperatures there is a considerable smearing out of detail.

It is interesting to consider the derivative of (2-46) in this case. We have, supposing Metal 2 is in the normal state,

$$\left.\frac{dI}{dV}\right|_{NS} = \frac{C}{e}\int_{-\infty}^{\infty} n_1(E)\, K(E, V, T)\, dE \quad , \qquad (2\text{-}49)$$

$$\text{where } K(E, V, T) = \frac{e}{kT}\,\frac{e^{(E + eV)/kT}}{\left[e^{(E + eV)/kT} + 1\right]^2} \quad . \qquad (2\text{-}50)$$

As pointed out by Bermon and Ginsberg[28], the function K is bell-shaped with its peak at the point of investigation, V = -E/e, but it also mixes in current contributions over a range determined by the width of K. When K is at half maximum its width is approximately

$$\Gamma = 3.5\,\frac{E + eV}{(kT)^2} \quad . \qquad (2\text{-}51)$$

Reversing our outlook we may say that, at low temperatures, only E states close to the proper value (-eV) are mixed in because K falls off rapidly. At T = 0°K, K becomes a δ-function and then the first derivative of the tunnelling characteristic is proportional to the density-of-states in the superconductor. As the temperature increases there is more smearing. It is also important to notice that the smearing has a further effect of fundamental importance in that the maximum slope of the characteristic is shifted from the position it assumes at T = 0°K, viz. V = Δ/e, to higher voltages, as may be seen by looking closely at Figure (2-4a).

(iii) S-S Case

When two different superconductors with gaps Δ_1 and Δ_2 ($\Delta_1 > \Delta_2$) are considered, there is found to be a sharp cusp-like peak at $(\Delta_1 - \Delta_2)/e$ followed by a region of negative slope, and then there is a sharp increase at $(\Delta_1 + \Delta_2)/e$. The structure at $(\Delta_1 - \Delta_2)/e$ is actually a logarithmic singularity while that at $(\Delta_1 + \Delta_2)/e$ is a step-wise jump. The sharpness of both these features is related to the use of the BCS density-of-states result (2-44) in which there is a divergence at the gap edge.

(c) Coherence Effects in Tunnelling

One of the triumphs of the BCS theory was to show that coherence effects are responsible for the observed behaviour of superconductors in experiments on acoustic attenuation, electromagnetic absorption and nuclear spin relaxation. Earlier phenomenological theories could not give an internally consistent interpretation of these results.

In the case of electron tunnelling coherence effects cancel out, because it is the energy of the quasi-particles that determines whether or not a tunnel current will flow. In acoustic and electromagnetic experiments, on the other hand, there is scattering from one $\vec{k}$ state to another and in nuclear relaxation spin flip is involved: these processes are therefore sensitive to the occupation of specific $\vec{k}$ states and to the nature (scalar, vector, etc.) of the coupling of these states to the external probe. Tunnelling places no such restrictions on the $\vec{k}$ states; only compatibility with energy considerations is required. This leads to the interesting result that an electron emitted from a superconductor through a tunnel barrier is to be regarded as coming partially from each of two different Bloch states.

To see this, consider again the wave function for the ground state of the superconductor

$$\Psi = \prod_{\vec{k}} (u_{\vec{k}} + v_{\vec{k}} b_{\vec{k}}^{+}) \Phi_0 \quad ,$$

remembering that for an energy minimum

$$v_{\vec{k}}^{2} = \frac{1}{2}\left[1 - \frac{\epsilon_{\vec{k}}}{(\epsilon_{\vec{k}}^{2} + \Delta_{\vec{k}}^{2})^{1/2}}\right] .$$

The occupation of Bloch states may be interpreted graphically as in Figure (2-5).

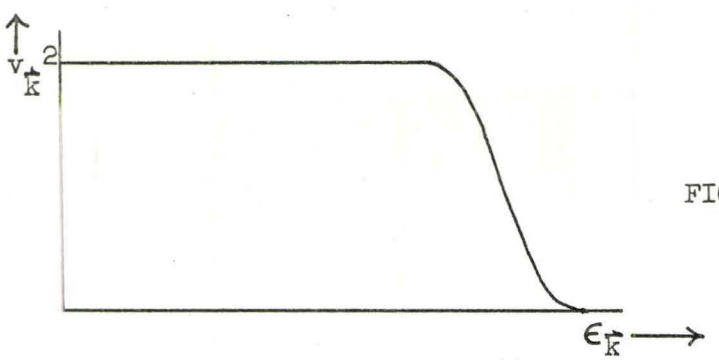

FIGURE (2-5)

We would rightly conclude that the Bloch energy is no longer a good label for the electrons; there should be included the superconducting interaction energy, $\phi_{\vec{k}}$ say, too so that a new energy, $\eta_{\vec{k}}$, determined by

$$\eta_{\vec{k}} = \epsilon_{\vec{k}} - \phi_{\vec{k}} \quad ,$$

would be used to describe the electron states. The population of these $\eta_{\vec{k}}$ states would have a sharp cut-off at a new (lower) Fermi energy in contrast to the smeared $\epsilon_{\vec{k}}$ cut-off. It is obvious that $\epsilon_{\vec{k}}$ and $\phi_{\vec{k}}$ would have to have very different functional dependences on $\vec{k}$. However, it would be misleading to take $\eta_{\vec{k}}$ too seriously since the superconducting

interaction is a co-operative one and the condensation energy can hardly be divided up among the quasi-particles in a term like $\phi_{\vec{k}}$. We therefore keep the Bloch state description.

From the result (2-27), the application of the B-V operator $\gamma^{+}_{\vec{k}}$ destroys the partial occupation of $(\vec{k}\uparrow , -\vec{k}\downarrow)$ by a Cooper pair and substitutes complete occupation of the $\vec{k}\uparrow$ state by an electron just as the $C^{+}_{\vec{k}}$ operator would when acting on the vacuum state. The state $-\vec{k}\downarrow$ is then completely empty. In tunnelling we have the addition and removal of single electrons.

The probability with which an electron in the Bloch state $\epsilon_{\vec{k}}$ can be excited out of the ground state to give a non-Cooper-interacting quasi-particle (or electron) is $v_{\vec{k}}^{2}$, the probability of the state occupation. There is a complementary probability $u_{\vec{k}}^{2}$ $(= 1 - v_{\vec{k}}^{2})$ that an electron in the Bloch state $\epsilon_{\underline{\vec{k}}}$ can be so excited where $\epsilon_{\underline{\vec{k}}} = -\epsilon_{\vec{k}}$. Both excitations require the same energy $E_{\vec{k}} = (\epsilon_{\vec{k}}^{2} + \Delta_{\vec{k}}^{2})^{1/2}$, if $\Delta_{\vec{k}} = \Delta$ for all $\vec{k}$.

This is the origin of the disappearance of coherence factors in the tunnelling theory. Excitations of energy $E_{\vec{k}}$ are partly in the Bloch state $\epsilon_{\vec{k}}$ and partly in the state $\epsilon_{\underline{\vec{k}}}$.

If they tunnel to a normal metal, where $\Delta = 0$ and in which, therefore, the excitation energy of quasi-particles is $E_{\vec{k}} = \epsilon_{\vec{k}}$, then the electron enters the state $\epsilon_{\vec{k}}$ (above the Fermi surface).

For tunnelling into a second superconductor the coherence factors that occur relate to the emptiness of the Bloch states in the second metal, rather than their occupation, but again the simple result follows, i.e. no dependence on coherence factors.

The above argument is equally true whether we describe the excitations in terms of electrons or of holes since each appears in conjunction with the other at all times. The dispersion curve for electrons is identical to the dispersion curve for holes because of this inseparability. (Excited real pairs require some generalization of the argument but that need not worry us here.)

Figure (2-6a) shows the situation in a pictorial form. A few pair states are indicated. Solid lines denote occupation (i.e. probability of finding electrons) and dotted lines denote vacancy (i.e. probability of finding holes). Their lengths correspond to $v_{\vec{k}}^2$ and $u_{\vec{k}}^2$ respectively. The $\gamma_{\vec{k}}^+$ operator changes the situation to that shown in Figure (2-6b).

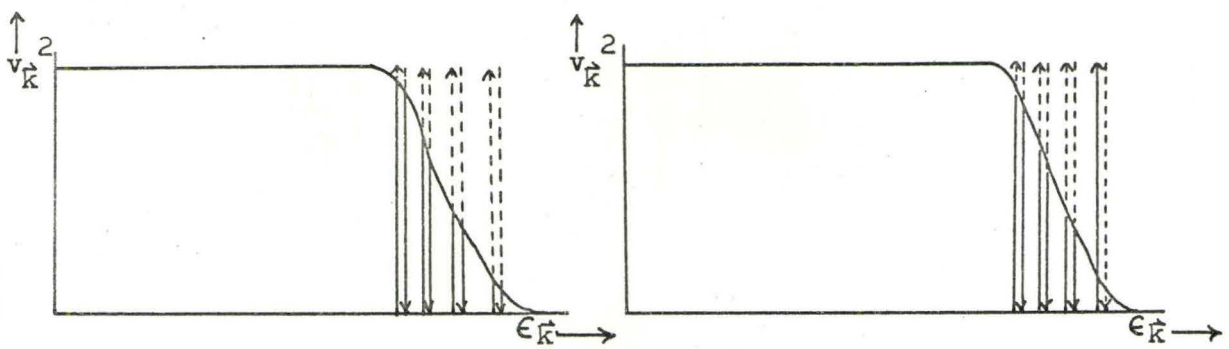

FIGURES (2-6a) AND (2-6b)

Now an electron and hole are both created. There is a redistribution of the pair occupation of the other pair states to compensate for the blocking of this one pair state. (For the particular case of breaking up the pair states at the Fermi surface no adjustment is necessary.)

The electrons and holes may be shown pictorially in two different regions and each is separated by an energy interval Δ from the superconducting ground state (see Figure (2-7)). It is very important to note that conservation-of-states requires that these states do not exist until the excitations are created. As they are created, there is a corresponding destruction of states in the Cooper-interacting sea.

Furthermore, the gap decreases at the same time. Each destroyed pair state contributes one state to the electron region and one state to the hole region of Figure (2-7) (strictly true only if we still choose to ignore the excitation of real pairs).

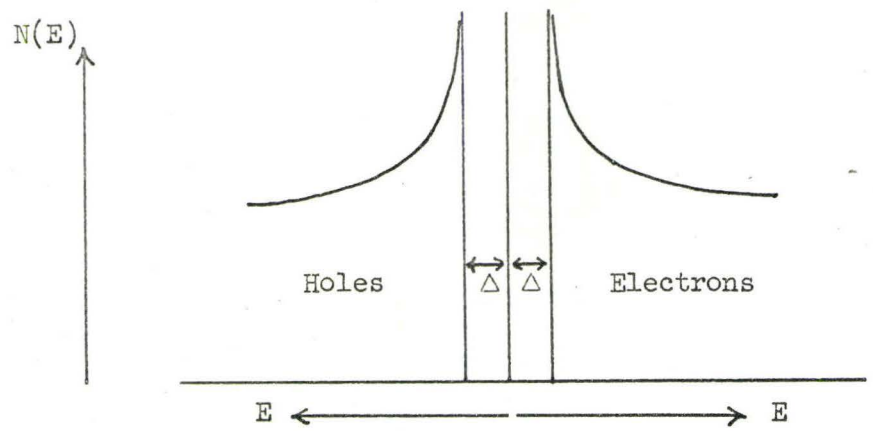

FIGURE (2-7)

In the light of these considerations we conclude that the conventional semiconductor picture should not be pushed unduly in interpreting tunnelling results — for one thing it improperly assumes permanence of states.

Schrieffer[29] discusses some aspects of the situation in more detail.

(d) The Josephson Effect

Josephson[30] has shown that in the case of tunnelling between two superconductors there must be considered the contribution of electron pairs. It is possible for a bound pair to flow from one side of a barrier to the other in the absence of an applied potential. In effect there exists a region of weak superconductivity right through the barrier.

One might at first sight conclude that the probability of the pair tunnelling process would be negligible in comparison with single-particle tunnelling. This is true for the case of a normal metal but with superconductors the long-range order extends sufficiently into thin barriers to provide a superconducting bridge and thus a significant DC supercurrent flow. Josephson arrived at the result through consideration of a modified Bogoliubov transformation which acts on the ground state to produce a new ground state containing two electrons more than the original, and then he followed the many-body procedure developed by Bardeen[31] and Cohen et al.[32].

A further interesting possibility is for an electron pair to fall through a small potential as it tunnels. Conservation of energy is achieved by emission of a photon of the appropriate frequency (determined by $h\nu = 2eV$, where ν is the frequency and V the potential drop). In the absence of an external circuit to withdraw such tunnelled pairs there is set up an AC current.

We have observed both the AC and DC Josephson effects. Some of the observations on the AC effect antedate their appearance in the published literature but they do not add to what has now been determined by other workers[33-37]. Furthermore, they do not constitute a major part of the work reported here. For these reasons we do not discuss the theory in any detail but merely point out that excellent discussions have been given by Josephson[38] and Anderson[39].

CHAPTER 3. SAMPLES AND EQUIPMENT

3.1. SAMPLES

(a) Films - General Procedure

As might be expected, the fabrication of a tunnelling barrier, some tens of Angstroms thick, presents a considerable challenge. For one thing, the host metals should be smooth and free of contamination. Moreover, the barrier material should bind well to the metals to prevent sample rupture during severe thermal cycling.

Vacuum deposited metal films[40] with thermally grown oxides fulfil these requirements well in many cases. Since separate problems are encountered with each metal, it is first convenient to consider the basic steps in sample preparation.

A soda-glass microscope slide, or part thereof, was used as a substrate. It is important to clean the slides thoroughly as even small amounts of contamination can seriously affect the results. To remove bulk contaminants the slides were outgassed, in batches, at 200°C for 2-3 hours, under a vacuum of 1 Torr. Then, as they were used, the surface of each slide was further cleaned by washing with a commercial cleanser (Ajax), made up to a paste-like constituency with water. To check whether or not the slide was finally grease-free, it was held in a pair of forceps and distilled water was sprayed on it. A continuous film of water covers the whole slide if no grease is present, otherwise grease spots are clearly visible. Finally the substrate was dried by wrapping

it successively in a number of lint-free soft paper tissues (Kimwipes). The substrate was not touched by hand from the time the final cleaning started until sample preparation was complete.

After cleaning, the substrate was placed in the vacuum coating unit, and metal films were deposited on it in a geometry determined by the mask used. Typically the first-deposited film was a long, narrow strip. This was then oxidized either in the coating unit or, if necessary, elsewhere. Finally, further cross-strips were deposited to give a pattern of the form shown in Figure (3-1).

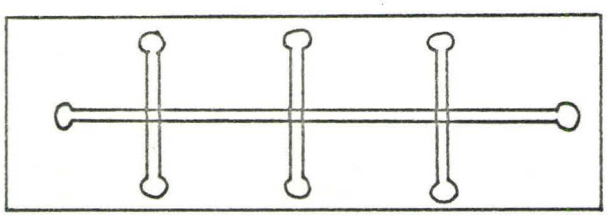

FIGURE (3-1)

The blobs at the end of the strips are helpful in fastening electrical leads to the films and they can be separately deposited if a metal different from that of the strip is desired.

Most of the time indium was used to fasten the copper wire leads to the films after they were deposited. It gives good contacts and stands up well to thermal shocks. For indium films it was necessary to use a lower-melting-point solder, such as Wood's metal.

Using this procedure, tunnelling samples have been made involving the following combinations:

Al - I - Al	Sn - I - Sn	Pb - I - Pb
Al - I - In		Pb - I - Sn
Al - I - Sn		Pb - I - In
Al - I - Pb		

where the first-named metal in each series refers to the first-deposited,

or base, layer. The term "I" is used for the insulating barrier which is an oxide of the first-deposited metal. The second-deposited metal is often referred to as the cover layer.

When discussing the penetrability of the tunnel barriers the electrical "resistance" is often quoted. This is in analogy with metals, which obey Ohm's law, and thus have a linear current-voltage (I-V) relationship. At low bias, the barriers do have a linearity in their I-V curves, but there is no power dissipation when a current flows through them.

The type of experiment being done determines what barrier resistance is to be used. For straightforward gap measurements, about 1 to 10 ohms is desirable. Higher resistances reduce the tunnelling current (exponentially dependent on thickness) unnecessarily, at the expense of a relatively large leakage current (usually only linearly dependent on thickness of barrier); this spoils the definition of the I-V characteristics. Josephson current studies require lower resistances, of the order of 10^{-2} to 10^{-1} ohms, to ensure stability of the current against thermal and electromagnetic fluctuations as discussed by Anderson[39]. On the other hand, the electrical circuit we use to investigate phonon structure in the characteristics requires higher resistance samples, in the range 10 to 100 ohms.

Generally, the thickness of our metal films has not been measured. We estimate it to be in the region of 1000 to 2000 Å except in the studies of anisotropy where thicker films are needed. Then, a four-terminal arrangement was used in conjunction with a potentiometer to determine their resistance at room temperature and 77°K. From a knowledge of the

temperature dependence of the " ideal" resistivity it was possible to apply Matthiesen's rule to separate out the " impurity" resistance and thus get a measure of the film thickness. A travelling microscope is convenient for film width measurements. In both lead and indium we have found that annealing takes place at room temperature and in fact the impurity resistance is negligible. Only room temperature resistance measurements need be made once this has been established. Aluminium does not anneal as quickly and measurements at both temperatures are necessary.

(b) Films - Specific Considerations

(i) Aluminium

Aluminium is very suitable as a base layer since it oxidizes in atmosphere to form a thin coherent Al_2O_3 film. Usually a few minutes' oxidation is adequate to give a suitable tunnelling barrier. The widely accepted Mott-Cabrera[41] theory of oxidation of aluminium actually assumes that tunnelling of electrons through the oxide is necessary to further oxide growth, once the metal has been covered with a monolayer of alumina. It is therefore to be expected that, if the growth is prematurely terminated through the deposition of a cover layer, a tunnel current will flow through the oxide on application of a potential across the barrier. Shorter oxidation times lead to lower resistance barriers. We have found that oxidation at reduced pressure may give lower resistances but quite often in such cases there are contributions from other undesirable current flow mechanisms. Humidity seems to have a catalytic influence on the oxidation rate; growth is much faster in the presence of some moisture.

Handy's[42] conclusion, that tunnel resistances are greater if the second-deposited metal has a large atomic radius, is supported by our observations on Al-I-M samples (where M is the second metal).

Anodization of aluminium[43,44] has been used on a wide scale commercially to produce a protective oxide coating on the metal. Measurements by other workers indicate that the thickness of the oxide depends on the potential applied. About 12 Å per volt is quoted. We have carried out some anodization attempts on aluminium thin films using ammonium tartrate and ammonium citrate solutions as electrolytes. The technique is particularly unsuited to the production of tunnelling barriers. With air oxidation the oxide seems never to grow much beyond the required thickness; with anodization there is an immediate growth on insertion of the metal into the electrolyte of approximately (1.7 x 12) Å ($\triangleq$20 Å) corresponding to the effects of the electrochemical potential of aluminium. In the very region of thickness where control is most needed it is not available. Further difficulties are that the electrolytic solution tends to dislodge films from the substrate unless elaborate cleaning and degassing are used, and also that the current flow seems to concentrate at certain spots in the film giving a pitting action and a quite inhomogeneous oxide. Cleaning and drying after anodization prior to deposition of a second metal introduce further problems. From our experience we do not recommend the use of wet processes in tunnel sample preparation.

In the case of Al-I-M samples, the strips used have been 1 mm wide for both metals, giving a junction area of 1 mm^2. The results of a room temperature investigation of air oxidation in the production of Al-I-Al tunnel samples are included in the next Chapter, along with the

low temperature measurements. Tungsten helical coils were used as the filaments in the coating unit for the evaporation of aluminium. Strong[45] has shown that, even though alloying of the tungsten occurs at high temperature, the tungsten is reprecipitated from the melt as the aluminium evaporates and there is no significant contamination in the aluminium film deposited. The aluminium used was 99.999% pure (supplied by A. D. Mackay, New York).

A great disadvantage in working with aluminium is that it has a low transition temperature (1.175°K for bulk material) which leaves only a small temperature range in which it can be investigated in the superconducting state with a pumped He^4 cryostat.

(ii) Lead

Lead does not oxidize quickly at room temperature. An oxide grown on it, either at room temperature or above, is not usually coherent — in some places it is quite thick and in others almost non-existent. Since lead has a high transition temperature (7.18°K for bulk material) and has the additional interesting feature of being a strong-coupling superconductor it is desirable to make Pb-I-M samples for examination.

Evaporation of the metal poses no problems; it readily wets, and evaporates from, molybdenum boats. Some idea of film thickness can be obtained by watching the hot filament through the glass bell-jar on the coating unit during evaporation. It is best to terminate the deposition once a continuous film has formed rather than prolonging it to get a thick film, because oxidation can be troublesome in the latter case.

To achieve a suitable barrier we have carried out an extended set of sample fabrications under widely differing oxidation conditions. These ranged from a few minutes to 100 hours oxidation time at temperatures from ambient to the melting point of lead. The pressure of the air used was varied in value from less than 10 Torr to 1 atmosphere. Sometimes water vapour was added in the belief that it might act as a catalyst. None of these samples gave good tunnelling characteristics.

The second metal deposited in most cases was either lead or tin.

Success was finally achieved through the use of a pure oxygen atmosphere, with oxidation for 2 - 3 hours at 75°C giving barriers of 10 - 50 ohms[*]. It is possible to rationalize the success of this method as being due to the increased probability of formation of oxide nucleation centres over the surface of the metal. With pure oxygen this probability is increased fivefold over that in air. The oxide is then perhaps coherent from the beginning, rather than developing at isolated sites and growing laterally in a "cabbage-leaf" pattern. The "cabbage-leaves" would not be expected to fit together well: hence the high probability of current flow by processes other than tunnelling, i.e. shorts.

Aluminium oxide (sapphire) is the second hardest naturally occurring substance known. There is no danger of damaging the barrier that grows on aluminium by evaporating the second metal at too high a temperature. This is a real danger in the case of oxides on lead and tin. The lowest possible filament temperature should be used in the second evaporation; it should not, however, be so low as to prolong the evaporation beyond, say, 1 minute, because then the condensing film

---

[*]We are indebted to Dr. W. W. Smeltzer for this suggestion and much other general instruction concerning oxidation of metals.

becomes increasingly contaminated by residual atmosphere in the vacuum chamber. Damage to the oxide frequently occurs, however, when a thick lead layer is deposited on top of a lead-lead oxide base.

Since shorts appear randomly, it is advisable to work with narrow films and thus reduce the probability of their occurrence. We have worked mostly with films 0.010 inches wide.

(iii) Tin

It seems to be easier to grow an oxide tunnelling barrier on tin in air at room temperature than on lead. We have had some success under these conditions but the barrier resistances are invariably quite low. Higher resistance samples can readily be produced under conditions comparable to those for lead. Somewhat paradoxically, tin requires a longer oxidation time at 75°C than does lead for the production of a given barrier resistance, even though tin oxidation is easier at the lower temperature.

Tin has a lower melting point (232°C) than lead (327°C) but it requires a higher evaporation temperature to give film deposition in a reasonable time. This introduces a complication. The condensing atoms have a kinetic energy determined by the temperature of the filament source: on striking the substrate they exhibit some mobility which leads to an agglomerated structure evidenced by a milky appearance. Such milky films will not readily grow a tunnel barrier. It is therefore important to avoid excessive heat input to the source, since this in turn heats the substrate by radiation and agglomeration is then enhanced. In practice it is best to use relatively high power heating of the source for a minimal period — just long enough to give a continuous film. The

second film is evaporated under the same conditions to avoid damage to the oxide layer.

Molybdenum boats have been used as filaments for all our tin evaporations. As with lead, narrow (0.010 inches) films have been used for most experiments.

(iv) Indium

We have not attempted to oxidize indium. The discussion on agglomeration in the previous section applies, a fortiori, to the evaporation of indium which has an even lower melting point (156°C) than tin. Indium, too, evaporates from molybdenum boats.

The lead, tin and indium used had a rated purity of 99.9999% (supplied by Cominco).

(v) Other Barriers

Successful tunnel barriers, reported in the literature[46,27], have been made with, presumably evaporated, thin film insulators such as BaF_2, or by deposition of monomolecular organic layers. We have attempted to evaporate thin layers of silicon monoxide but there is great difficulty in controlling the thickness within the required limits and, when cooled, it often peels off as a result of differential contraction. Experience suggests that the natural oxide, if it can be grown, is much the best choice as barrier material.

Another technique, about which we have reservations, is the deposition of a layer of Al_2O_3 by slow evaporation of aluminium in a low pressure oxygen atmosphere. This has been used on metals other than aluminium[47,48] but we feel there is a danger that not all of the

aluminium oxidizes. The presence of small amounts of metallic aluminium could seriously influence the results, since the experiment probes only a thin surface layer.

(c) Lead Single Crystals

We have made an extensive search to find a method of preparing a junction of which one member is a lead single crystal. All attempts so far have been quite unsuccessful.

Basically, two different approaches have been tried. One was to prepare the surface of a commercially-obtained lead single crystal by etching and electropolishing; the second was to grow a single crystal in vacuum with a clean smooth surface.

The commercial lead crystal was a cylinder 6 inches long and 3/4 inch in diameter. Slices about 1/4 inch thick were cut off in a spark cutter (Metals Research Ltd., Cambridge, England, Type SMD), at the slowest available speed to minimize damage. The time taken to cut through was of the order of 10 hours. The crystal slice was then electropolished[49]; with either of two electrolytes, namely (a) one involving perchloric acid, ethanol, and ether (which must be handled with extreme caution), or (b) one consisting of sodium acetate, glacial acetic acid and water. The former requires a high current density which caused spitting of the lead to some extent and undesirable heating of the solution. Even when the crystal was etched in hot electrolyte, both solutions failed to give a surface that even approached the smoothness of a thin film. The operations of cleaning and drying the crystal when the electropolishing had been completed were always open to the suspicion that some impurities were being left behind, even though the surface was shiny. The procedure was to wash the polished surface with distilled

water and then methanol, by spraying from a wash bottle. We have compared our attempts at electropolishing with those that give successful results for cyclotron resonance experiments; they are comparable in quality. The sample fabrication was completed by oxidizing the polished surface, masking off the major portion of it with G.E. 7031 lacquer and finally depositing a thin film of either tin or lead across the unmasked area. Aluminium foil leads were attached with a silver paste. The geometry of the finished sample was as shown in Figure (3-2). Sometimes several junctions were made simultaneously on the same crystal face.

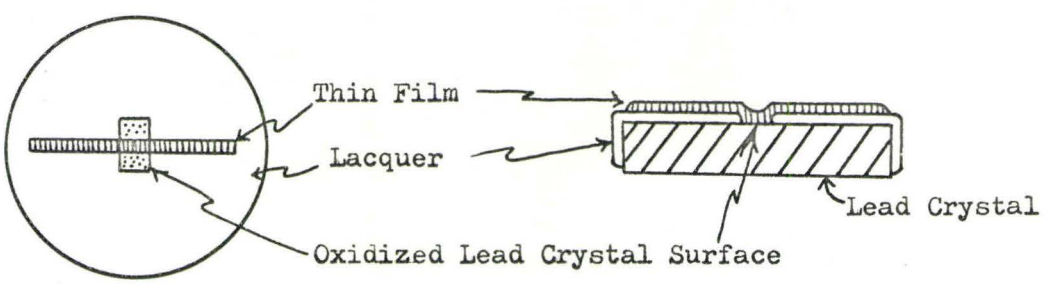

FIGURE (3-2)

Over 30 samples prepared along these general lines were cooled to helium temperatures. None showed clear evidence of tunnelling. Usually there were shorts but sometimes the barrier resistance was very high, of the order of megohms. Different crystal orientations were tried and in fact slices from two different crystals were used. An end piece that had not been spark cut was also tried. The crystals were of good quality; when examined in a neutron scattering spectrometer they exhibited a mosaic spread of less than 30 minutes of arc (the divergence of the instrument).

Dietrich[50] has reported successful tunnelling experiments on bulk tantalum prepared by electropolishing. We can only surmise that perhaps the better oxidation qualities of tantalum are sufficient to compensate for the disadvantages of the preparation technique.

The second method we have tried is a dry process. Following Zavaritskii's[51] work on tin crystals we have attempted to grow lead crystals with clean surfaces by pouring molten lead on to glass in vacuum. Unfortunately the glass cannot be separated from the lead after cooling! The chemical bond is exceedingly strong. No such difficulty exists with tin on glass as we have verified. Lead also sticks to silica, mica, and cleaved sodium chloride. It has recently come to our attention that graphite is a suitable crucible material and preliminary tests bear this out.

3.2. EQUIPMENT

(a) Vacuum Coating Unit

An Edwards model 12E3 vacuum coating unit was used for the metal film evaporations; usually a vacuum of 5×10^{-6} Torr or better was obtained. A liquid air trap, in the form of a spirally-wound length of 3/8 inch copper tubing fed from a pressurized liquid air dewar, was built into the throat of the diffusion pump to reduce backstreaming of diffusion pump oil and to condense water and other vapours present. Usually, however, it was not necessary to use the trap to achieve the required vacuum.

A similar copper tube was soldered to the substrate mount for cooling the microscope slides to liquid air temperature, if desired, before film deposition.

The 12E3 unit has a 12-inch bell-jar, a four-position rotary filament-holder to allow successive evaporations without breaking the vacuum, a radiant heater to heat substrates, and an ionic bombardment device for substrate cleaning.

We have fabricated a large variety of masks from 1/16 inch aluminium sheet using a milling cutter to give well-defined slots. Composite masks have been made for use in multiple evaporation runs. The masks have been kept as close to the substrate as possible during evaporations — the usual separation has been of the order of 0.025 inches.

(b) Electrical Circuitry

(i) DC Circuit

For energy gap measurements (and observation of Josephson currents) a DC current-sweep circuit has been used. It is shown in Figure (3-3).

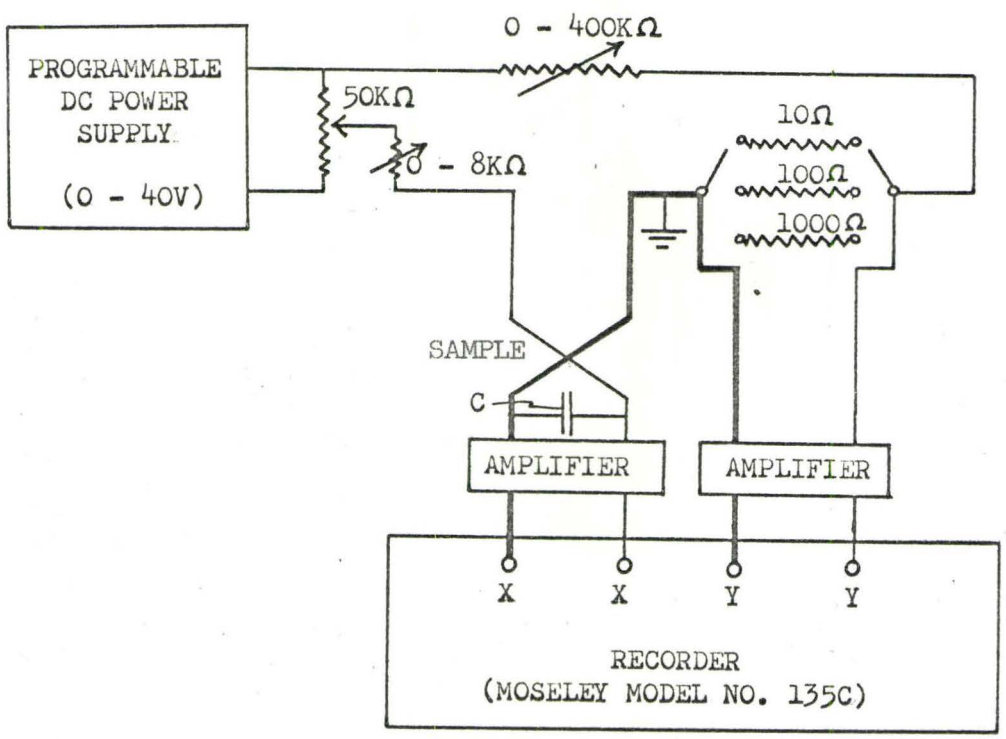

FIGURE (3-3)

The power supply is programmed by a motor-driven potentiometer and the circuit parameters are variable to cope with sample barrier resistances from approximately 10^{-3} ohms to approximately 10^{5} ohms. The DC amplifiers have a continuously variable gain of from 1 to 11,000.

Current through the sample is monitored on the Y-axis of the recorder and potential developed across it on the X-axis. The function of the 1000 μfd capacitor, C, is to suppress noise in the circuit, when necessary. Shielded or co-axial cables are used where possible.

(ii) Harmonic Detection Circuit

This circuit has been designed and built by Dynes and Campbell and is described in detail by Dynes[52]. It applies a small-amplitude sinusoidal modulation signal, $V_1 \sin \omega t$, to the sample at angular frequency ω and detects the resulting current through the sample at ω, or harmonics of ω, with a narrow band lock-in amplifier (NBLIA). The output of the amplifier is displayed on the Y-axis of the recorder while the DC bias is plotted along the X-axis. The signals at ω and 2ω can be regarded as proportional to the first and second derivatives, dI/dV and d^2I/dV^2, of the tunnelling characteristic.

To see this, suppose the potential developed across the sample is

$$V = V_o + V_1 \sin \omega t = V_o + \delta V \quad , \qquad (3\text{-}1)$$

where V_o is the DC bias and V_1 is the amplitude of the modulation. Let us further suppose that the current flow through the sample is written in expanded form as

$$I(V) = I_o + \left(\frac{dI}{dV}\right)\delta V + \frac{1}{2!}\left(\frac{d^2I}{dV^2}\right)(\delta V)^2 + \frac{1}{3!}\left(\frac{d^3I}{dV3}\right)(\delta V)^3 + \ldots \text{ etc.}$$

$$= I_o + \left(\frac{dI}{dV}\right) V_1 \sin \omega t + \frac{1}{2!}\left(\frac{d^2I}{dV^2}\right) V_1^2 \sin^2 \omega t + \ldots \text{ etc.}, \quad (3\text{-}2)$$

where $I(V)$ is the current that flows when the potential developed is V and I_o is a contracted form for $I(V_o)$.

By continuing the expansion and collecting terms we find:

$$I(V) = \left[I_o + \frac{1}{4}\left(\frac{d^2I}{dV^2}\right) V_1^2 + \frac{1}{64}\left(\frac{d^4I}{dV^4}\right) V_1^4 + \ldots\ldots\ldots\ldots\right]$$

$$+ \sin \omega t \left[\left(\frac{dI}{dV}\right) V_1 + \frac{1}{8}\left(\frac{d^3I}{dV^3}\right) V_1^3 + \frac{1}{192}\left(\frac{d^5I}{dV^5}\right) V_1^5 + \ldots\ldots\ldots\right]$$

$$+ \cos 2\omega t \left[-\frac{1}{4}\left(\frac{d^2I}{dV^2}\right) V_1^2 - \frac{1}{48}\left(\frac{d^4I}{dV^4}\right) V_1^4 + \ldots\ldots\ldots\ldots\right]$$

$$+ \sin 3\omega t \left[-\frac{1}{24}\left(\frac{d^3I}{dV^3}\right) V_1^3 - \frac{1}{384}\left(\frac{d^5I}{dV^5}\right) V_1^5 + \ldots\ldots\ldots\ldots\right]$$

$$+ \cos 4\omega t \left[\frac{1}{192}\left(\frac{d^4I}{dV^4}\right) V_1^4 + \ldots\ldots\ldots\ldots\ldots\ldots\ldots\right]$$

$$+ \ldots \text{ etc.} \quad (3\text{-}3)$$

Clearly, the signal detected at frequency ω will have contributions from higher odd derivatives as well as the first derivative of the characteristic. And these higher order contributions, at frequency ω, depend on V_1^3, V_1^5, ... etc. as can be seen from equation (3-3). When the modulation amplitude, V_1, is changed in our experiments by a factor of as much as 8 there is no noticeable change in the curve shapes apart from slight smearing at higher levels. We conclude that only the first-derivative term contributes significantly at ω.

A similar result obtains for the second derivative at frequency 2ω.

The essentials of the circuit are shown in Figure (3-4). The modulation and DC circuits are connected in parallel. Typical values of the DC circuit parameters are included to illustrate that the sample now "sees" a power source of low impedance. Changes in sample conductance do not significantly affect the potential developed across the 1 ohm resistor. It is important that this should be so if voltage is to be the independent variable in the derivatives. Usually a fundamental frequency of about 1100 c/s was used.

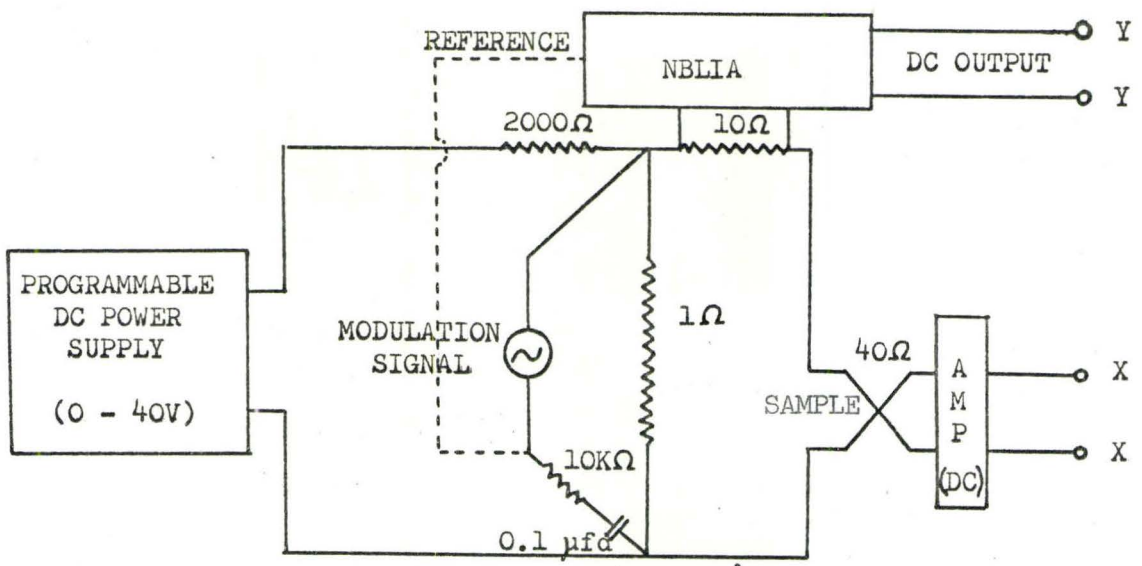

FIGURE (3-4)

(c) Cryostat

Most of the work was carried out in a conventional slit-silvered glass two-dewar system as shown in Figure (3-5). Temperatures of 1.20°K were obtained with an Edwards 3000 litres/min rotary pump. The helium vapour-pressure was measured on mercury and oil manometers and on a McLeod

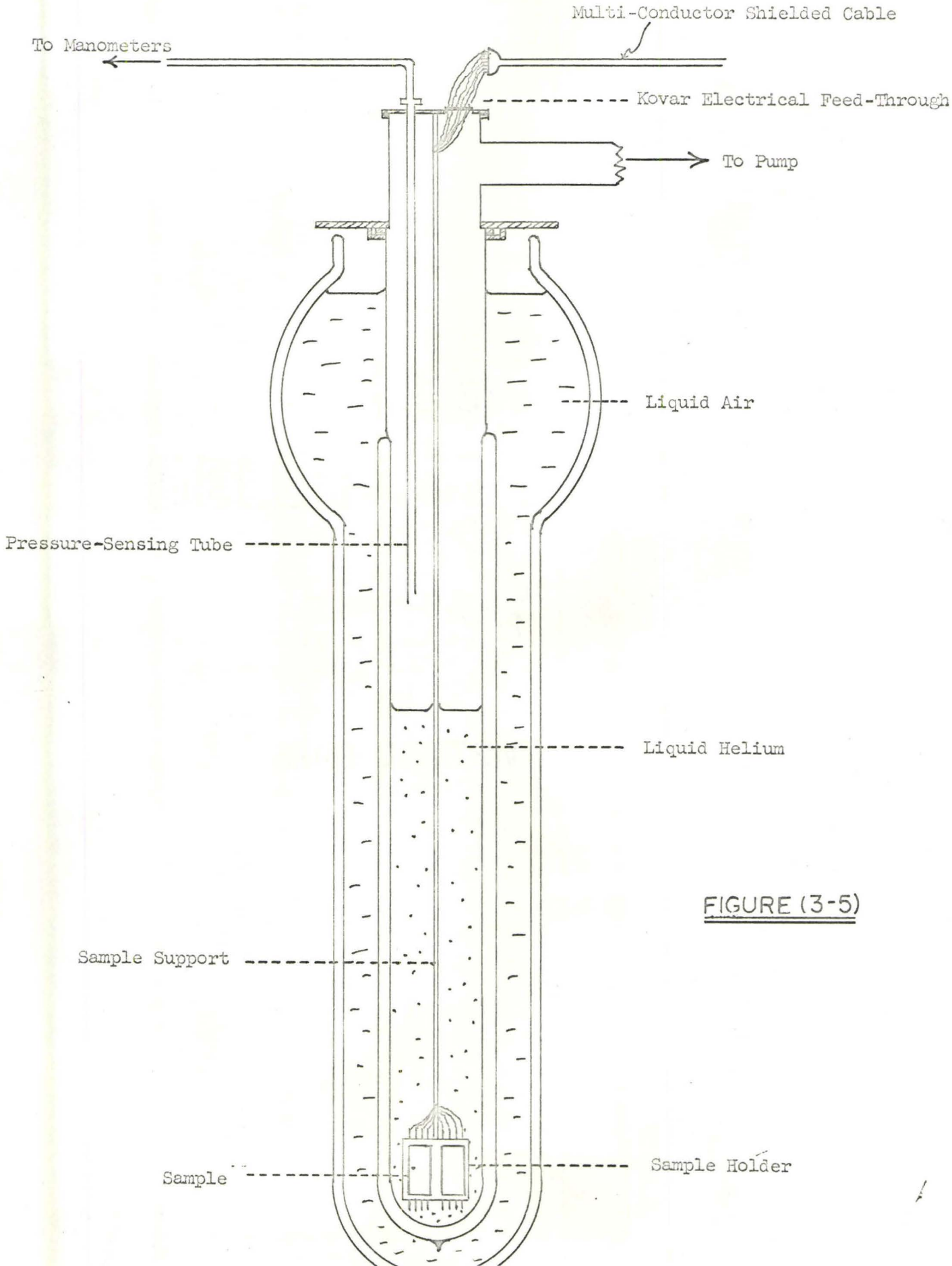
Multi-Conductor Shielded Cable
To Manometers
Kovar Electrical Feed-Through
To Pump
Liquid Air
Pressure-Sensing Tube
Liquid Helium
Sample Support
Sample
Sample Holder

FIGURE (3-5)

gauge which had been calibrated earlier against a precision McLeod (Manostat Corporation). A Pirani gauge was used, but only as a convenient monitor, below 5 Torr to detect any fluctuations in pressure. Conversion from vapour pressure to temperature was done through the T_{58} scale[53]. The pressure-sensing tube was inserted into the cryostat separately; it was not connected to the pumping line. A Cartesian manostat was used to stabilize the vapour pressure of the pumped liquid during recording periods made at higher temperatures.

At one stage in the research we experienced difficulty in observing the superconducting transition of aluminium. This inspired a careful look at the temperature measuring techniques at the lowest temperatures. A pressure-sensing tube of adjustable height (Figure (3-6)) was installed to investigate whether or not pressure drops were occurring between the liquid helium surface and the fixed end of the old pressure-sensing tube. The results are recorded in Table (3-1); h is the distance from the liquid helium surface to the end of the tube.

TABLE 3-1

h(cm)	Pirani Reading (Units of 10^{-3} Torr)	McLeod Reading (Units of 10^{-3} Torr)
13	970	632 ± 4
11	950	625 ± 4
6.5	950	625 ± 4
3	950	625 ± 4
1	950	625 ± 4
- 0.5	not noted	640 ± 4

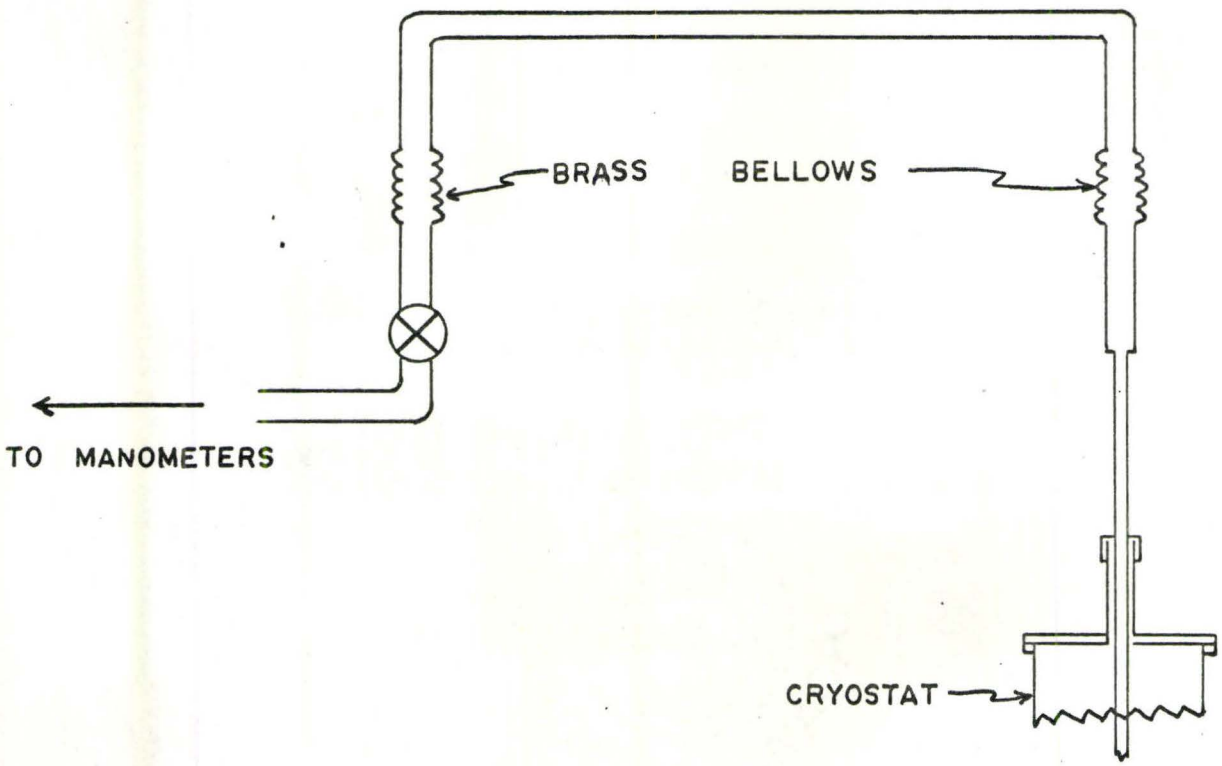

ADJUSTABLE PRESSURE - SENSING TUBE

FIGURE(3 - 6)

The last reading corresponds to the sensing tube dipping into the liquid. No sensible pressure drops occur in the cryostat. Thermomolecular corrections[54] to the pressure never amount to more than 0.25% in the tube and are neglected here.

To get to lower temperatures than available in the two-dewar cryostat, a three-dewar system was constructed with helium in the two inner dewars (Figure (3-7))[*]. The outer bath could be pumped down to 2°K and the inner one was connected to the 3000 litres/min pump. A temperature of 1.05°K was achieved. The system has disadvantages. For example, the inner dewar is very fragile because of its long supporting neck; transfer of liquid helium to the system, especially to the outer helium dewar is then a hazardous process. Furthermore, pumping on the outer helium bath is of little benefit because it lowers the level of the helium liquid and therefore reduces the shielding effect on the inner dewar. The experiment did serve to point out that there is significant heat leak to a helium bath from the sides as well as the top in a conventional dewar system: it also gave rather good evidence of superconductivity of aluminium at these lower temperatures.

Another dewar system that we tried, involved using the innermost helium dewar of the previous experiment in a liquid air bath only. Rather interestingly the same ultimate temperature (actually 1.16°K) was achieved, as with the original two-dewar system. Presumably the reduction in helium-film reflux is balanced by the pumping constriction which the narrow neck introduces.

---

[*]We are grateful to Dr. D. H. Douglass for this suggestion.

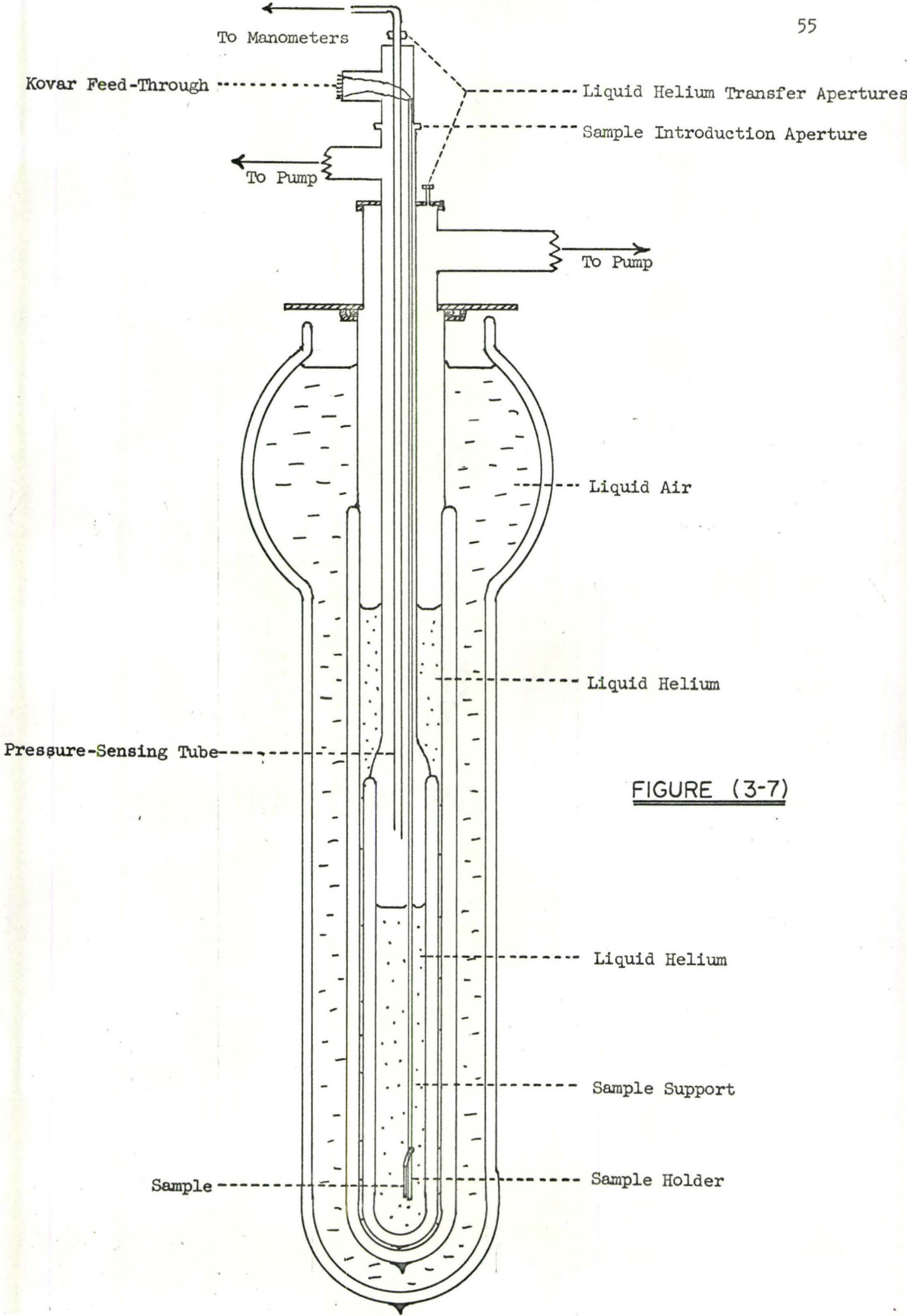
To Manometers
Kovar Feed-Through
Liquid Helium Transfer Apertures
Sample Introduction Aperture
To Pump
To Pump
Liquid Air
Liquid Helium
Pressure-Sensing Tube
Liquid Helium
Sample Support
Sample
Sample Holder

FIGURE (3-7)

(d) Sample Holder

Many different sample holders were used during the course of the project. The most useful type allows the samples to be introduced to, and removed from, the cryostat while there is liquid helium present. This permits quick cooling of the samples; it also allows the examination of several samples with one dewarful of liquid and repairs to be carried out on electrical contacts which may break after the experiment starts.

(We have found that Sn-I-M and Pb-I-M samples are more likely to give good tunnelling curves if cooled suddenly, and soon after preparation. Diffusion is perhaps responsible for their deterioration at higher temperatures. In the case of tin the phase transition from the white to grey modification may also be relevant.)

To minimize heat leaks to the sample all leads in the dewar were of 0.003 inches diameter copper magnet wire (SWG 40) with enamel insulation. Also, the support from the sample to the top of the cryostat was usually 0.15 inches diameter thin-wall stainless steel tubing, but sometimes even this was eliminated by letting the sample mount rest on the bottom of the dewar. The latter step is now realised to be unnecessary. Figure (3-8) shows a typical sample holder.

(e) Magnet Coil

Round the dewar a magnet coil with a few turns of copper wire was placed at sample height and it provides a small magnetic field which is useful in studies of the Josephson effect. It gives a field of approximately 25 gauss at the sample, per ampere of current through the coil.

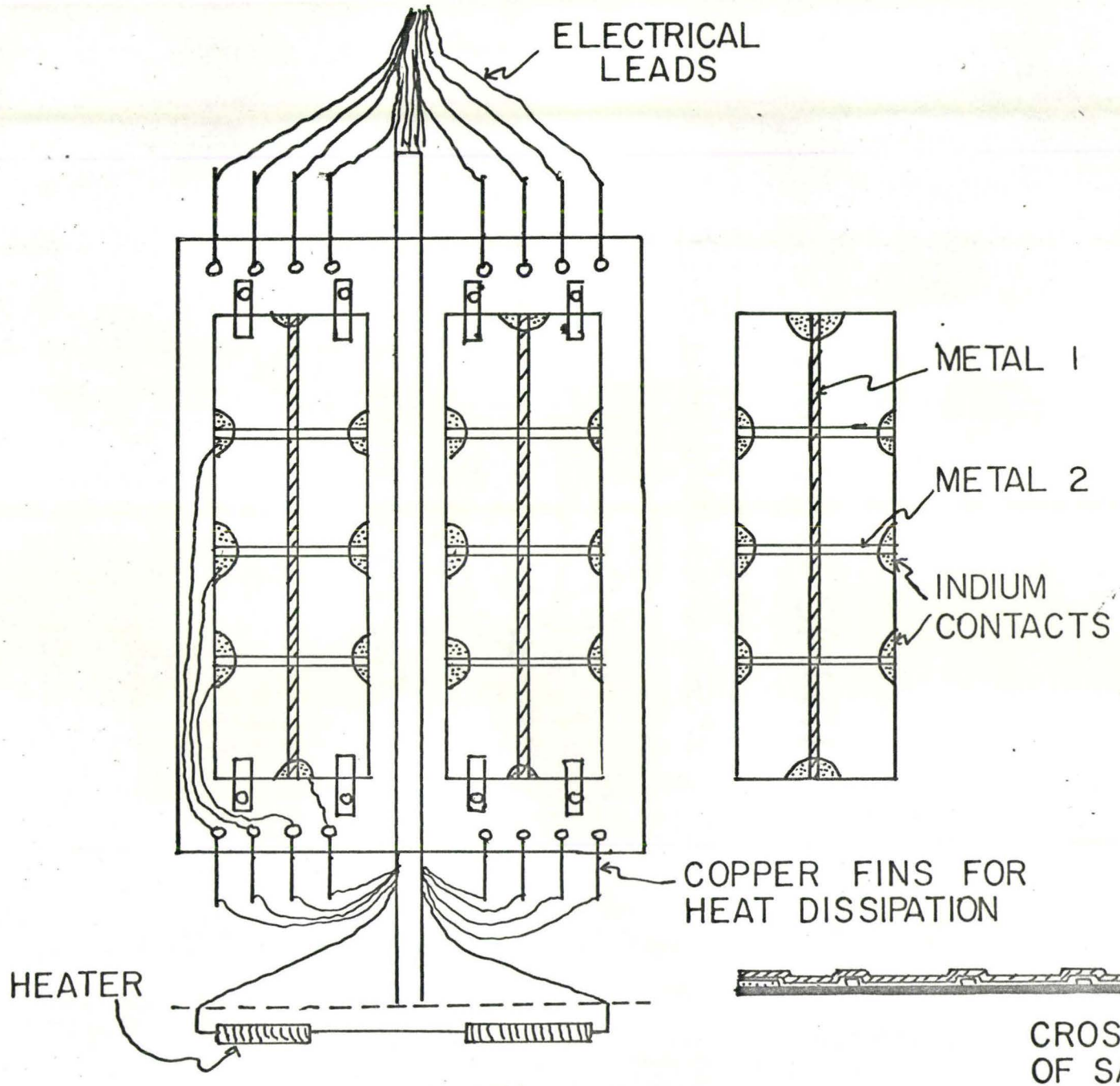

FIGURE (3-8)

SAMPLES AND HOLDER

CHAPTER 4. RESULTS AND DISCUSSION

4.1. TUNNELLING BETWEEN NORMAL FILMS

As a preliminary to the study of superconductors by the tunnel effect, some Al-I-Al samples were prepared and examined at room temperature mainly for the purpose of establishing techniques. The first-deposited aluminium film was oxidized in the atmosphere for periods ranging from 45 to 160 hours. All told, over 50 samples with 1-mm wide films were prepared under these conditions and only about 10% of them had shorts. Good, but not perfect, correlation exists between the observed resistances and the oxidation time. To illustrate the results obtained, the characteristics of seven representative samples are plotted on linear and semi-logarithmic scales in Figures (4-1) and (4-2). From these it is easy to see that the predicted dependence of tunnelling resistance on bias is borne out: up to about 200 mV the current is a linear function of applied potential; beyond, it approaches exponential behaviour. The characteristics show that a sample may have a higher resistance than another at low bias, but "cross-over" in the characteristics can occur at higher bias to reverse the relationship. This may arise either from different tunnelling barrier energy contours (denoted by $\phi(x)$ in Figure (2-3)), or the presence of additional current flow mechanisms contributing to different extents, in such samples. The fact that deviation from linearity becomes significant beyond about 200 mV would support the view that the metal-to-oxide work function is of the order of 1 electron-volt as deter-

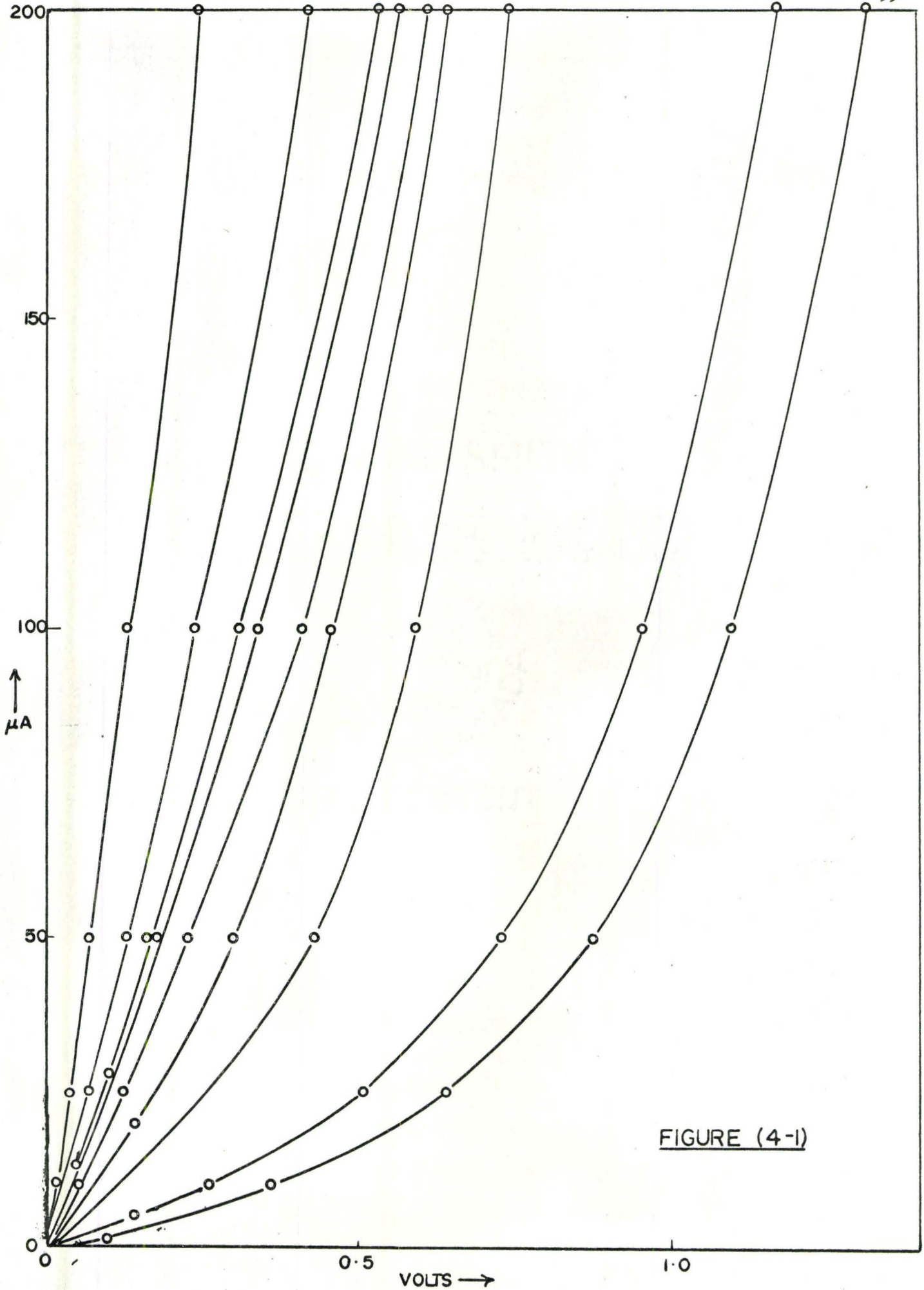

FIGURE (4-1)

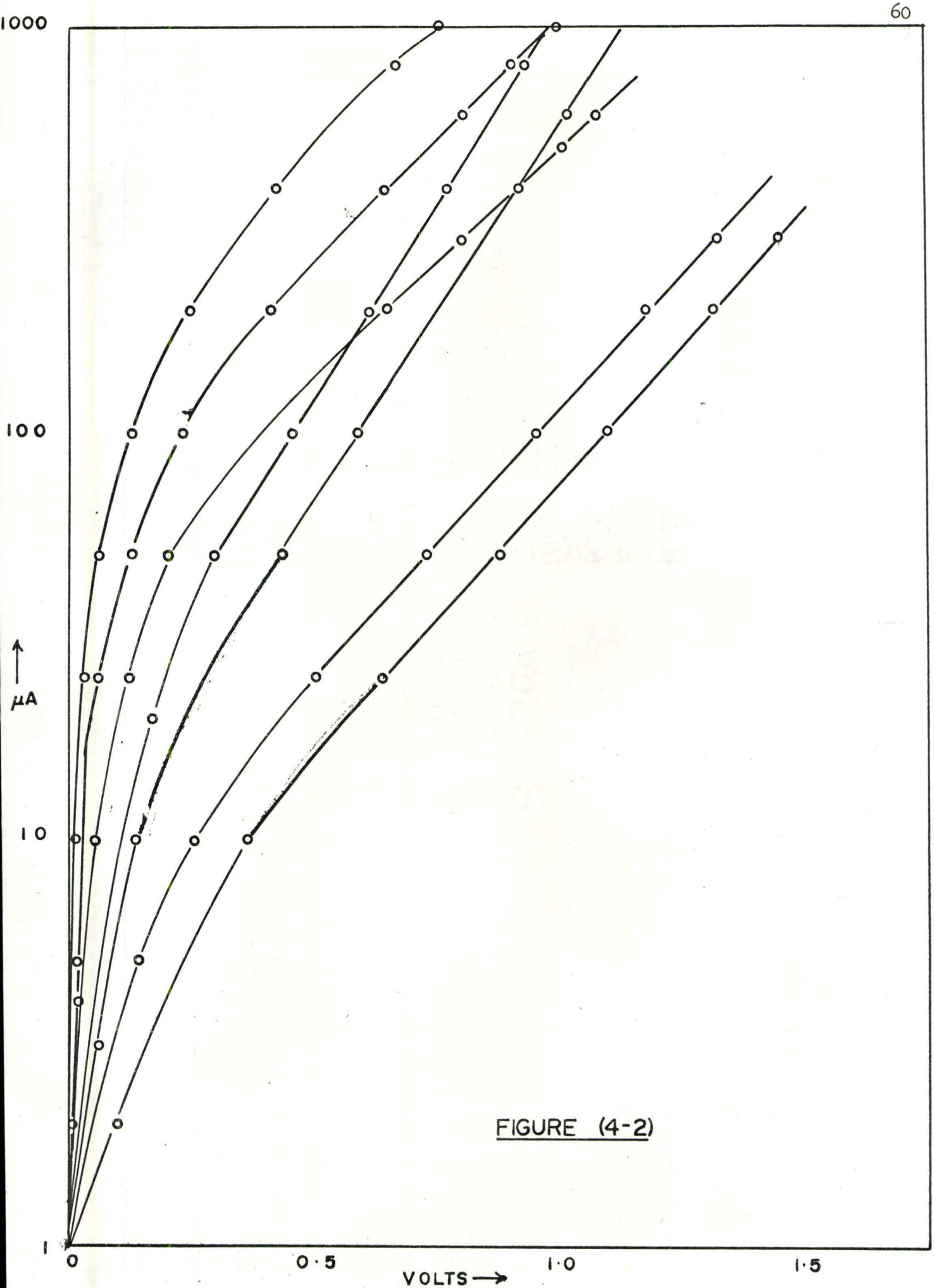

FIGURE (4-2)

mined in Schottky emission observations[55] rather than 4 to 5 electron-volts as has sometimes been used in tunnelling calculations. This point has been made by Holm[56] who discusses the question of charge transfer between metals in detail.

On the presumably reasonable assumption that tunnelling was responsible for the observed characteristics, the technique was extended to measurements at low temperatures as documented below.

4.2. TUNNELLING BETWEEN THIN SUPERCONDUCTING FILMS

(a) I-V Characteristics

(i) Al-I-M Samples

Some of the results obtained on Al-I-In, Al-I-Sn, Al-I-Pb and Al-I-Al samples are shown in Figures (4-3) to (4-6) respectively.

Figure (4-3a) corresponds to the case of a sample above the transition temperature for aluminium but below that for indium. The effects of the energy gap in indium are evident. The temperature was 1.18°K when this curve was taken. Other samples at lower temperatures, one at 1.15°K and one at 1.12°K, illustrate the rather abrupt change that occurs as the aluminium becomes superconducting. These are plotted in Figures (4-3b) and (4-3c).

The variation of the characteristics with temperature for an Al-I-Sn sample in the range 4.2°K to 1.14°K is shown in Figure (4-4a) and the lower temperature results of Figure (4-4b) were obtained in the three-dewar system described in the previous Chapter (Section 3.2.(c)). Figure (4-4c) is included to illustrate the fact that the aluminium film transition temperature shows variations from one sample to another. Here the aluminium is clearly superconducting at 1.15°K whereas no sign of its having undergone a transition is evident in Figure (4-4a) at 1.14°K.

FIGURE (4-3)

Al-I-In

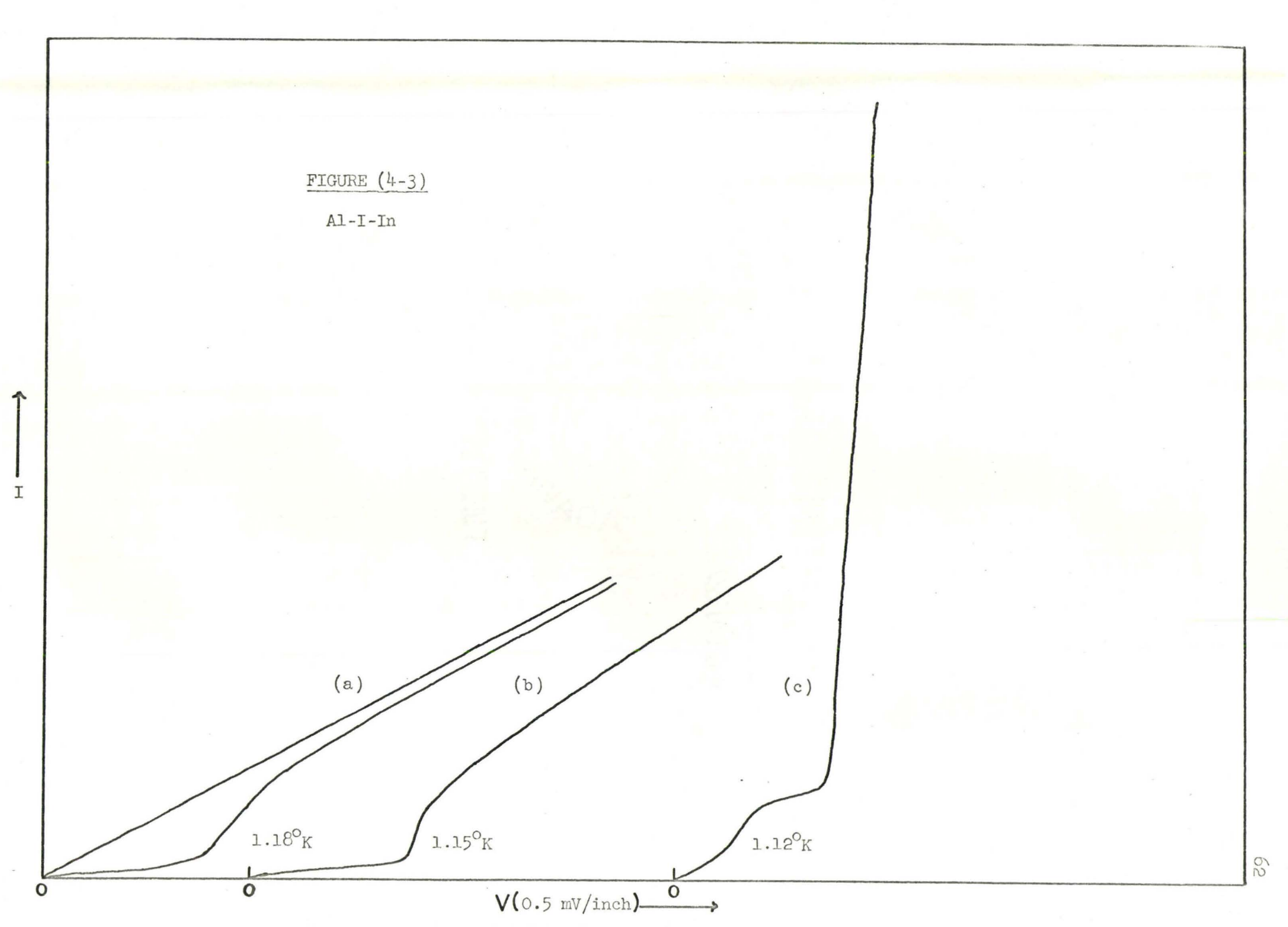

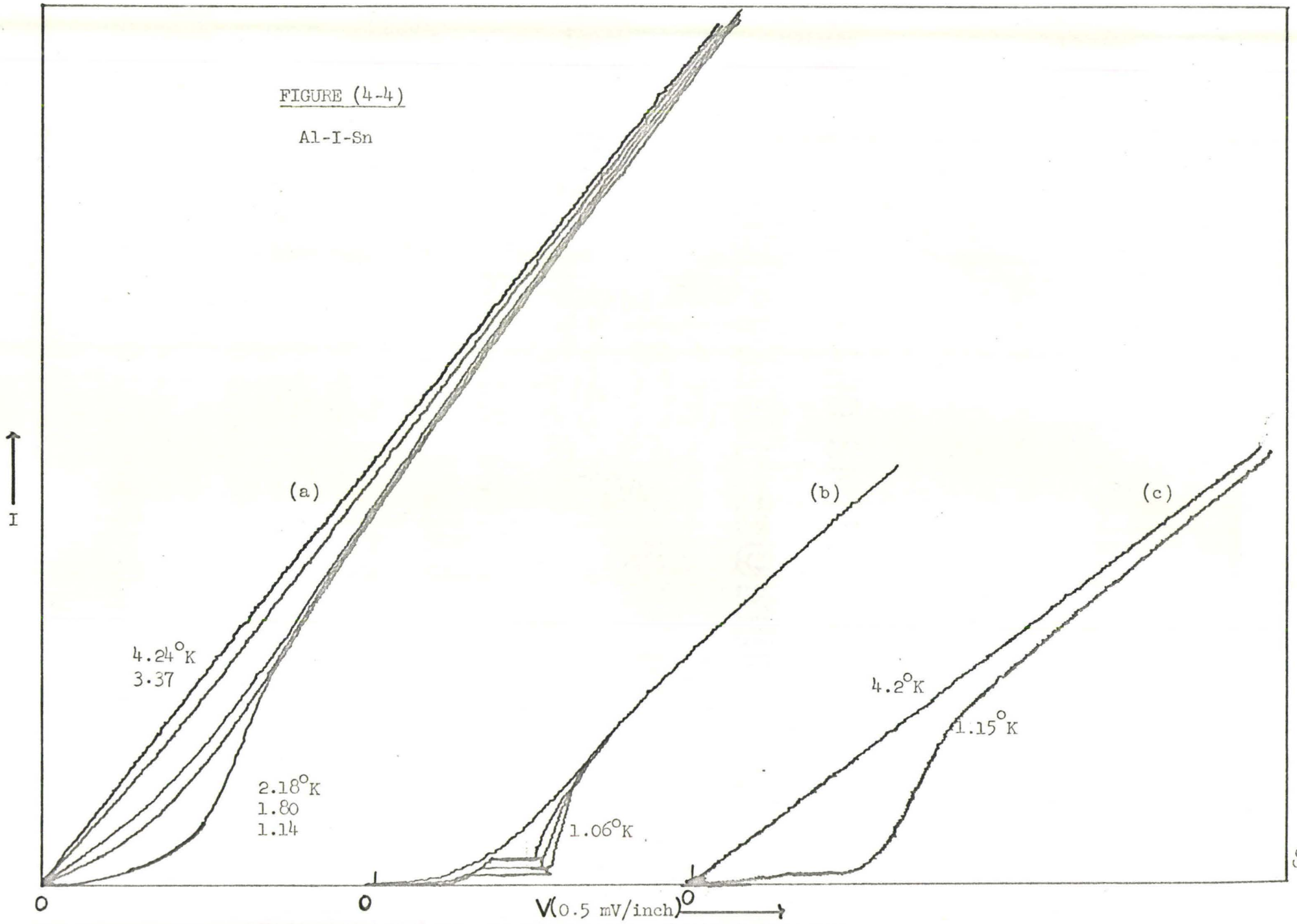
FIGURE (4-4)
Al-I-Sn
I
(a)
(b)
(c)
4.24°K
3.37
2.18°K
1.80
1.14
1.06°K
4.2°K
1.15°K
0
0
0
V(0.5 mV/inch)

An Al-I-Pb sample gave the result of Figure (4-5a); a separate plot of the 1.14°K curve (Figure (4-5b)) indicates the onset of the double superconductor behaviour. In Figure (4-5c) the tunnelling characteristic is plotted to higher applied potential to show non-linearity in the curve associated with the phonon spectrum in lead.

Finally, Figure (4-6) is a record of results obtained on Al-I-Al samples. Curve (a) may be considered as typical. There is a definite non-linearity but of the type one associates with N-S samples rather than S-S samples. Curves (b), (c) and (d) are results from exceedingly thin films.

In their pioneering experiments, Giaever and co-workers[57] obtained elegant curves from Al-I-M samples through the use of aluminium films showing transitions as high as 1.8°K. Thinner films, they noted[58], showed higher transition temperatures with the onset of the effect evidently occurring at 300 Å or thicker. No details were given as to the method of thickness measurement. Douglass and Meservey[59] have also found transitions above the bulk value even at a thickness of 9800 Å, measured interferometrically. Strongin et al.[60] have established that stress does not account for the effect and suggest[61] that a Ginzburg surface layer of high critical temperature is responsible for the observations. The thickness of this layer they assume to be about 20 Å. This concept inspired the experiment which produced curves (b), (c) and (d) where an attempt was made to produce aluminium films less than 100 Å thick. No reliable method of thickness measurement was available to us in this laboratory. Certainly resistance measurements do not suffice because they suggest that the films used to obtain curve (a) are thinner than those for (b), (c), and (d). For the record, the resistances and

FIGURE(4-5a)

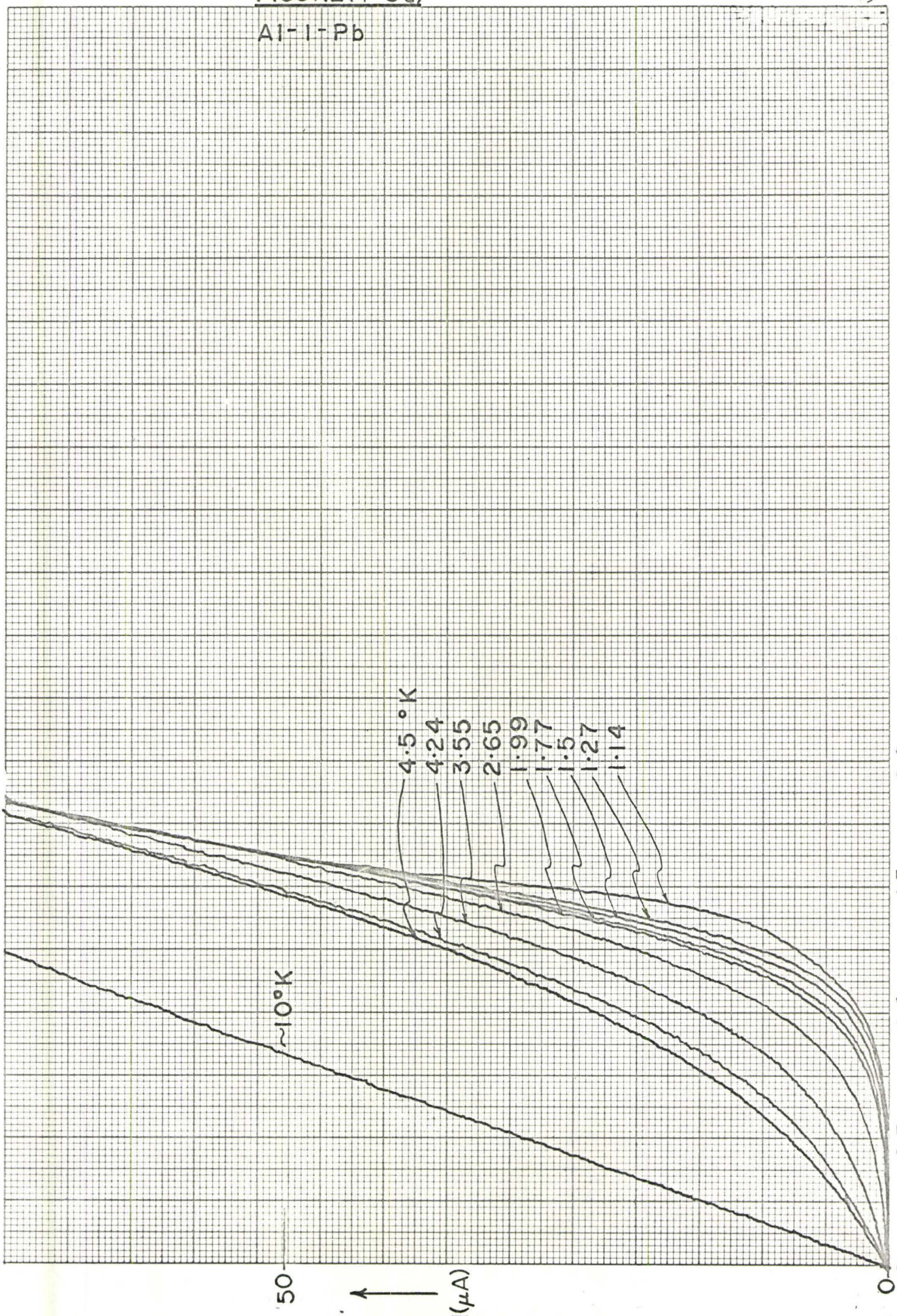
Al-I-Pb
4·5 °K
4·24
3·55
2·65
1·99
1·77
1·5
1·27
1·14
~10°K
50
I(μA)
0
0·5
1·0
1·5
2·0
V(mv)

FIGURE(4-5b)

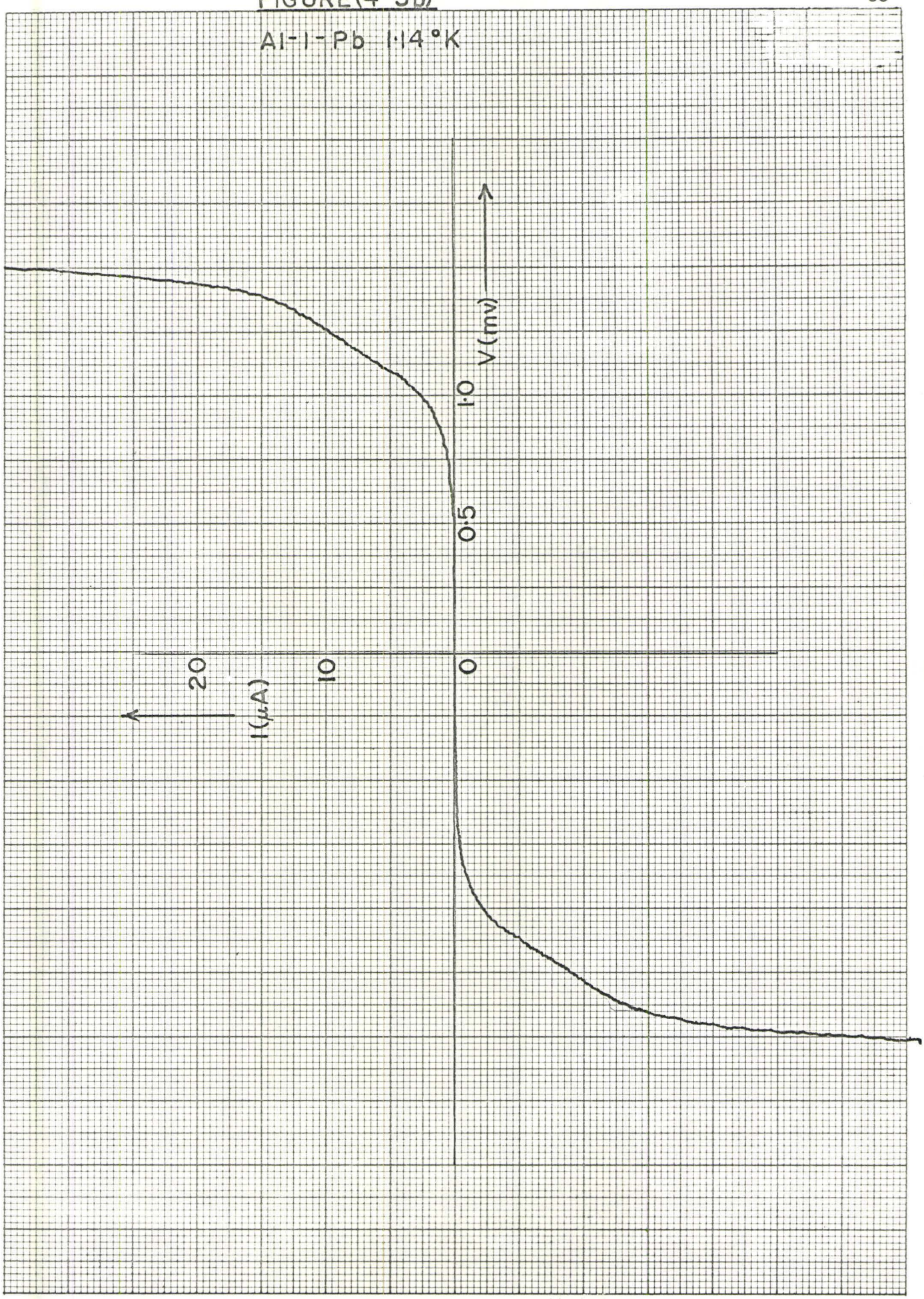

FIGURE (4-5c)

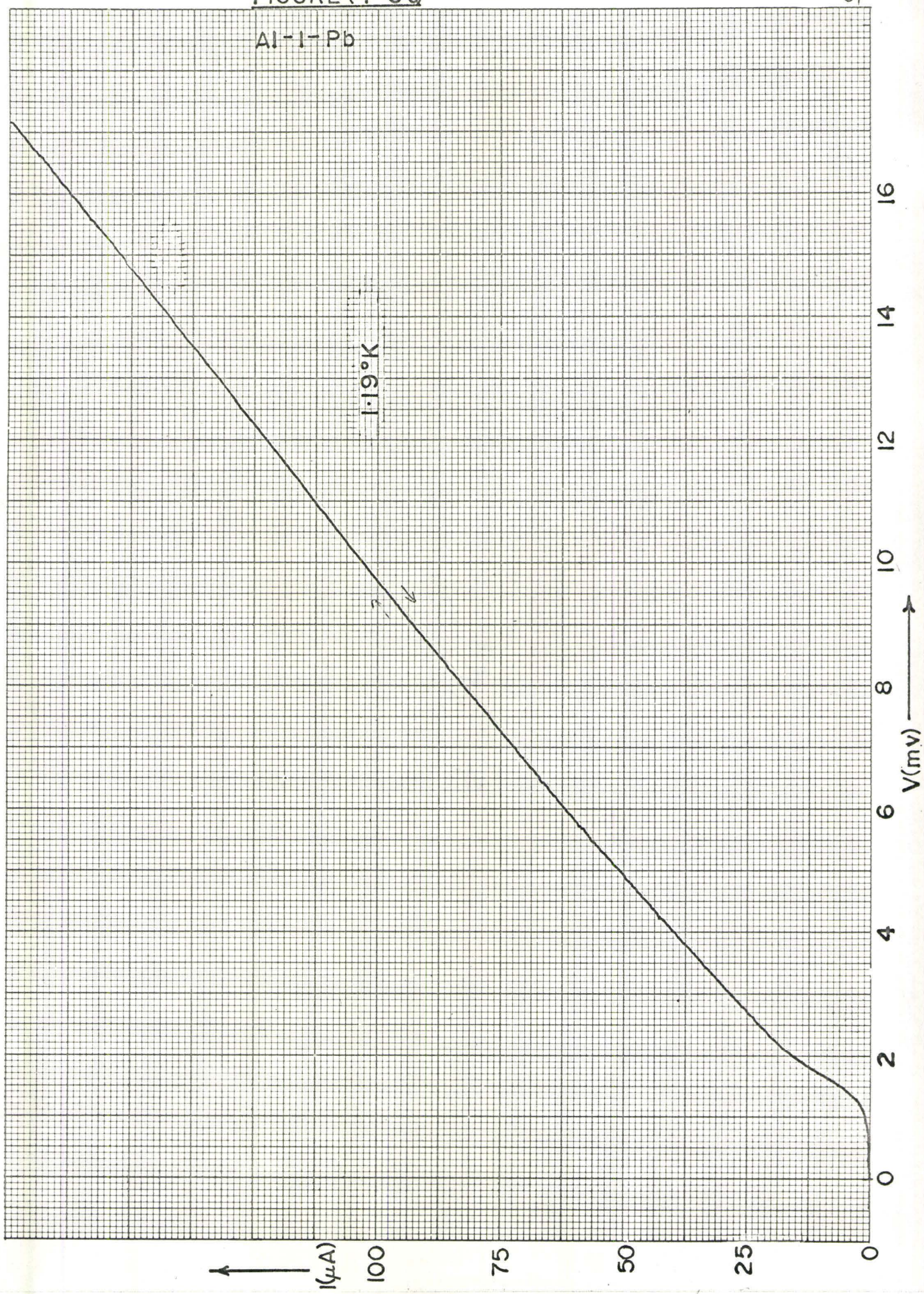

FIGURE (4-6)

Al-I-Al

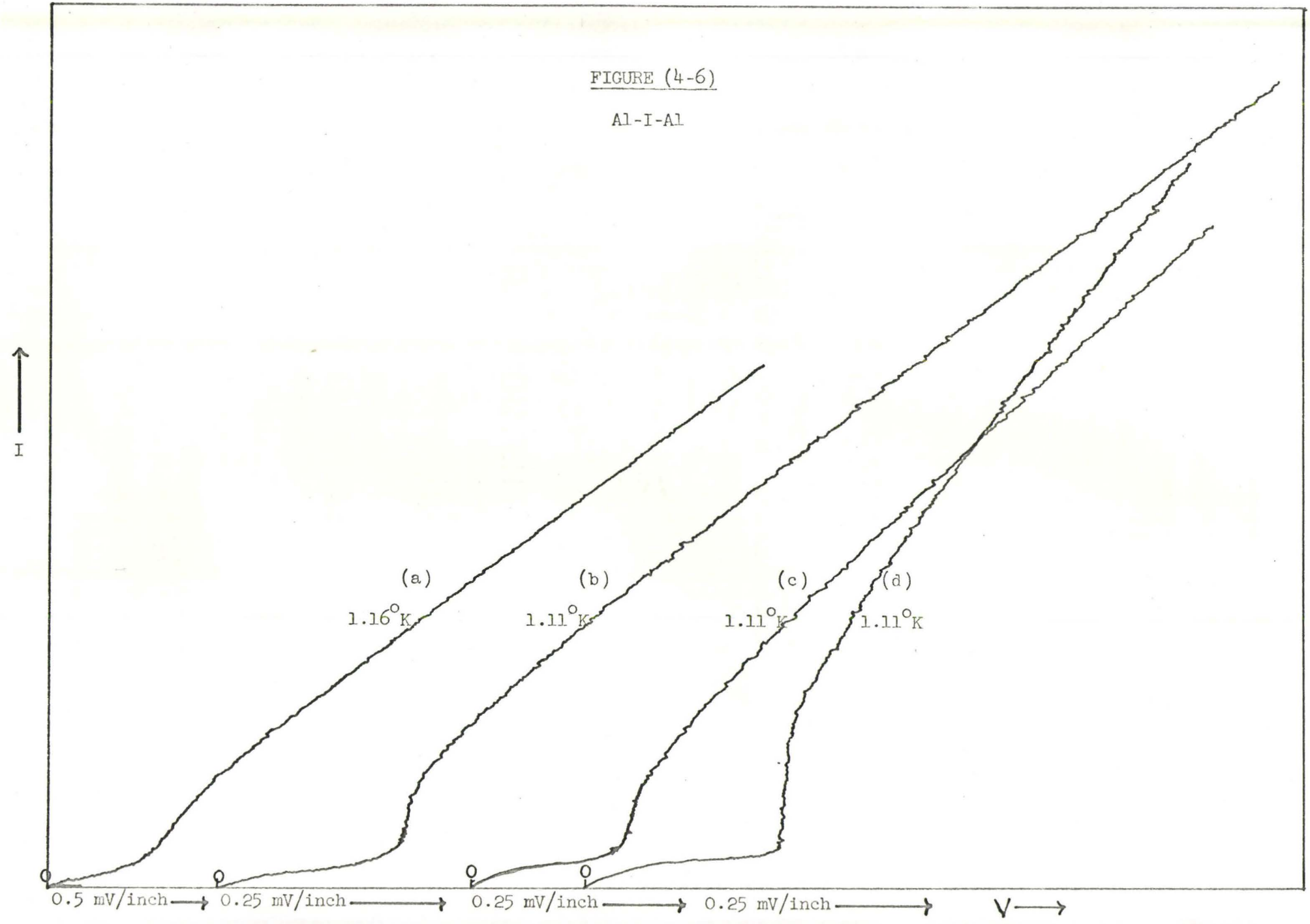

measurable dimensions of the aluminium films used to obtain curves (a), (b), (c), and (d) are listed in Table (4-1).

TABLE (4-1)

Curve	Film	Resistance at 300°K	Length	Width	Thickness
(4-6a)	1st-deposited	1700 ohms	2.6 cm	0.25 mm	17 Å
	2nd-deposited	630 ohms	1.3 cm	0.25 mm	23 Å
(4-6b)	1st-deposited	130 ohms	2.6 cm	1.7 mm	33 Å
	2nd-deposited	45 ohms	1.3 cm	1.6 mm	50 Å
(4-6c)	1st-deposited	130 ohms	2.6 cm	1.7 mm	33 Å
	2nd-deposited	21 ohms	1.3 cm	1.6 mm	110 Å
(4-6d)	1st-deposited	130 ohms	2.5 cm	1.7 mm	33 Å
	2nd-deposited	120 ohms	1.3 cm	1.1 mm	28 Å

A resistivity value for aluminium of 2.8×10^{-6} ohm-cm was used in the calculations. No claims are made regarding the meaningfulness of the thickness determined in this way. Obviously surface and inter-crystallite boundary scattering are the dominant sources of resistance. Nothing is gained by making further measurements at 77°K because variation in texture from one film to another makes meaningless any average thickness that might be determined from application of Matthiesen's rule.

Thickness determinations by interferometric methods are probably better. What they measure in the case of open-textured deposits is open to debate but there should not be any serious problem when quickly-deposited metal films are under consideration.

With very thin films the I-V tunnelling characteristics can show great sharpness as is illustrated by the current rise at $2\Delta_{Al}/e$ in

Figure (4-6d). It compares favourably with results obtained at 0.5°K on Al-I-Al by Adler[62]. (We believe smearing at temperatures significantly below the transition is associated with energy gap anisotropy.)

(ii) Sn-I-Sn Samples

The characteristics of two Sn-I-Sn samples are shown in Figures (4-7a) and (4-7b). The first was prepared by oxidizing the tin in air, while the second sample was oxidized in an oxygen atmosphere. Josephson DC and AC effects are present in the first sample but there are rather serious leakage currents below the "striking potential" of $2\Delta_{Sn}/e$. Leakage is very low in the second sample.

(iii) Pb-I-M Samples

Lead has a transition temperature (7.18°K) above that easily attainable in a simple cryostat. The variation of Pb-I-Pb tunnelling characteristics in the liquid helium temperature range is shown in Figure (4-8a) while in (4-8b) the phonon effects beyond the gap are seen to stand out more clearly than in the Al-I-Pb samples.

A number of Pb-I-Sn curves (Figure (4-9)) illustrate well the change that occurs in the characteristic when tin becomes superconducting. Quenching of the Josephson DC current, when necessary, was achieved with a magnetic field of only 5 gauss, applied in the plane of the films.

The last type of sample attempted, Pb-I-In, yielded the plots in Figure (4-10). They are not good, but suggest that such samples can be prepared. A puzzling tendency to show unstable oscillation between different voltages when the current was held constant can perhaps be explained in terms of shorts, with resistance values comparable to the

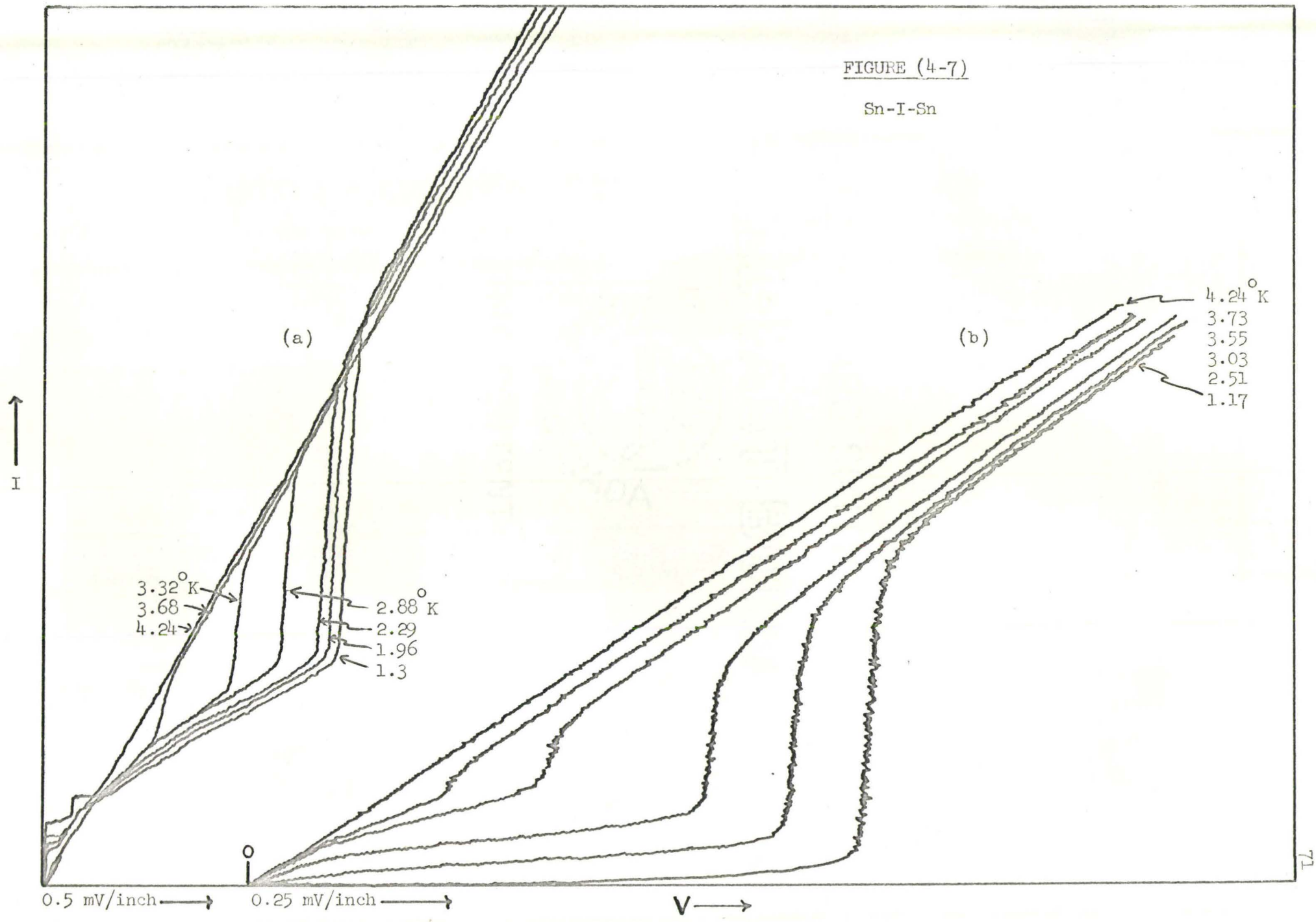
FIGURE (4-7)
Sn-I-Sn
(a)
(b)
4.24° K
3.73
3.55
3.03
2.51
1.17
3.32° K
3.68
4.24
2.88° K
2.29
1.96
1.3
I
0
0.5 mV/inch
0.25 mV/inch
V

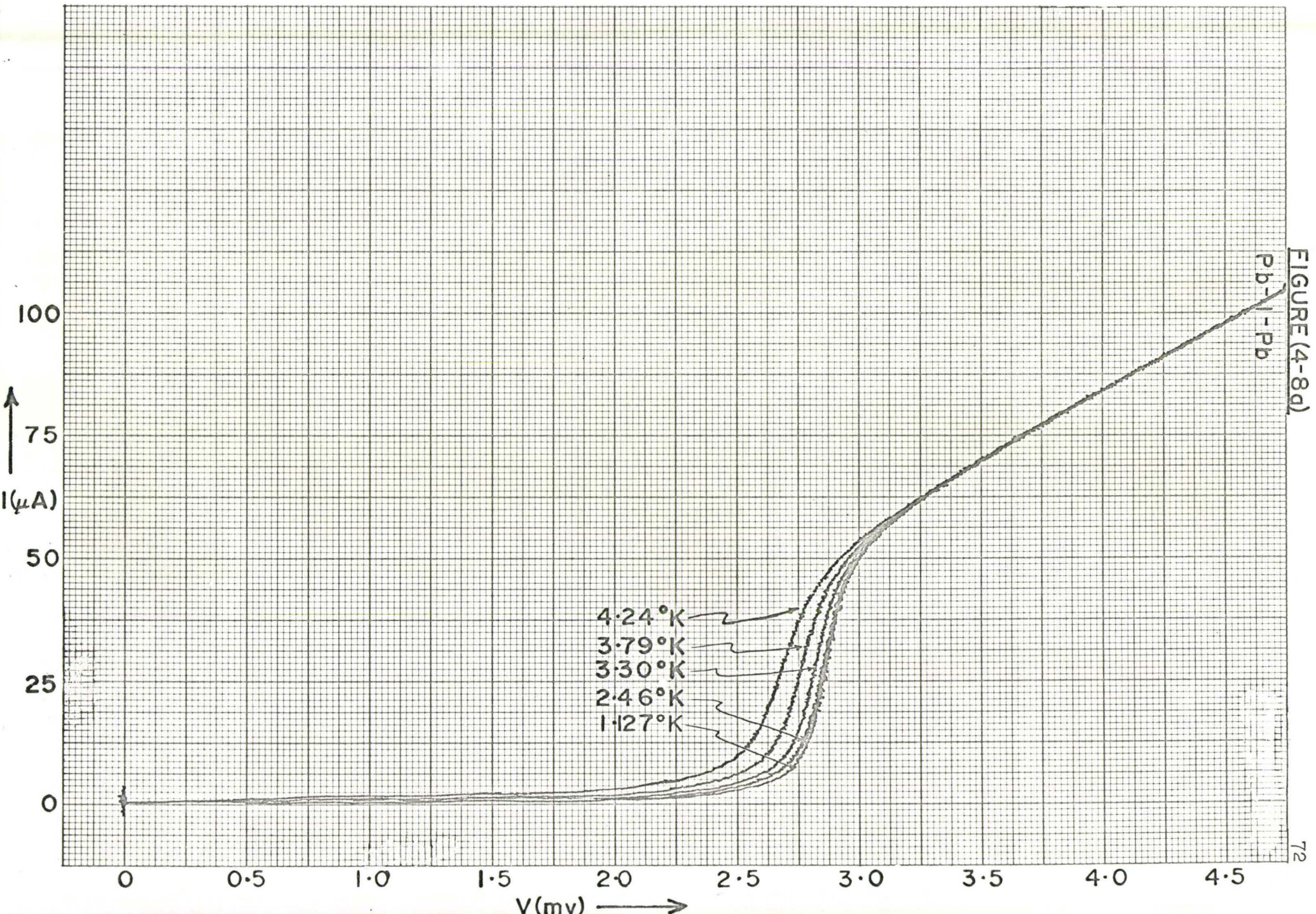
100
75
I(μA)
50
25
0
4·24°K
3·79°K
3·30°K
2·46°K
1·127°K
0
0·5
1·0
1·5
2·0
2·5
3·0
3·5
4·0
4·5
V(mv)
Pb-I-Pb

FIGURE (4-8a)

FIGURE (4-8b)

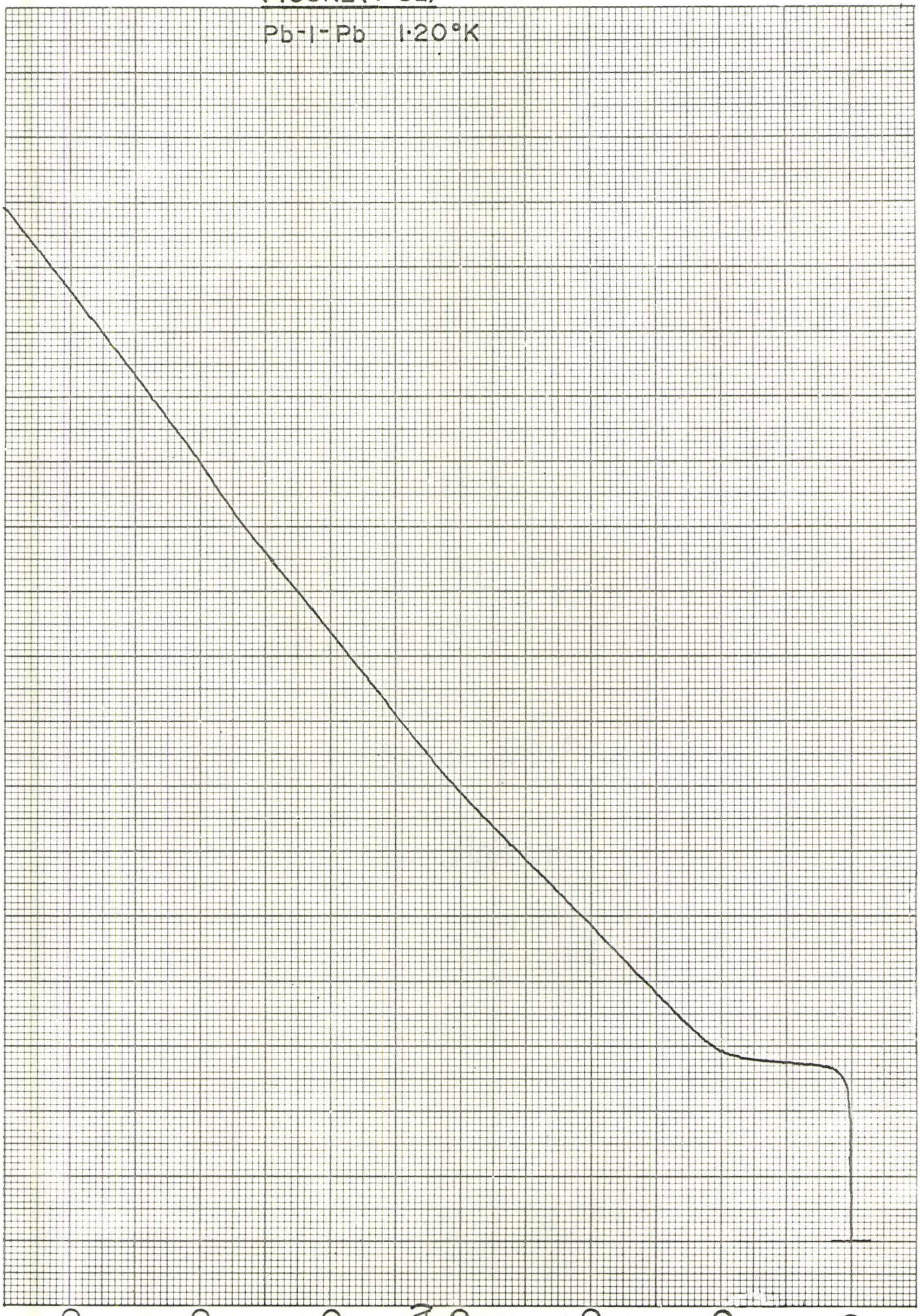

FIGURE (4-8c)

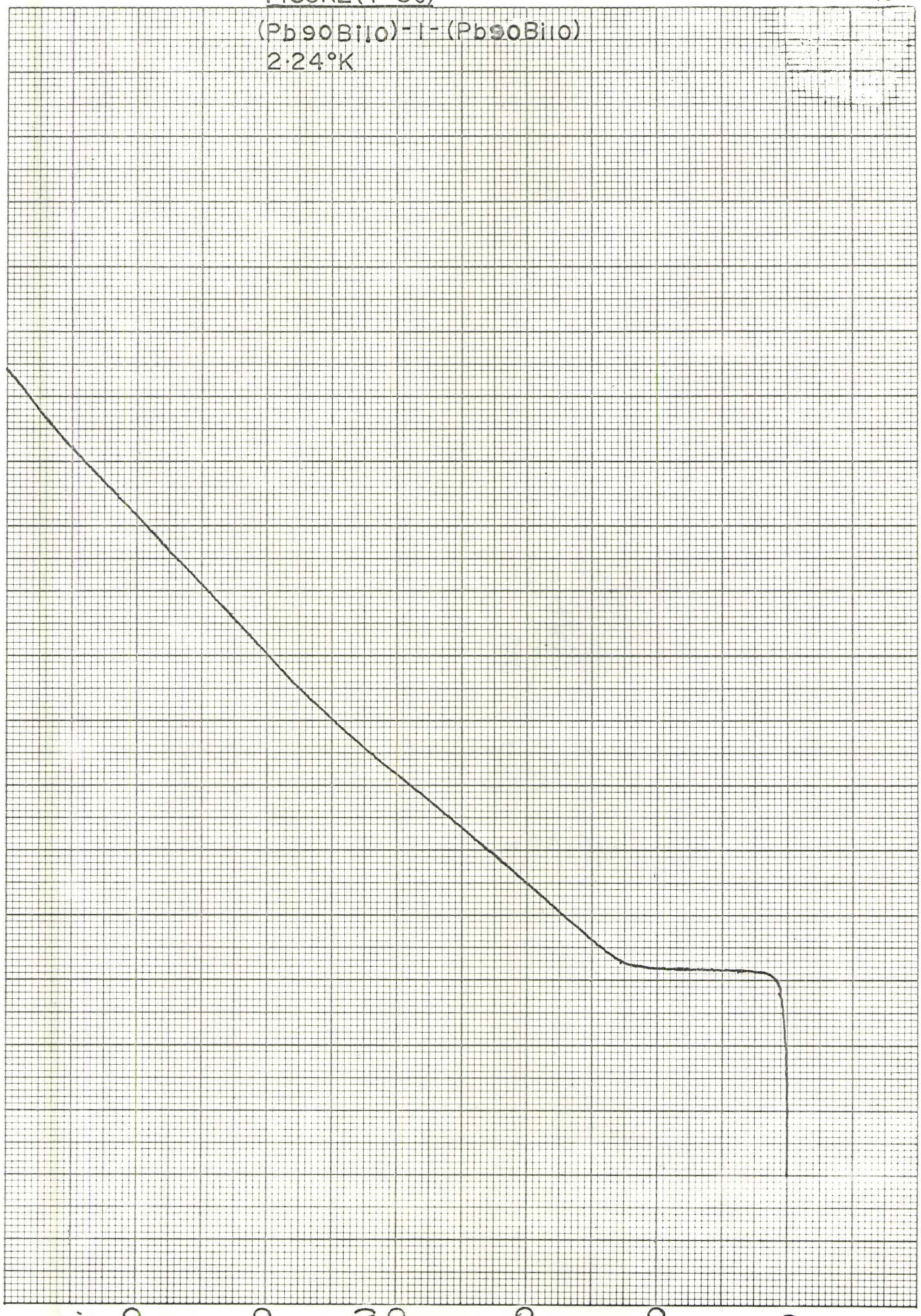
(Pb90Bi10)-I-(Pb90Bi10)
2.24°K
0
2
4
6
8
10
12
14
V(mv)
500
400
300
200
100
0
I(μA)

FIGURE (4-9)

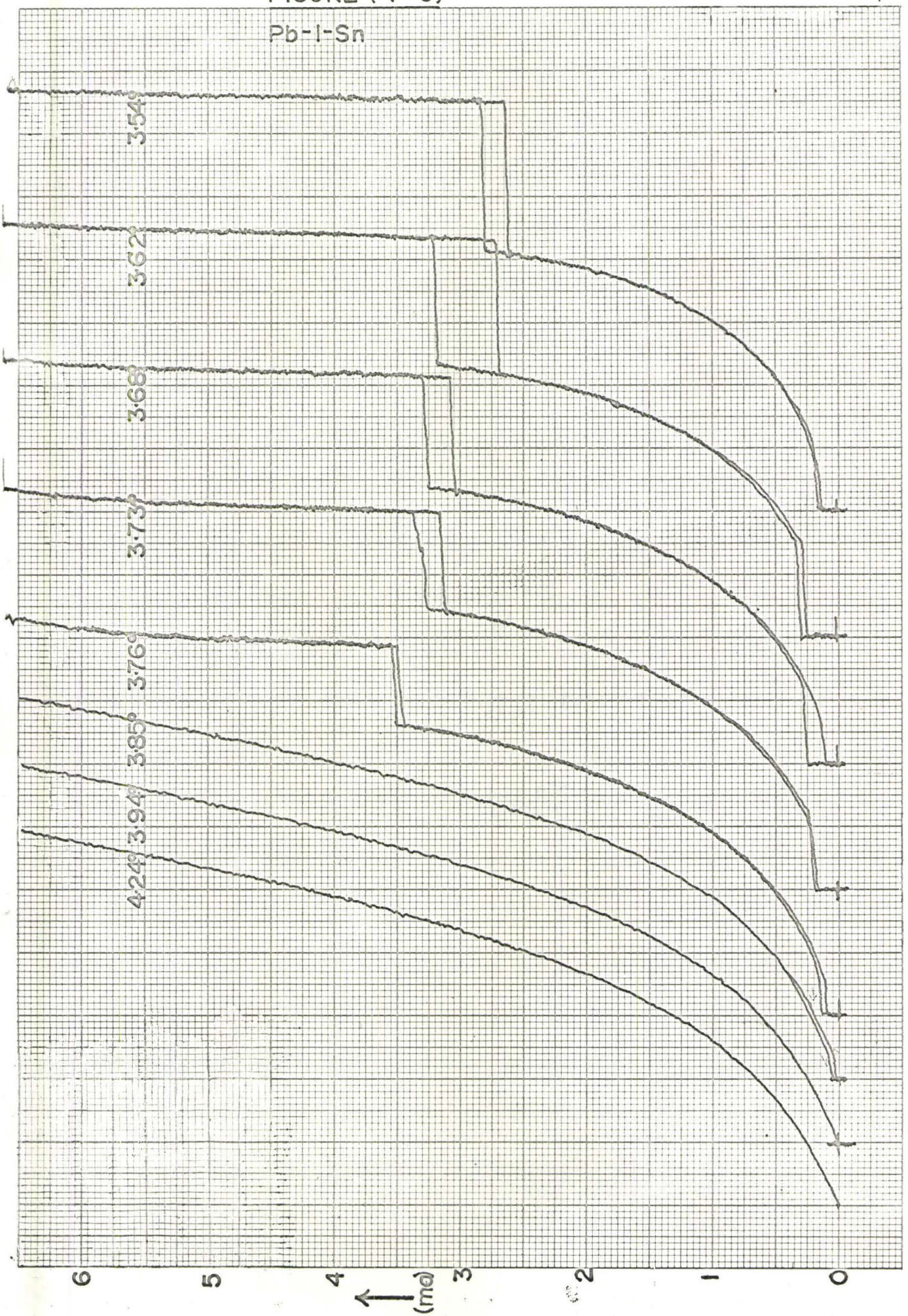

FIGURE (4-9)

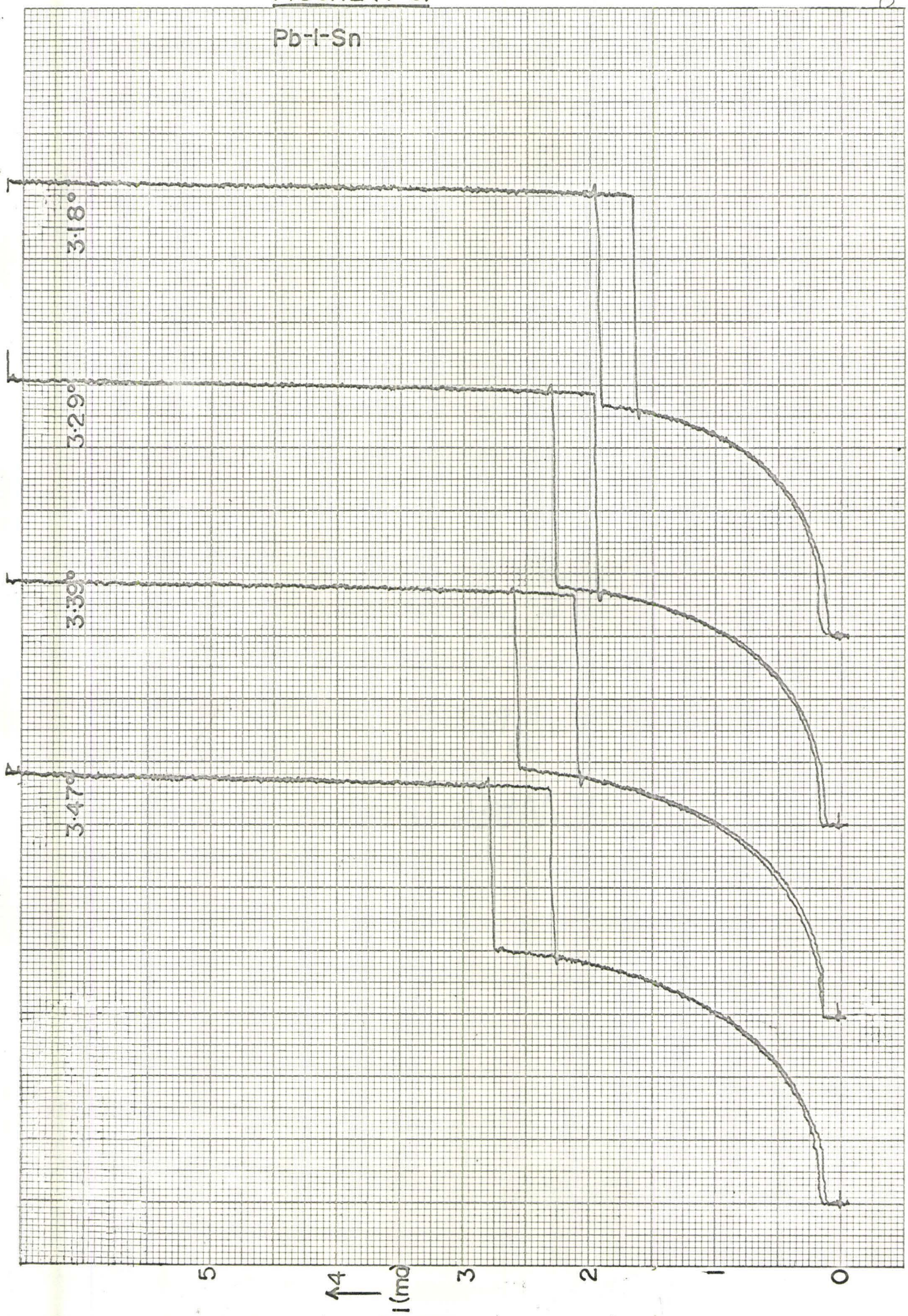

FIGURE (4-9)

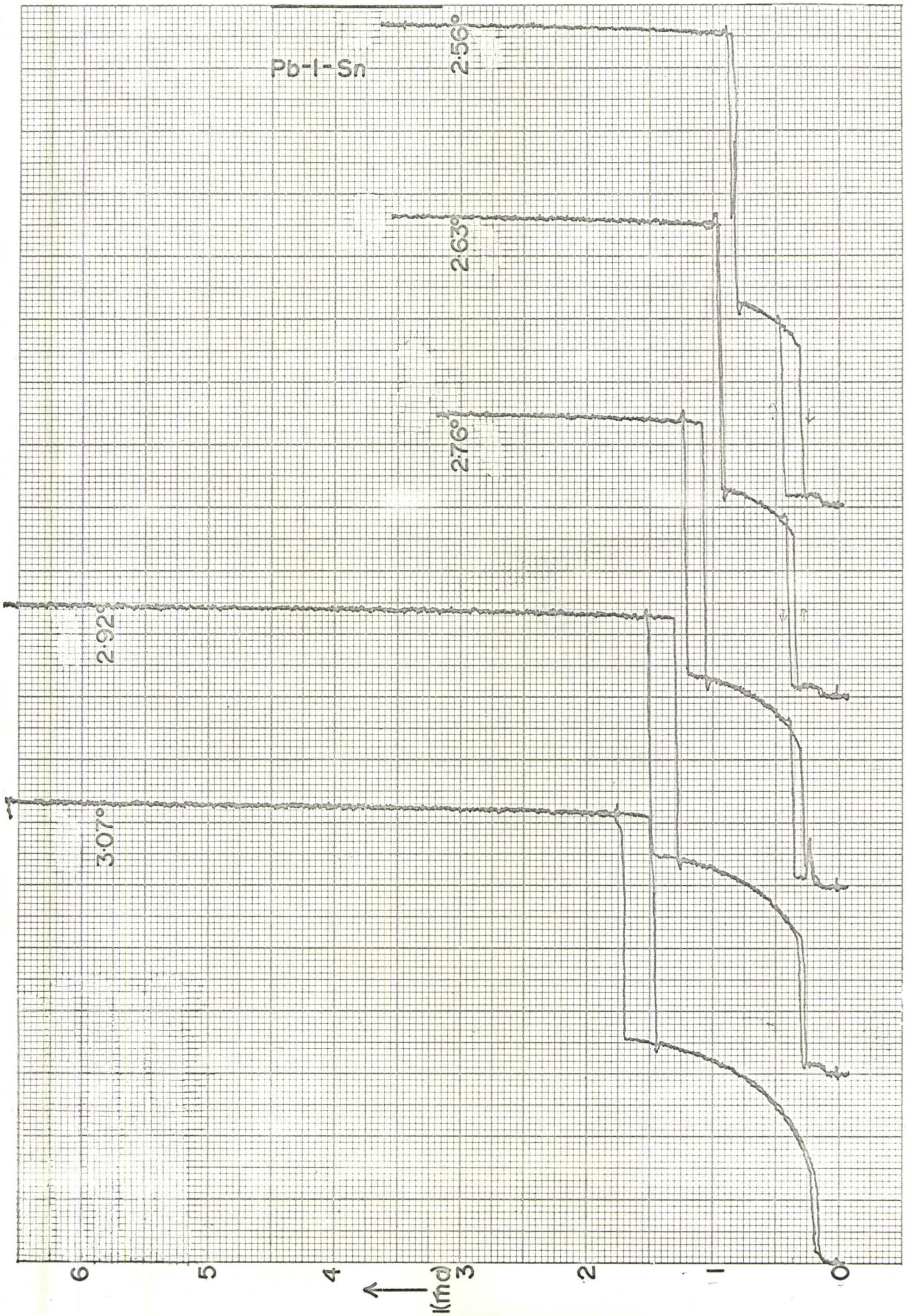

FIGURE (4-9)

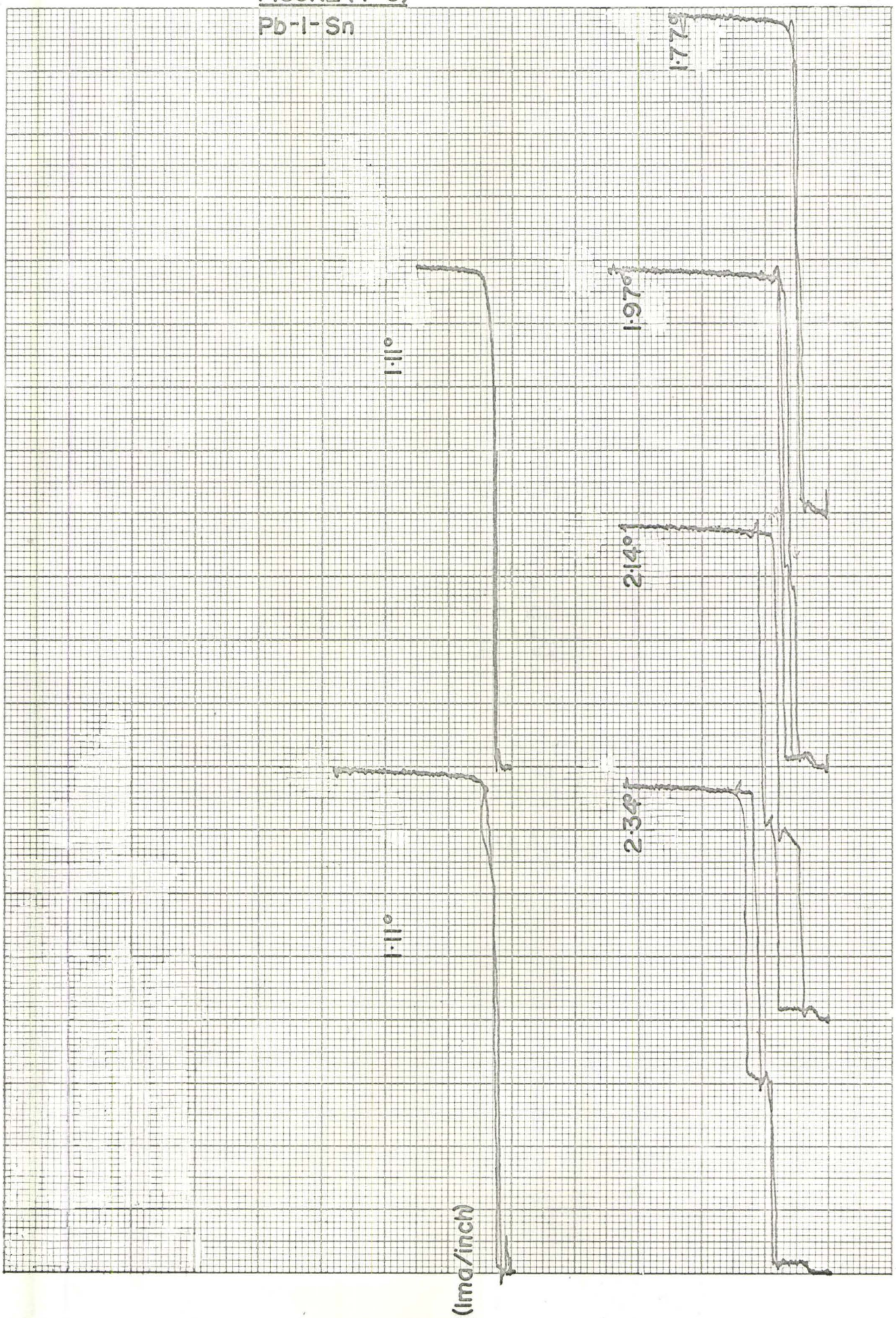

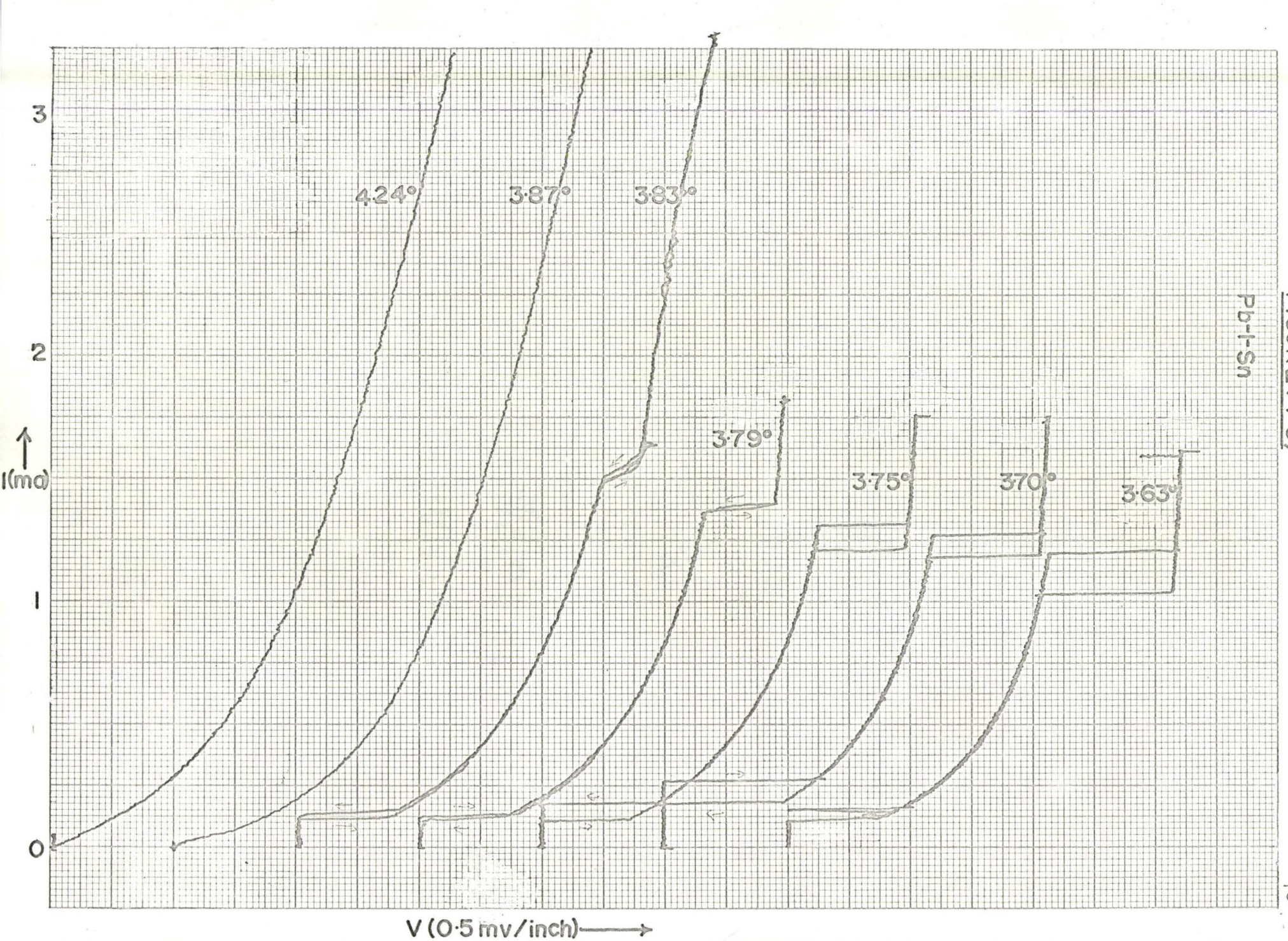

FIGURE (4-9)

FIGURE (4-9)

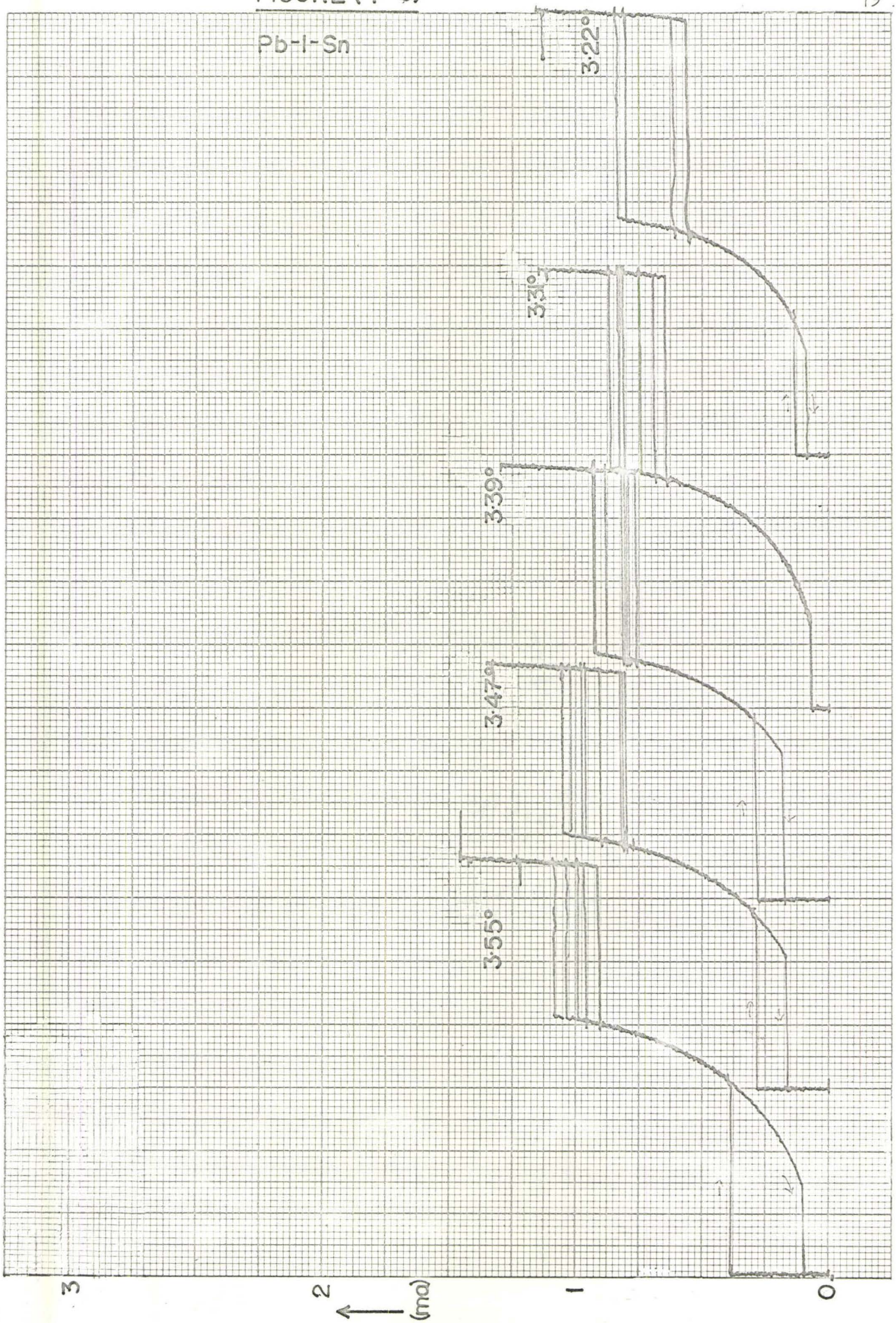

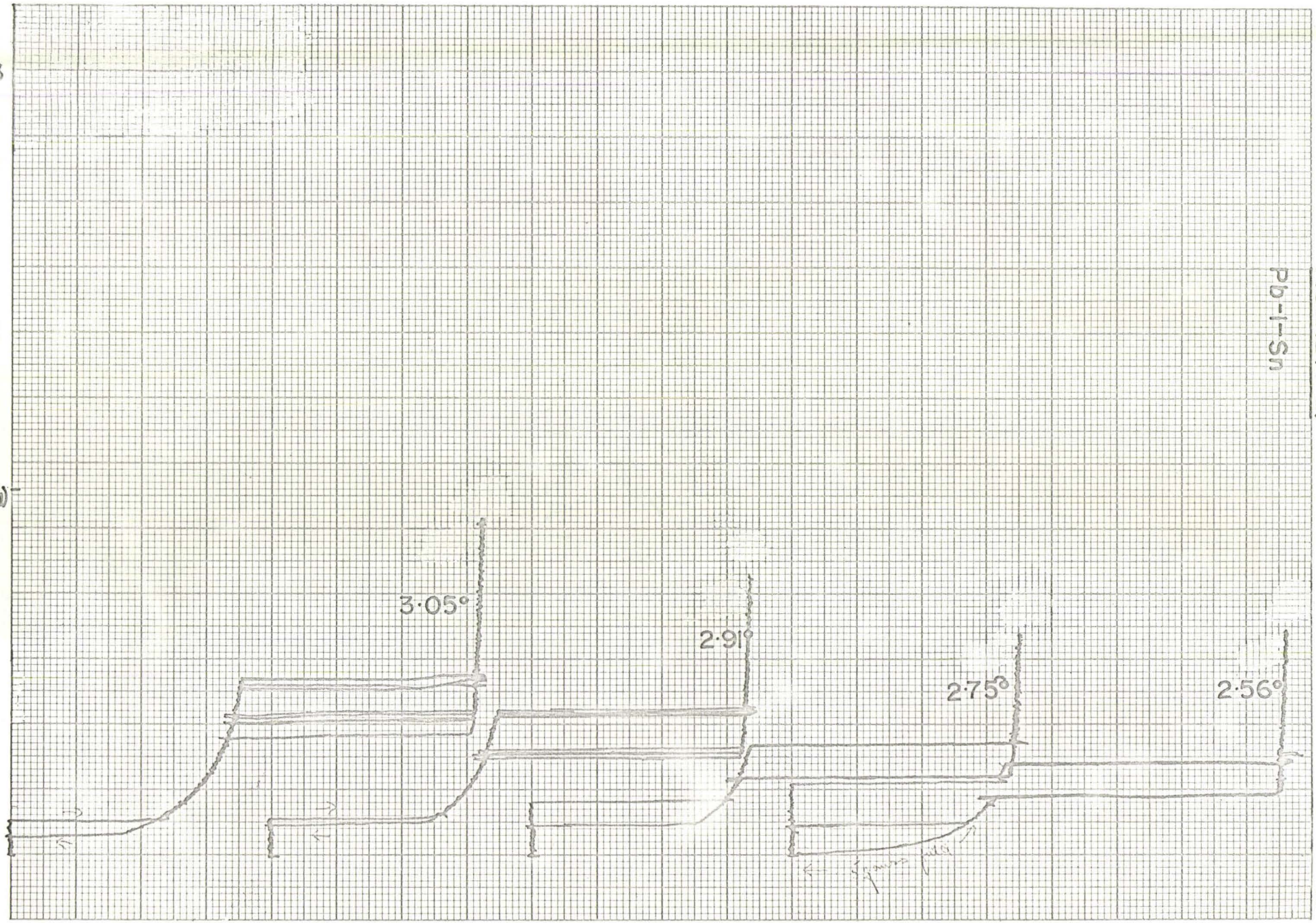

FIGURE(4-9)

Pb-I-Sn

FIGURE (4-9)

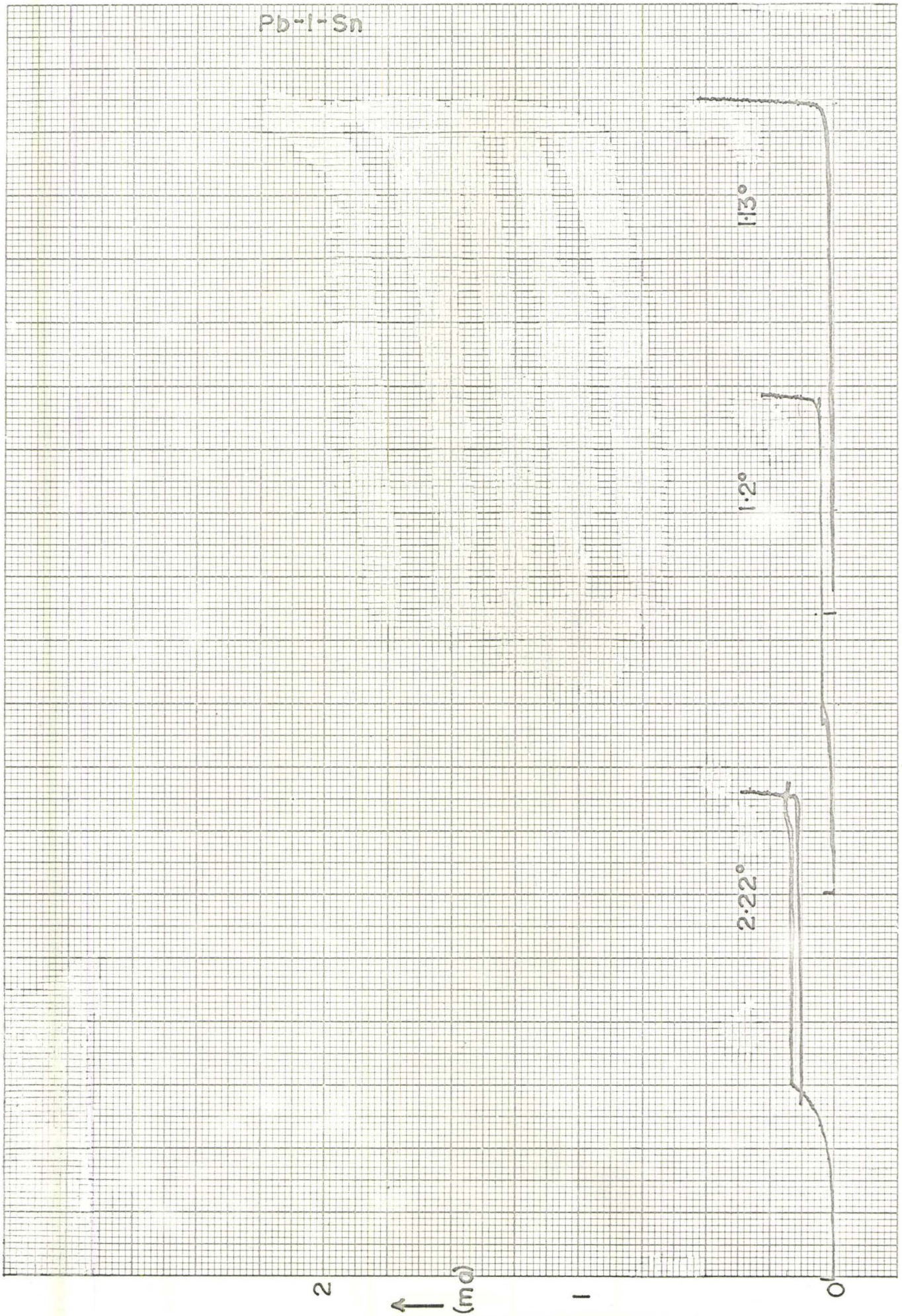

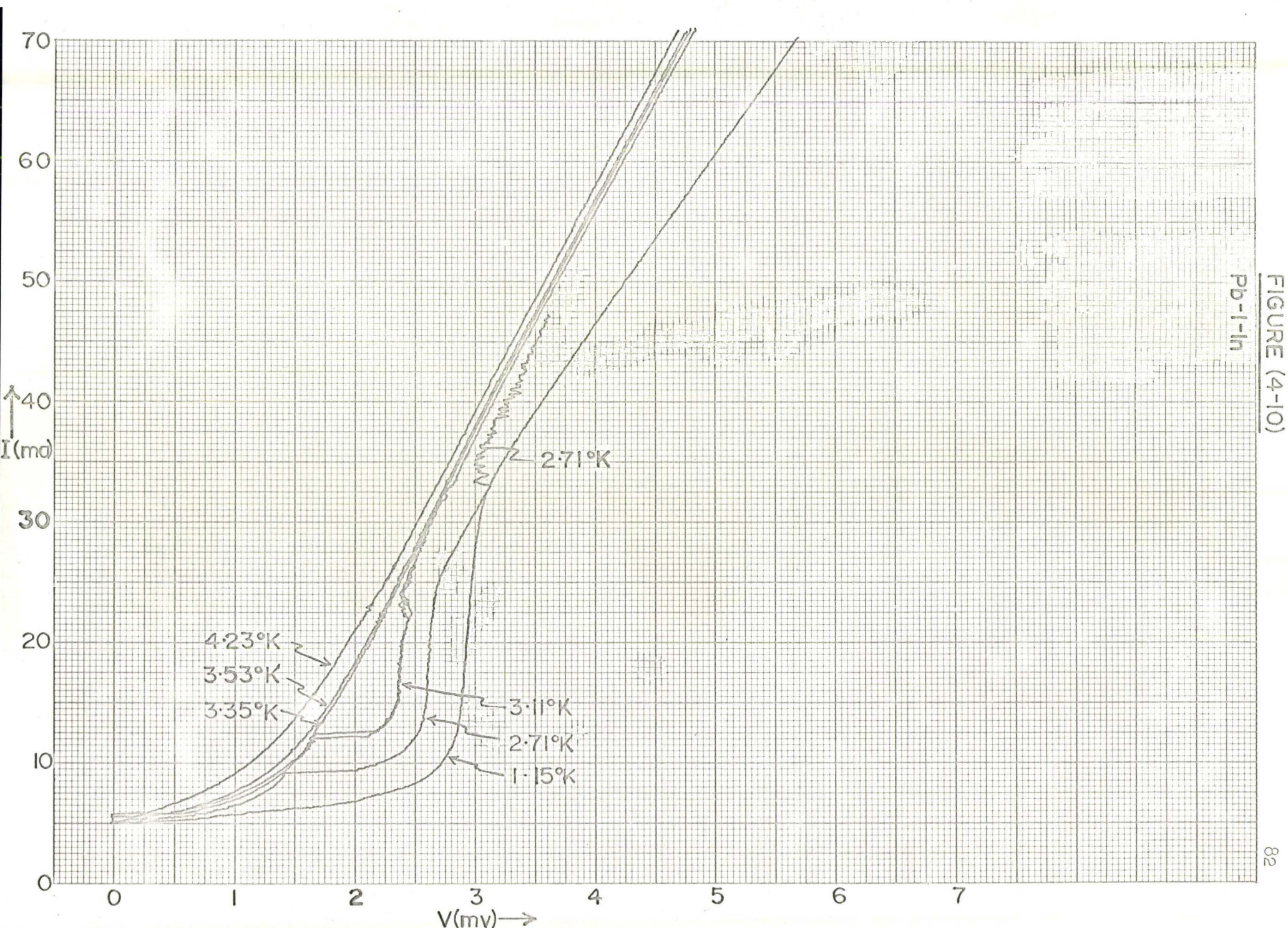

FIGURE (4-10)
Pb-I-In

tunnelling resistance. The general form of the curves was repeatable after thermal cycling. No instability occurred at 1.15°K or above the indium transition temperature. The current rise at $(\Delta_{In} + \Delta_{Pb})/e$ seems to be at much too high a potential (2.90 mV approximately) to agree with values obtained for these quantities from our other experiments. Further samples will have to be examined before definite conclusions are reached, but the irregular behaviour of the 3.11°K and 2.71°K curves, in particular, would suggest the readings are not to be trusted.

(b) Evaluation of Energy Gaps from I-V Characteristics

Referring back to Figure (2-4) and the discussion on density-of-states, we recall that N-S samples do not readily give exact information on the energy gap without tedious numerical calculation, but S-S samples should give a well-defined cusp in the characteristic at $(\Delta_1 - \Delta_2)/e$ and a sharp rise at $(\Delta_1 + \Delta_2)/e$ where Δ_1 and Δ_2 are the gaps in the two materials. Good definition depends on the existence of a unique value for the energy gap in each material.

If multiple gaps exist, there will be smearing of the rise at $(\Delta_1 + \Delta_2)/e$, because, instead of the contribution of the full density-of-states, N(E), at a given potential, there will be a gradual build-up from components of strength $N_\alpha(E)$, $N_\beta(E)$, $N_\gamma(E)$, ... corresponding to the density-of-states of quasi-particles exhibiting gap values Δ_α, Δ_β, Δ_γ, ... respectively. Of course,

$$\sum_{\ell} N_\ell(E) = N(E) \qquad \text{where } \ell = \alpha, \beta, \gamma, \text{ etc.}$$

The build-up of current will begin at the potential relevant to the smallest gap and will be complete when that relevant to the largest gap

is attained; the interval determines the smearing. Anisotropy is discussed in detail later (Section 4.3.(a)) in connection with thick films.

A likely source of further smearing occurs near the transition temperature when there are a great many excited quasi-particles. Then there is a high scattering probability, a short lifetime, and, as a result, smearing of the energy gap. The results on Al-I-Al (curve (d) is sharper than curves (b) and (c)), on Sn-I-Sn in Figure (4-7b), and on Pb-I-Pb in Figure (4-8a) would certainly suggest that greater smearing occurs at higher (reduced) temperatures. Admittedly lead is not near its transition temperature at 4.2°K, but then it is a strongly-coupled superconductor, and lifetime effects are expected to be important at lower reduced temperatures than for a weakly-coupled counterpart. The limit on the sharpness obtained at low temperature, we claim, is determined by the anisotropy in the film. It is to be expected that the electrons in very thin films will have short mean-free-paths and, as a result, do not propagate far enough between scatterings (off impurities or boundaries) to acquire anisotropic properties — there is a mixing of states. This affords a ready explanation of why the Al-I-Al characteristic of Figure (4-6d) is so sharp, even though the sample is not at a particularly low reduced temperature. Inspection of the curve reveals that the major part of the current rise occurs in an interval of the order of 0.02 mV. Corresponding intervals in the tin and lead samples, where no pains were taken to prepare very thin films, are 0.08 mV and 0.20 mV, respectively. There is some indication in Figure (4-8a) that lifetime smearing is still important at 4.2°K for lead.

Further support for the idea of anisotropy smearing is found when an impurity is deliberately introduced to pure lead. The impurity

effectively reduces the mean-free-path of the electrons and produces a "dirty" superconductor[63]. Figure (4-8c) shows the I-V characteristic for such a sample (Pb 90 Bi 10) at 2.2°K (i.e. Alloy-I-Alloy). The current rise occurs in an interval of about 0.05 mV, which is much less than in the pure lead case. (A secondary effect is the slight increase in the value of the energy gap.)

Granted the existence of smearing, it is clear that some reasonable criterion must be introduced to arrive at energy gap values. For the I-V characteristics we use the following.

In cases of dissimilar metals, with significantly different gaps, as for example lead and tin, the I-V curve has been swept out repeatedly at each temperature and the limiting potentials to which the curve can be traced, on either side of the negative resistance region, are used to determine $(\Delta_1 + \Delta_2)/e$ and $(\Delta_1 - \Delta_2)/e$.

Where the same metal has been used for both films it is commonly only possible to identify the sharp current rise at $2\Delta/e$. We have chosen to neglect the initial region of high curvature in such characteristics as this point is approached, and we have used the potential at which the steep slope first appears to evaluate 2Δ. This, then, should identify the smallest gap and, if smearing is not great, the result should be a fairly typical value for the material. Figure (4-11) illustrates these criteria.

The compatibility of results for $2\Delta_{Sn}$ obtained from the Pb-I-Sn and Sn-I-Sn characteristics of Figures (4-7b) and (4-9), using the above procedure, is very good indeed. These results are plotted in Figure (4-12). The solid line is a BCS plot of the energy gap as a function of temperature, as in Figure (2-1), fitted to the values:

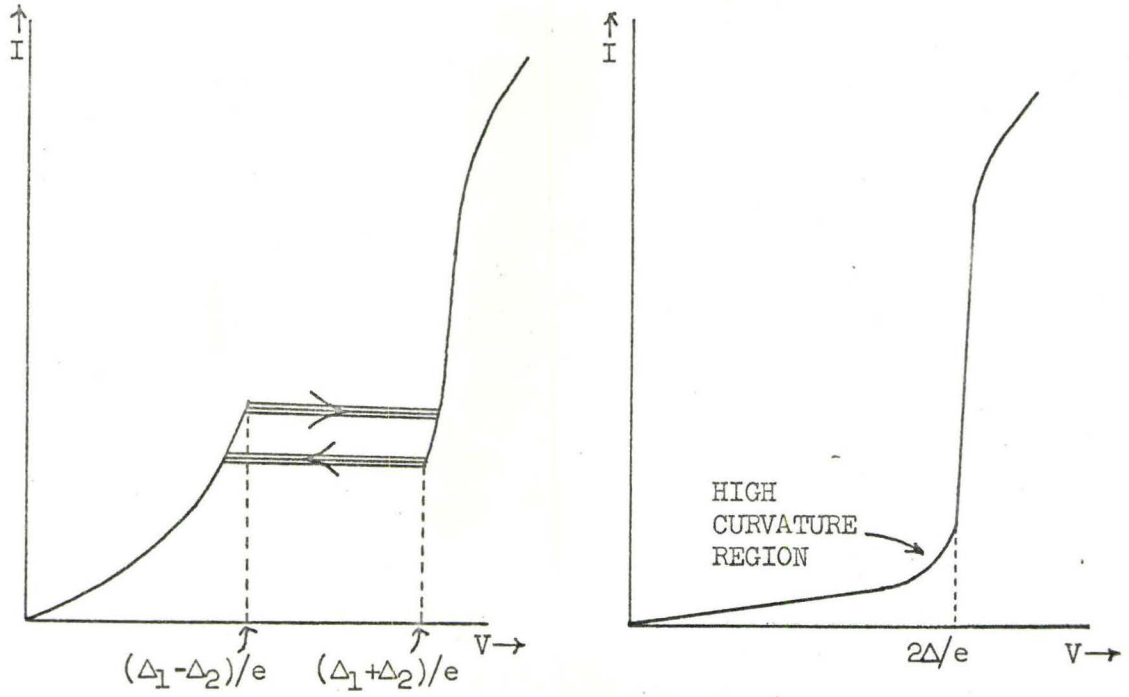

FIGURE (4-11)

T_c = 3.85°K, $2\Delta_{Sn}(0)$ = 1.22 meV. Somewhat smaller values for $2\Delta_{Sn}$ (1.08 to 1.11 meV) are given by the results on Al-I-Sn, but these characteristics are more smeared, and we therefore attach less significance to them.

Townsend and Sutton[64], using a slightly different criterion, found poorer agreement with BCS for the temperature dependence of the gap in tin in their experiments.

The best value for $2\Delta(0)$ in lead would seem, from the I-V characteristics of several Pb-I-Pb samples that we have examined, to be 2.70 meV. In Figure (4-8b) the current step region is readily distinguishable from the region of high curvature immediately below it, whereas (4-8a) is rather more smeared and the stipulated criterion cannot readily be applied to it. A value of 2.68 meV fits the Pb-I-Sn characteristics well. There seems to be a departure from BCS behaviour in the temperature dependence of the lead energy gap. Assuming that the film transition temperature is 7.2°K, then at 3.75°K a value of 2.54 meV

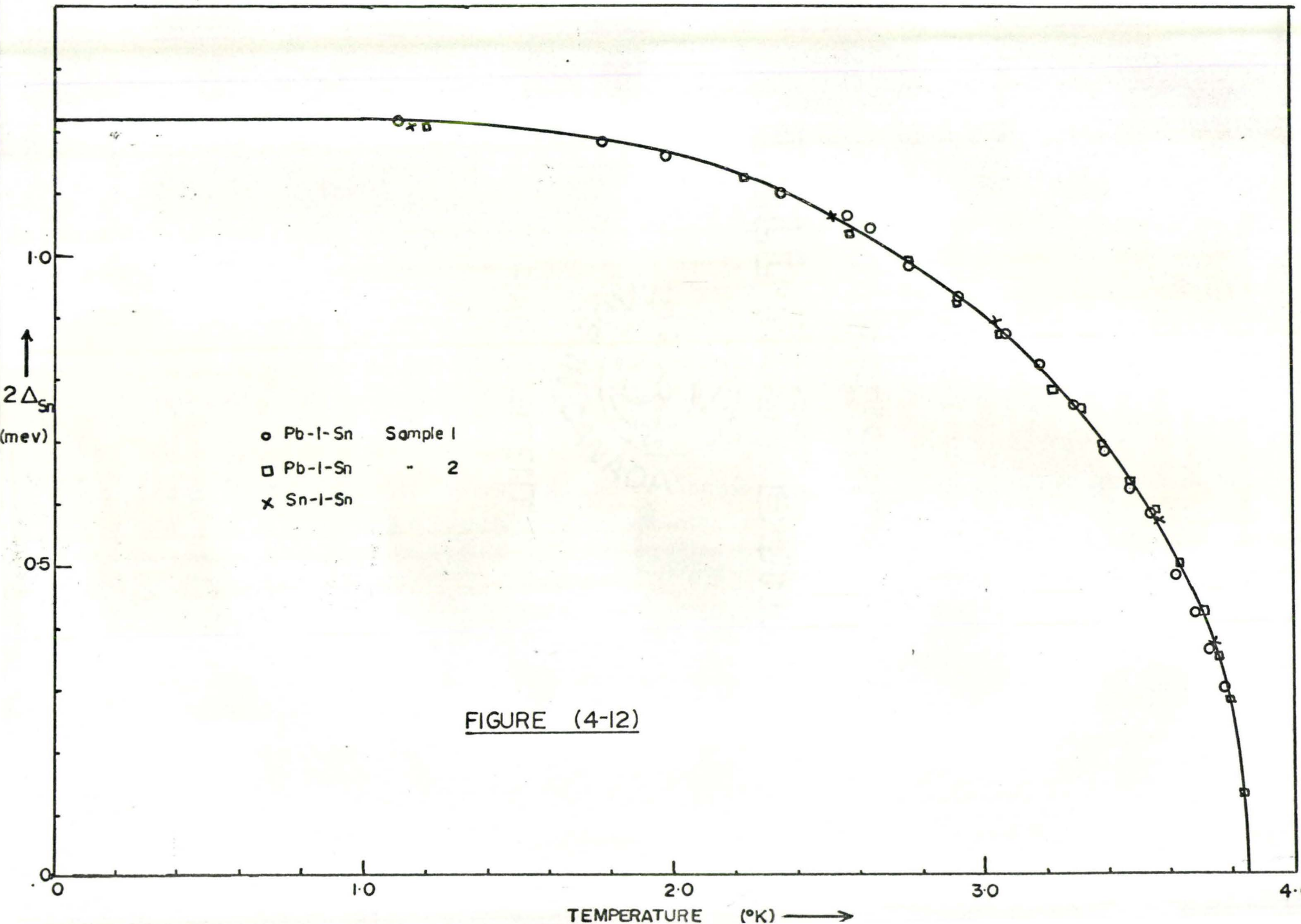
1·0
0·5
0
$2\Delta_{Sn}$
(mev)
o Pb-I-Sn Sample I
□ Pb-I-Sn - 2
× Sn-I-Sn
0
1·0
2·0
3·0
4·0
TEMPERATURE (°K) ⟶

FIGURE (4-12)

would be expected for 2Δ; the observed value in Pb-I-Sn samples is 2.61 ± 0.01meV (where the error refers to the range of values noted on the characteristic curves). This discrepancy lies outside the limits of experimental measurement error. Since the current rise at $(\Delta_1 + \Delta_2)/e$ in the Pb-I-Sn characteristics is quite sharp, even at $3.75^{\circ}K$, it seems unlikely that any argument invoking smearing to explain the discrepancy is justifiable. Perhaps the explanation is to be found in the theory of strongly-coupled superconductors. A recent calculation by Swihart, Scalapino and Wada[65] for lead found that, within the assumptions of their model, the reduced gap as a function of reduced temperature is within a couple of percent of the BCS weak-coupling expression. The deviation mentioned above is of this order.

Current flow in S-S samples below the striking potential, as is found at high reduced temperatures, is due to tunnelling of thermally excited real quasi-particles.

To determine the energy gap in indium from Al-I-In samples, it is best to study the first derivative of the characteristic, as is discussed below, because it is difficult to identify the point $(\Delta_1 - \Delta_2)/e$ on the original I-V curve. This problem would be circumvented if better Pb-I-In samples were available: measurements up to the critical temperature of indium would then be possible too. One of the I-V curves from an Al-I-In sample gives a result of $2\Delta(0) = 1.02$ meV (see Figure (4-3c)).

In the limited temperature range available below the transition temperature for aluminium, it is not possible to make useful temperature dependence measurements on the gap in aluminium. The largest value of 2Δ observed was 0.375meV at $1.11^{\circ}K$ (Figure (4-6d)).

(c) First Derivatives of Characteristics

Using the harmonic detection technique we have measured directly the first derivatives, dI/dV, of the tunnel characteristics of many samples.

Figure (4-13) shows a plot of dI/dV as a function of bias for an Al-I-In sample. The substrate was at room temperature during both depositions. The modulation signal applied to the sample was 50 μV peak-to-peak (p-p). A slight "kink" in the curve at 0.57 mV is possibly of instrumental origin.

An Al-I-Pb sample gave the derivative shown in Figure (4-14a). For the upper curve on this Figure the gain of the detector was increased in order to show up the detailed structure. The gap region is shown more clearly in Figure (4-14b). In (a) the modulation level was 250 μV p-p and in (b) it was 100 μV p-p and 200 μV p-p.

The plots shown in Figure (4-15) were obtained from Pb-I-Pb samples. From (4-15a), it may be seen that broadening of the peak at the gap edge becomes significant at a modulation level somewhere between 250 and 500 μV p-p. The temperature dependence of the derivative is shown in Figure (4-15b). A high-gain dI/dV trace beyond the gap region is shown along with the " parent" curve in Figure (4-15c); the modulation level was quite high when these curves were plotted, probably about 500 μV p-p or more. In general, the signals obtained from Pb-I-Pb samples are much stronger than those from Al-I-Pb samples.

(d) Discussion of First-Derivative Results

The first derivative of the characteristic is closely related to the density-of-states for excitations in the superconducting member of

FIGURE (4-13)

Al-I-In 1·16°K

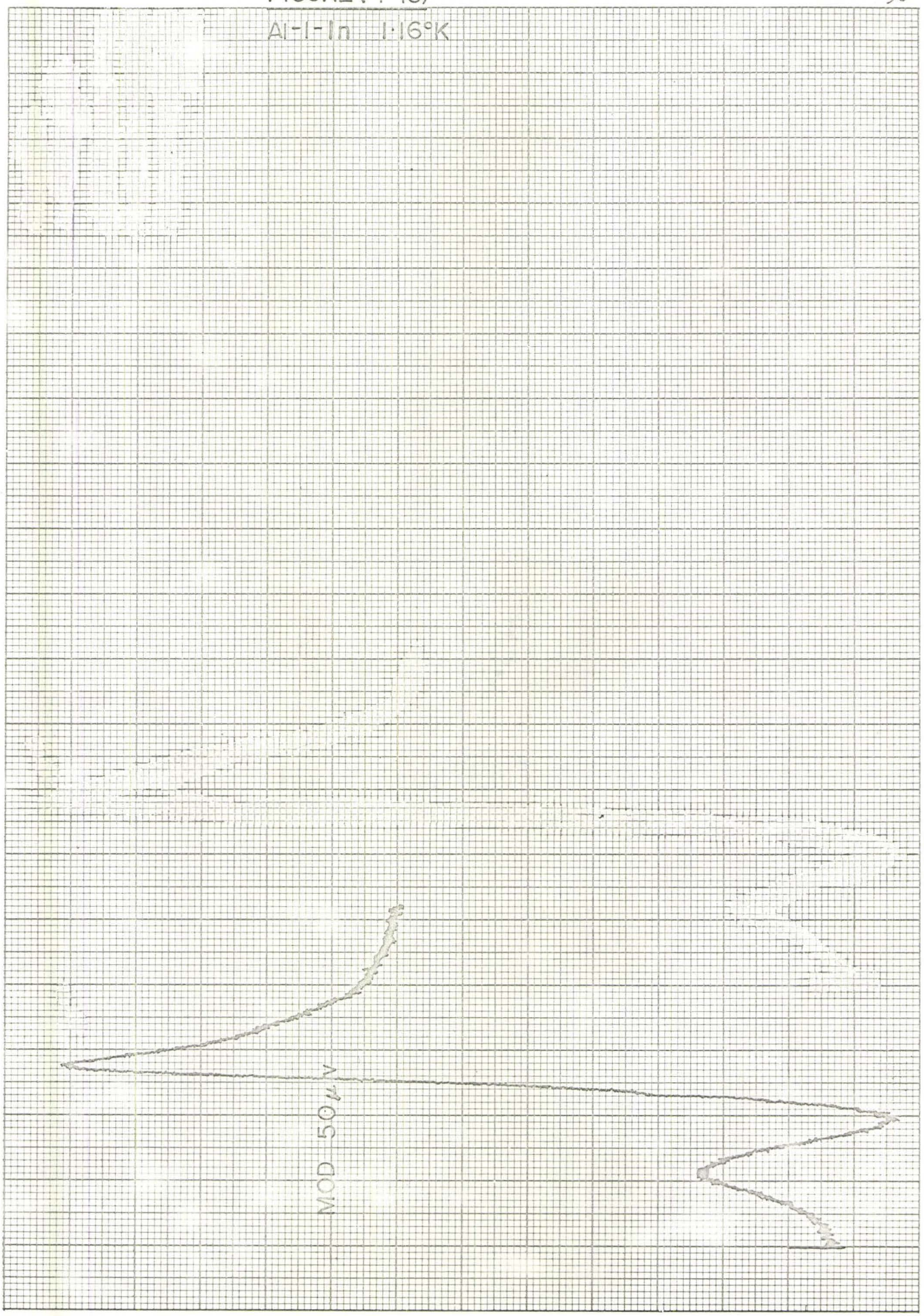

FIGURE(4-14a)


Al-I-Pb
1.19°K
MOD 250μV
1 SEC. FILTER
SWEEP 21mV/min
0
2
4
6
8
10
12
14
16
18
V(mv)→
←dI/dV

FIGURE (4-14b)

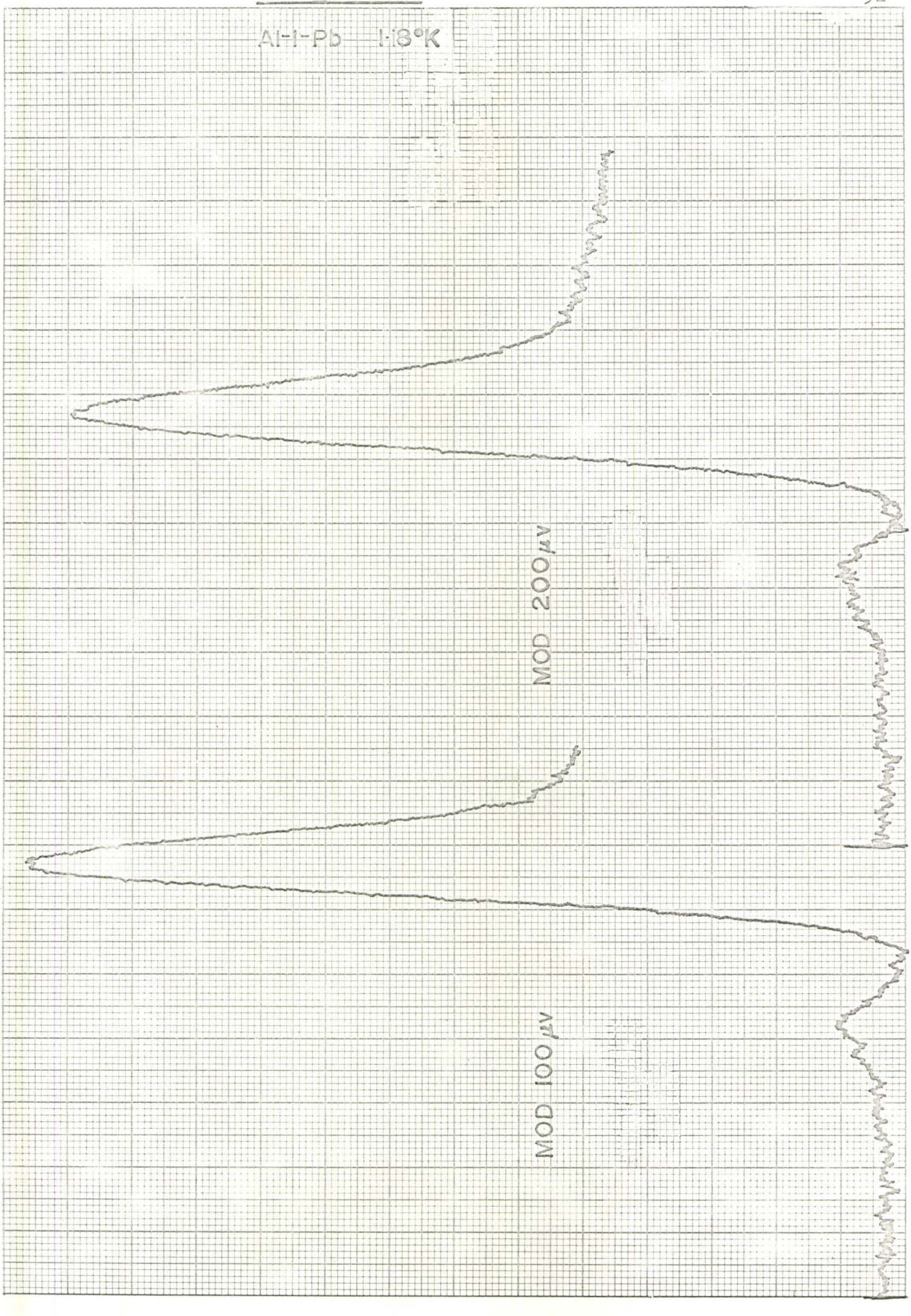

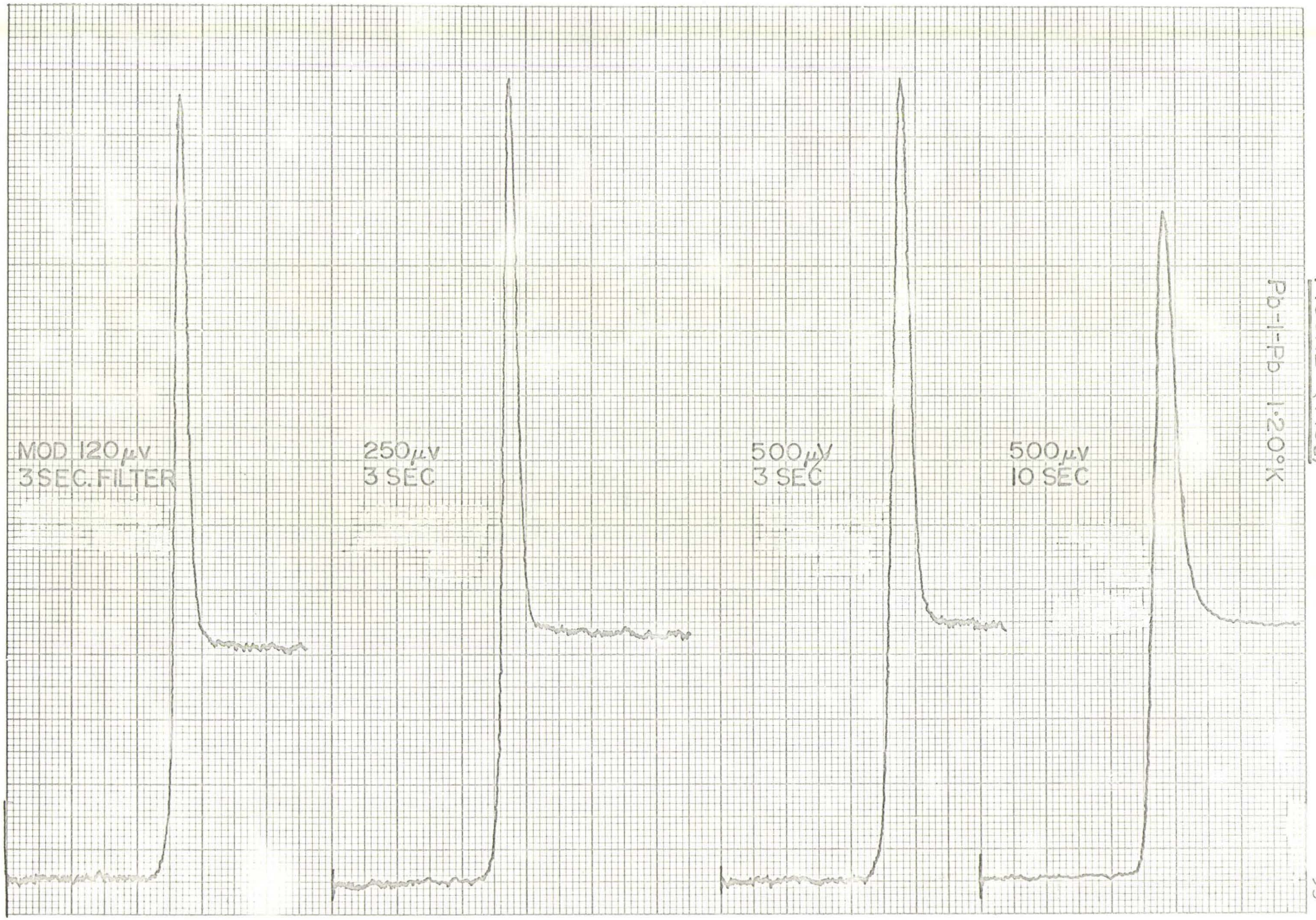
MOD 120μv
3 SEC. FILTER
250μv
3 SEC
500μv
3 SEC
500μv
10 SEC
Pb-I-Pb 1.20°K
dI/dV
V (2mv/inch)→

FIGURE (4-15a)

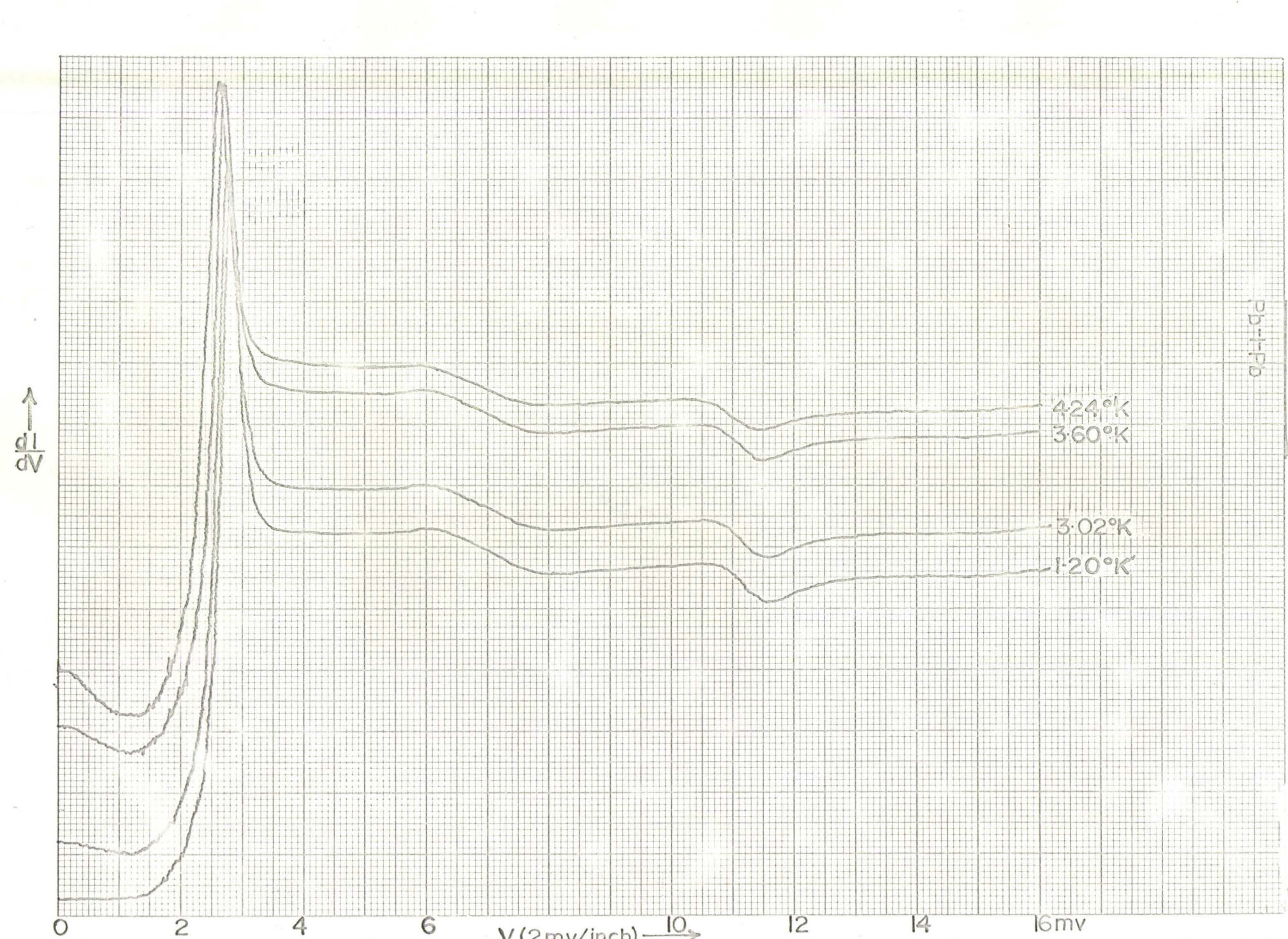

FIGURE (4-15b)

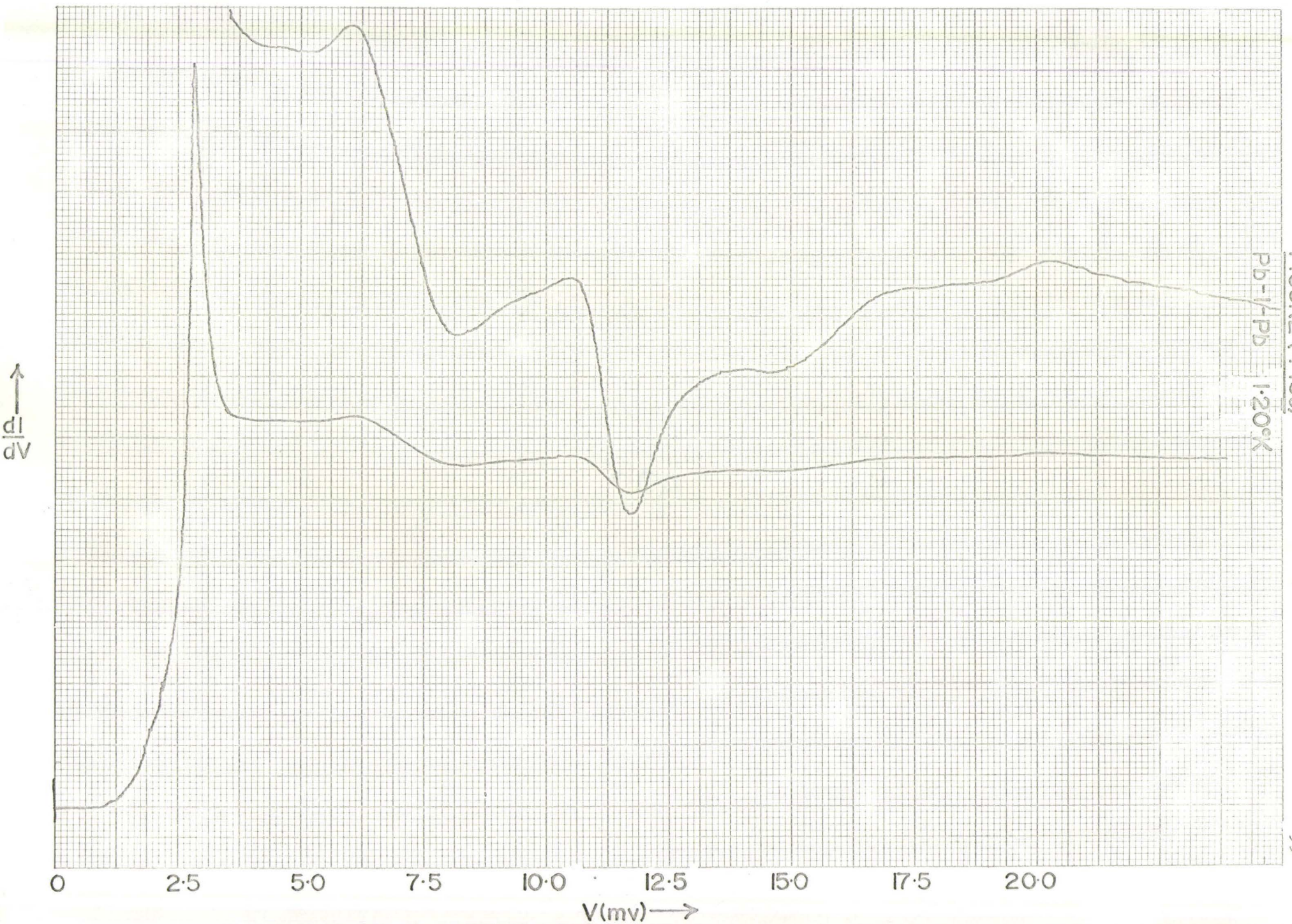

FIGURE (4-15c)
Pb-I-Pb 1·20°K

an N-S sample as discussed in Section 2.3.(b). With the circuit used, the differential conductance, dI/dV, is plotted directly as a function of bias. This is a considerable improvement over methods[28,51,58] which measure the inverse quantity, dV/dI, and then require numerical conversion.

According to equation (2-49), strict proportionality between the density-of-states for excitations and the differential conductance for N-S samples only holds true at T = 0°K. At non-zero temperatures, there is a mixing-in of current contributions from states within an energy range determined by the smearing of the Fermi surface in the normal metal.

If, on the other hand, two superconductors are being considered, there should be considerable sharpness, even at non-zero temperatures, provided anisotropy and lifetime effects do not constitute a further serious source of smearing. This is because the density-of-states peak at the edge of the energy gap, in one metal, is available for probing any detail in the density-of-states in the other metal. Undesired current contributions will still be mixed in at non-zero temperatures just as for N-S samples but the peaked nature of the density-of-states at the gap edge will tend to reduce the problems so introduced.

For a complete analysis a generalized form of equation (2-49) should be used with both metals superconducting and then the experimental curves could be fitted as has already been done for I-V characteristics by Shapiro et al.[27]. Without carrying out the detailed analysis much can still be determined from the experimental results.

For example, the sharp peak in Figure (4-15a) obtained from a Pb-I-Pb sample can unambiguously be identified with the density-of-states

peaking in lead. It is justifiable to take the position of the conductance maximum as defining the energy-gap width. Clearly this definition is not identical with the criterion applied to the I-V characteristics in Section 4.2.(b). The earlier criterion measures the smallest energy gap exhibited by any significant current component; the latter isolates the gap corresponding to the component which makes the strongest contribution to the total current. In the limit of perfect sharpness the results would coincide. We find ourselves forced to use the second criterion in the identification of multiple gaps, to be discussed below.

It is unlikely that a detailed fitting of the Pb-I-Pb conductance curves to numerical solutions would shift the gap value much from that corresponding to the peak in the curve (because of the curve's uncomplicated form). Results at the lowest modulation levels indicate a value of $2\Delta_{Pb}$ = 2.70 to 2.75 meV. Figure (4-15b) illustrates the fact that, in samples where both films are of the same metal, a low reduced temperature helps in the definition of 2Δ.

When a sample consists of two different superconductors, two peaks in the dI/dV curve may be expected, one at $(\Delta_1 - \Delta_2)/e$ due to thermally-excited real quasi-particles, and one at $(\Delta_1 + \Delta_2)/e$ due to virtually excited quasi-particles. The graphs for Al-I-In and Al-I-Pb (Figures (4-13), (4-14a) and (4-14b)) bear this out. Energy gap values of $2\Delta_{In}$ = 0.97 meV and $2\Delta_{Pb}$ = 2.79 meV, 2.73 meV may be identified from these conductance curves. For lead, these are near the values obtained from I-V curves. Only a detailed numerical analysis, along the lines already suggested, can give wholly reliable results. Thinner aluminium films would probably give much improved definition.

The modulation level has, in general, been kept at the highest value tolerable in order to get good signal-to-noise performance. The tolerable level is determined by when loss of detail begins to occur in the conductance curves. A few traces at different modulation levels suffice to establish this.

Our primary interest has been in applying this technique to identify multiple gaps and we have not carried out any numerical computations related to determining energy gaps from the results obtained on thin films.

The structure in the conductance curves for lead beyond the gap has been accounted for by Schrieffer et al.[18]. They approximated the phonon spectrum of lead by two Lorentzian functions, centred at 4.4×10^{-3} ev (ω_1^{t}) and 8.5×10^{-3} ev (ω_1^{ℓ}), corresponding to the transverse and longitudinal branches. Then they determined the complex energy gap parameter $\bar{\Delta}$ ($= \Delta_1 + i\Delta_2$) as a function of energy. The results showed that Re $\bar{\Delta}$ ($= \Delta_1$) goes through a maximum as quasi-particle energy, E, approaches $\omega_1^{t} + \Delta_o$ or $\omega_1^{\ell} + \Delta_o$ where Δ_o is the value of energy gap parameter at the gap edge. The value of Im $\bar{\Delta}$ ($= \Delta_2$) obtained shows two rapid rises, one at $\omega_1^{t} + \Delta_o$ and one at $\omega_1^{\ell} + \Delta_o$, because of the onset of emission of transverse and longitudinal phonons respectively. The calculation is analogous to that of the complex refractive index of a dielectric material[66] with two resonant frequencies.

Substitution of the calculated values in equation (2-44c),

$$N_T(E) = N_N(\epsilon) \quad \mathrm{Re}\left\{\frac{E}{(E^2 - \bar{\Delta}(E)^2)^{1/2}}\right\} \quad ,$$

gives good agreement with observed conductances. In particular, the two

sharp drops in the conductance (see Figures (4-14a) and (4-15c)) are readily understood because (2-44c) in expanded form is

$$N_T(E) = N_N(\epsilon) \left[1 + \frac{\Delta_1^2 - \Delta_2^2}{2E^2} \right] ,$$

and hence, if Δ_2 rises sharply, at the same time as Δ_1 passes beyond its maximum, a drop in $N_T(E)$ results.

(e) Second Derivatives of Characteristics

Figures (4-16a) to (4-16d) show the second derivative of a Pb-I-Pb sample at modulation amplitudes of 60 μV, 120 μV, 250 μV, and 500 μV (all peak-to-peak) respectively. Both lead films were quite thin, of the order of 1000 $\mathring{A}$. The sweep speed for tracing the curves must be kept low to accommodate the necessary filters in the system; otherwise there is a shift in position of the signals from their proper positions. In this experiment the sweep speed was 1 mV/min and all curves were traced out twice to check reproducibility. No variations were found except at the lowest modulation for which three curves are included. The temperature throughout the experiment was $1.200 \pm 0.005^{\circ}K$.

Corresponding results on Al-I-Pb at $1.20^{\circ}K$ are shown in Figures (4-17a) and (4-17b) at modulation levels of 250 μV and 500 μV peak-to-peak respectively. Again the films were thin, of the order of 1000 $\mathring{A}$.

(f) Discussion of Second-Derivative Results

It is possible to resolve more structure with the second-derivative technique than in first-derivative plots. This is useful in carrying further the investigation of the phonon structure reflected in the tunnelling density-of-states. Such experiments were first done by

FIGURE (4-16a)

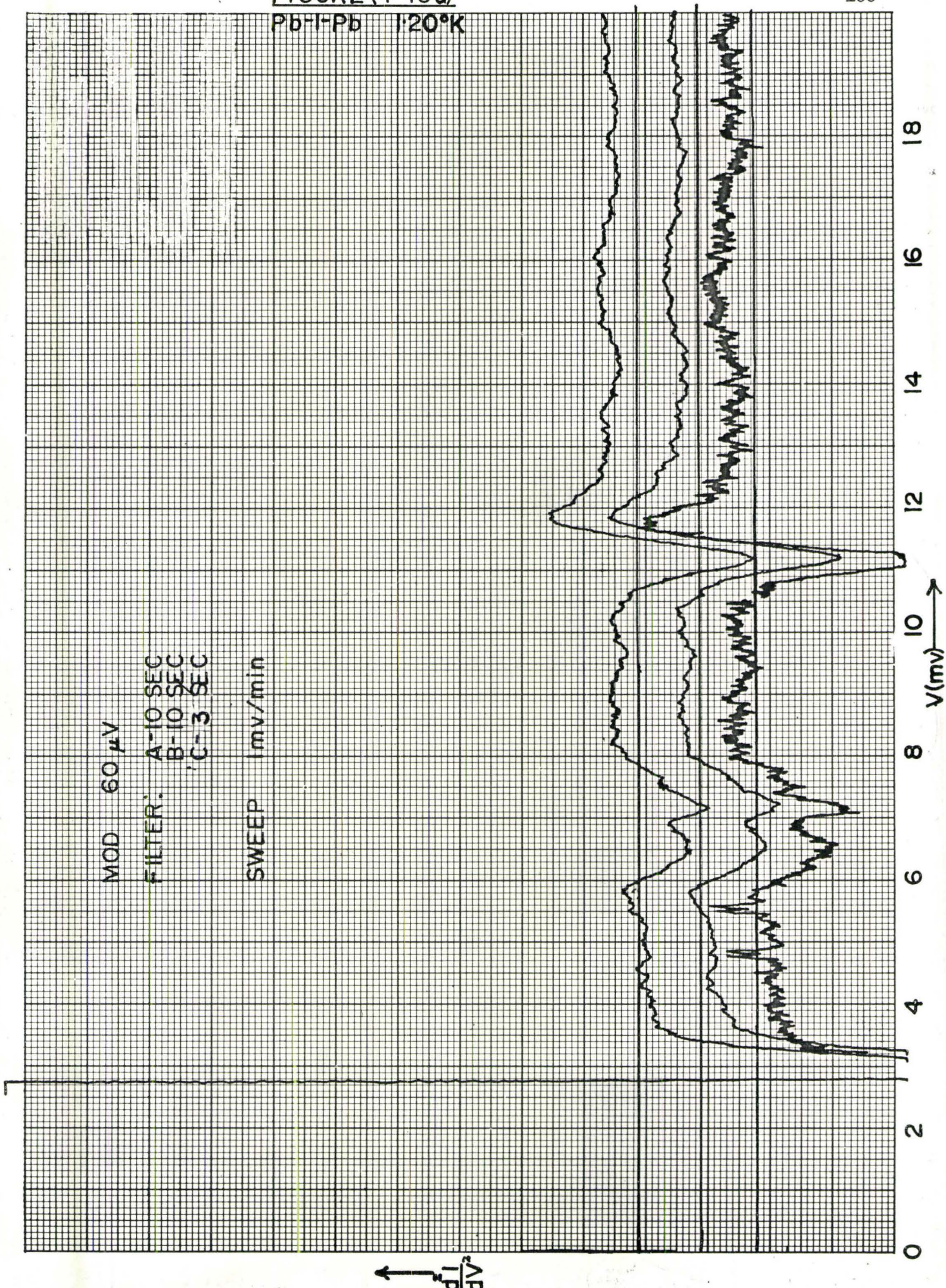
Pb-I-Pb 1.20°K
MOD 60 μV
FILTER: A-10 SEC
B-10 SEC
C-3 SEC
SWEEP 1mv/min
0
2
4
6
8
10
12
14
16
18
V(mv)
$\frac{dI}{dV}$

FIGURE (4-16b)

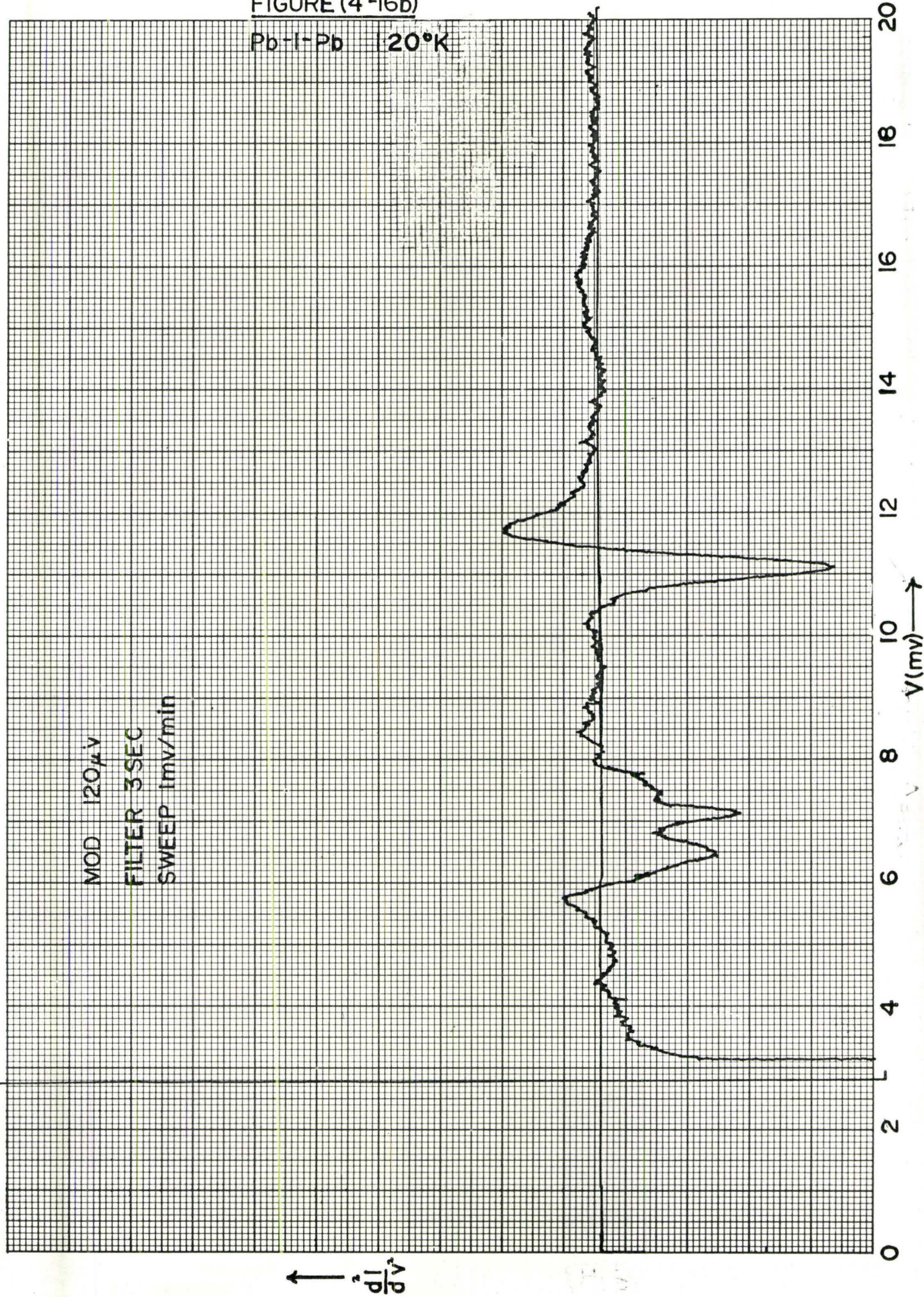
Pb-I-Pb 1.20°K
MOD 120μV
FILTER 3SEC
SWEEP 1mv/min
0
2
4
6
8
10
12
14
16
18
20
V(mv)
dI/dV

FIGURE(4-16c)

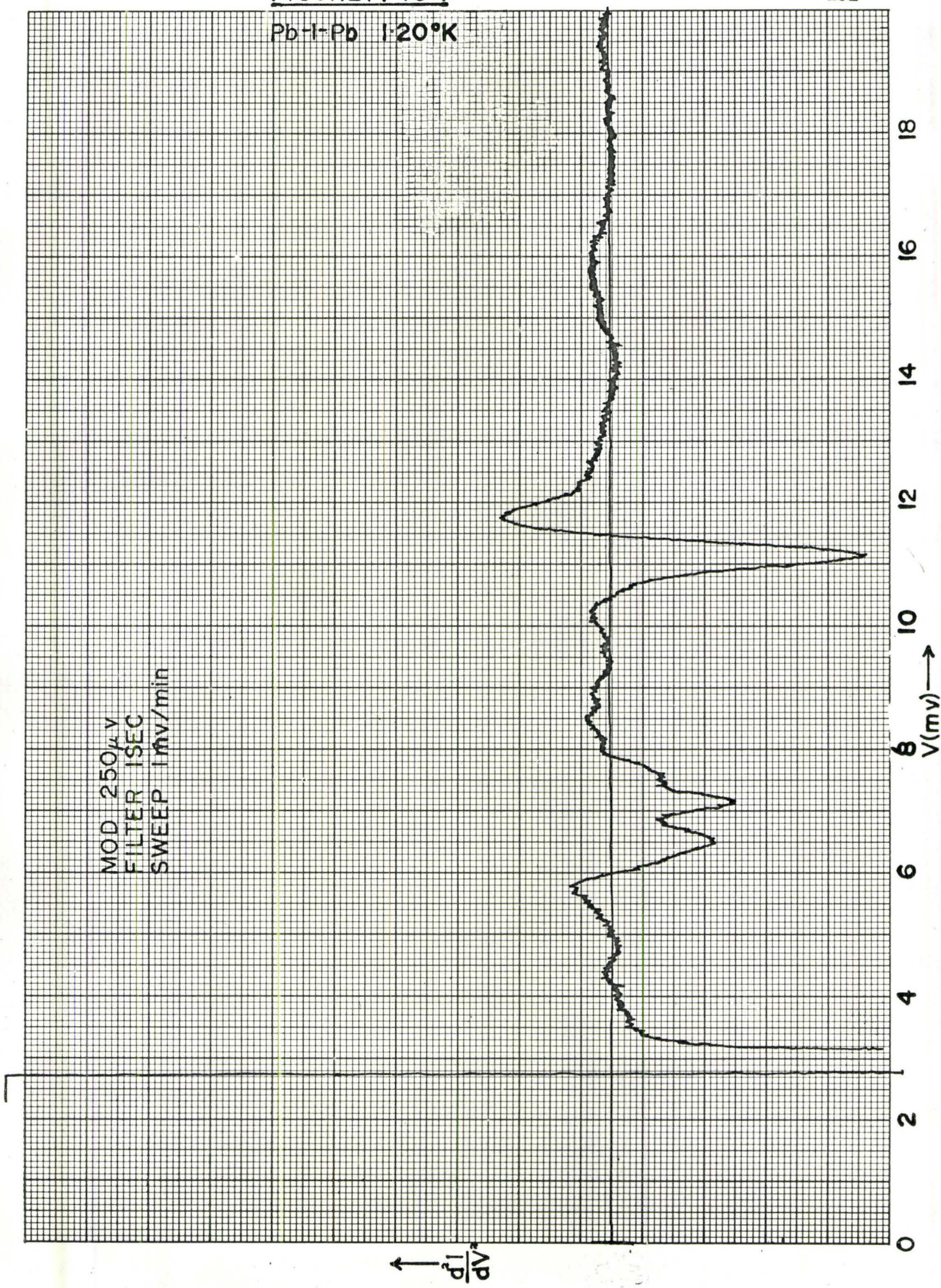
Pb-I-Pb 1.20°K
MOD 250μV
FILTER 1SEC
SWEEP 1mV/min
0
2
4
6
8
10
12
14
16
18
V(mv)
$\leftarrow \frac{d^2I}{dV^2}$

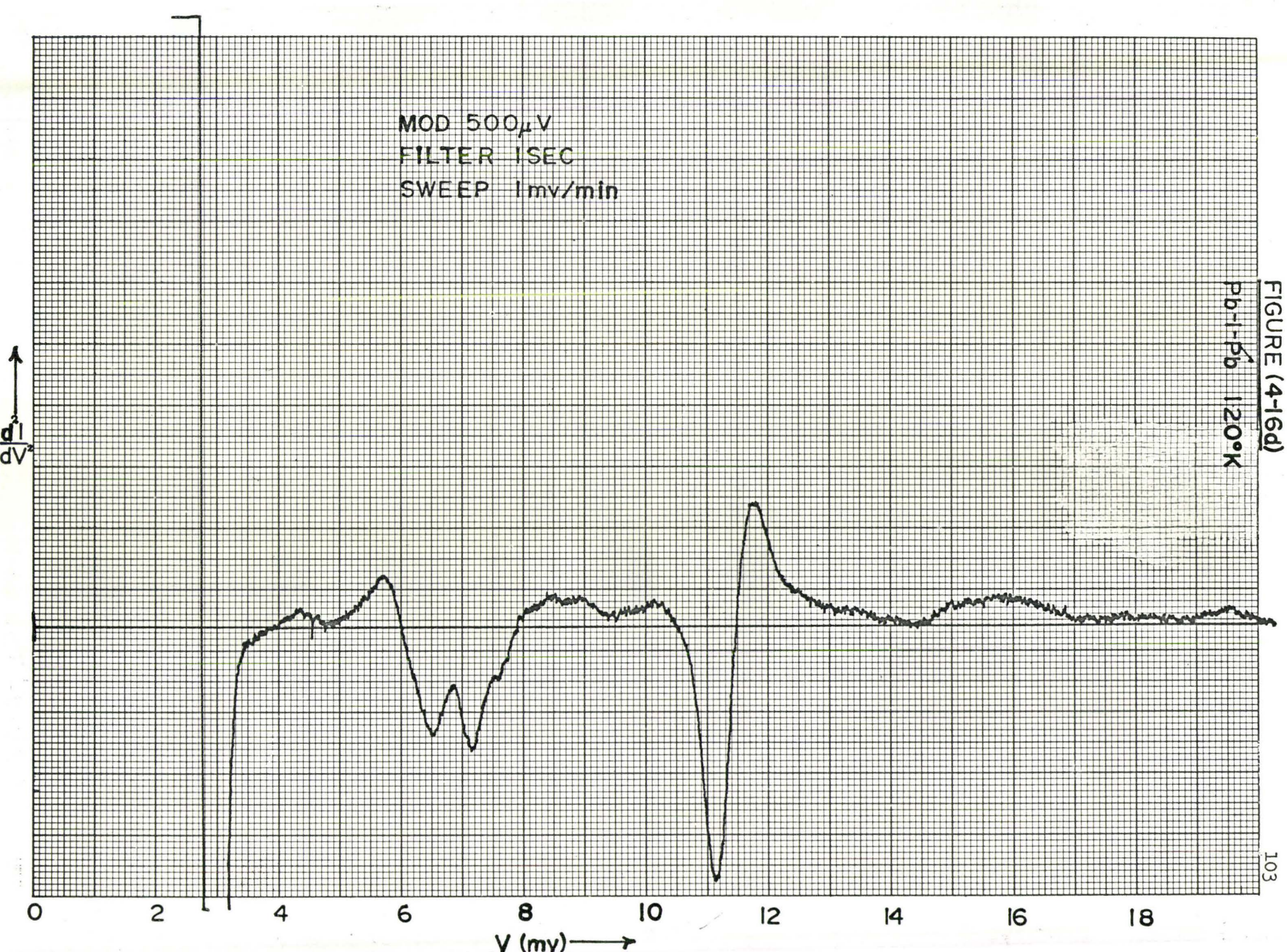
MOD 500μV
FILTER 1SEC
SWEEP 1mv/min
Pb-I-Pb 1.20°K
$\frac{d^2I}{dV^2}$
0
2
4
6
8
10
12
14
16
18
V (mv) ⟶

FIGURE (4-16d)

FIGURE (4-17a)

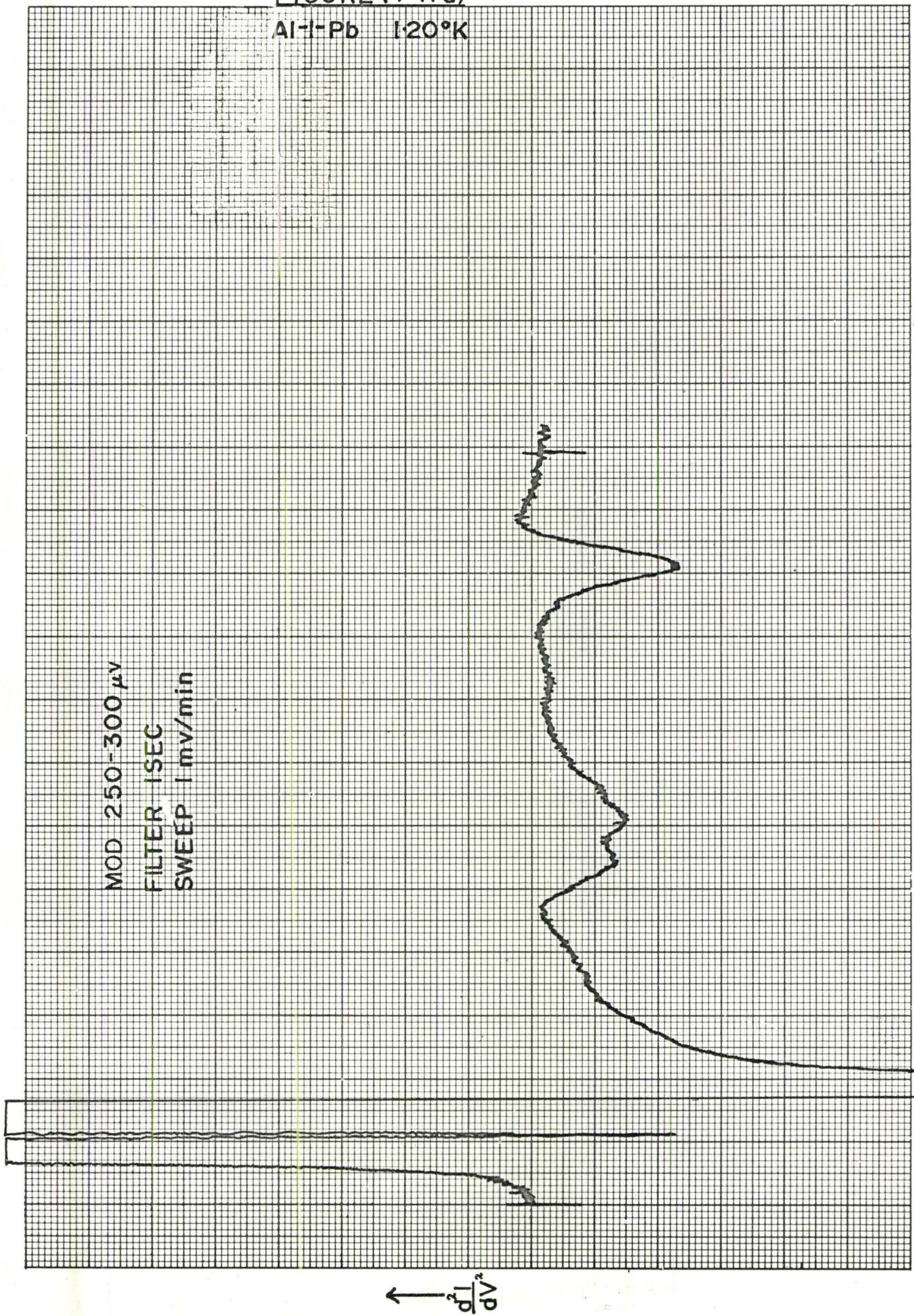
Al-I-Pb 1·20°K
MOD 250-300 μV
FILTER 1SEC
SWEEP 1 mV/min
0
2
4
8
10
12
14
V (mv)
$\frac{d^2I}{dV^2}$

FIGURE(4-17b)

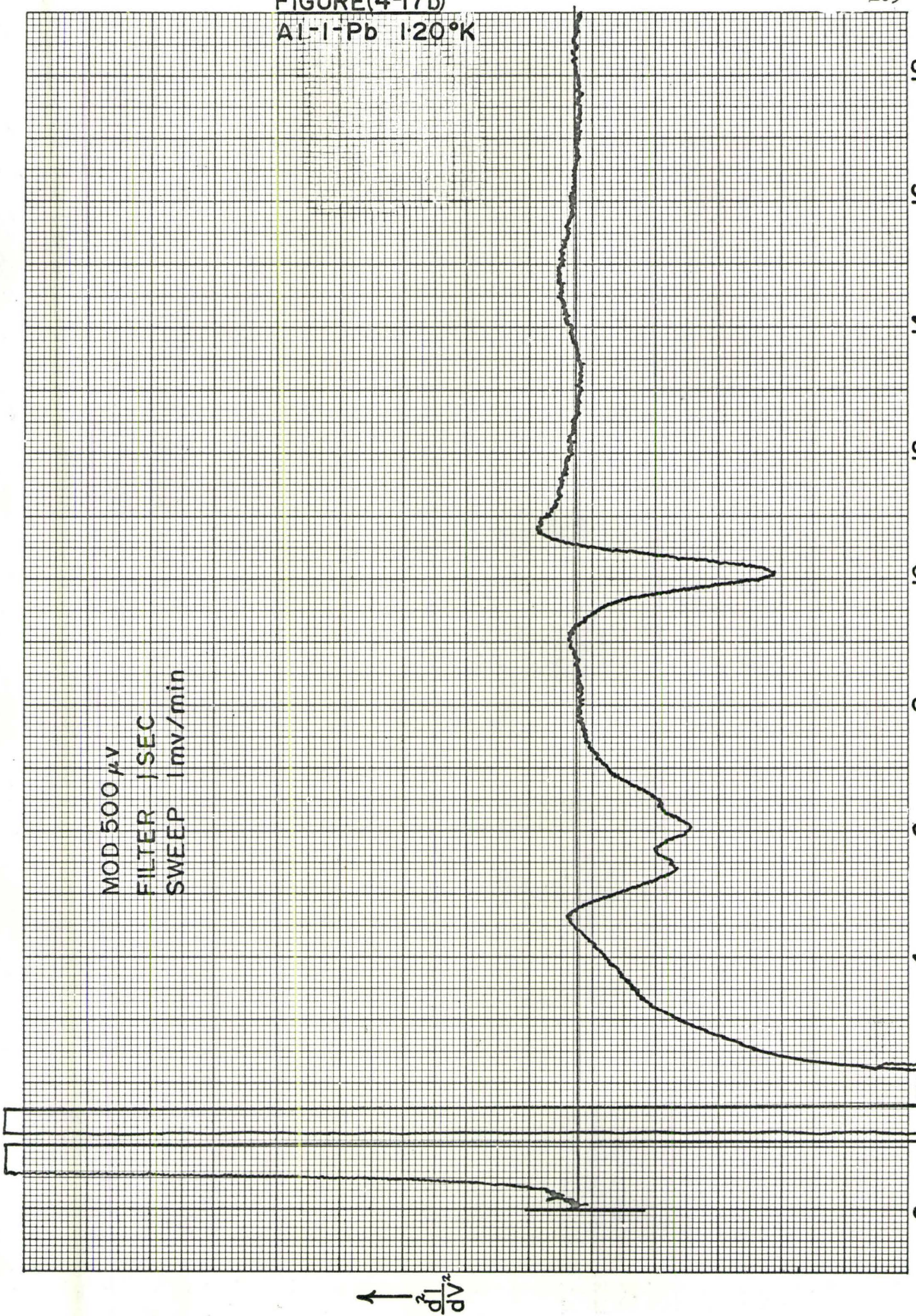
Al-I-Pb 1·20°K
MOD 500 μV
FILTER 1SEC
SWEEP 1mv/min
0
2
4
6
8
10
12
14
16
18
V(mv)
$\frac{d^2I}{dV^2}$

Rowell et al.[67,68] with a circuit that is presumably similar to that shown in Figure (3-4).

Scalapino and Anderson[69] have shown how to associate different types of Van Hove singularities[70,71] in the phonon frequency distribution, $g(\omega)$, with corresponding singularities in the second derivative of the tunnelling characteristic, d^2I/dV^2. A comparison between the main features of the phonon spectrum inferred in this way for lead, and the corresponding results from neutron scattering data[72], shows close agreement. Two factors, however, complicate the situation. Firstly, the information that may be obtained from the tunnelling experiments[73] involves not simply the phonon frequency distribution, $g(\omega)$, but its product with an unknown coupling parameter $\alpha^2(\omega)$. Some of the observed singular behaviour in $\alpha^2(\omega)g(\omega)$ may be due to anomalies in $\alpha^2(\omega)$. McMillan and Rowell[73] have rather successfully separated the effects arising from $g(\omega)$ and $\alpha^2(\omega)$ anomalies in the case of lead. A second complication is that neutron scattering data is normally taken for only a few crystallographic directions of high symmetry. It will not provide information on singularities in $g(\omega)$ at lower symmetry positions which may be revealed in the tunnelling curves. In this connection tunnelling is a useful tool for identification of such singularities.

We have developed the second-derivative technique for use in the investigation of thick films and alloys. Further results are recorded below.

(g) The Josephson Effect

Inspection of Figures (4-7a), (4-9) and (4-10) reveals a DC current flow at zero bias. This corresponds to the tunnelling of paired

electrons and may be a strong effect in samples with thin barriers. The maximum current that may be made to flow before the effect is quenched is very sensitive to applied (and self-) magnetic fields. We have been able to reduce it to zero in all samples with external fields of the order of 10 gauss. None of our junctions gave currents sufficiently stable against fluctuations (thermal and electromagnetic) to allow a demonstration of the periodic magnetic field dependence, as found originally by Rowell[74], or the temperature dependence predicted by Ambegaokar and Baratoff[75].

The extreme sensitivity to magnetic field arises because of coherence considerations. The superconducting state requires coherence of the pair wave functions; states in anti-coherence represent excitations as mentioned in Section 2.2.(c). Tunnelling of a pair from one superconductor to another will therefore proceed most easily if the two superconductors are coherent with respect to each other, i.e. if the pair wave functions in the two superconductors are locked together in phase. Such an ideal condition only exists, however, for a single block of superconducting material; once a barrier is introduced, decoupling of the two parts begins, and the probability of net pair flow is then modified by fluctuations in the relative phase between the two samples. A thick tunnel barrier causes such severe decoupling that fluctuations dominate and no net current flow is observed. A magnetic field applied in the barrier region can alter the current drastically by introducing relative-phase shifts in all parts of the barrier cross-section. This produces a situation analagous to Fraunhofer diffraction of light. To observe light intensity maxima and minima, the relative phase of different contributing light rays is adjusted by making observations at appropriate spatial

locations; to see Josephson DC current maxima and minima, the magnetic vector potential is suitably adjusted, by application of the appropriate magnetic field, in order to develop the necessary phase relationships for different current elements.

In our junctions, one handicapping feature has been self-field limiting as discussed by Ferrell and Prange[76]. Narrower films would be better suited to Josephson effect studies.

Figure (4-18) shows, in expanded form, some detail from the low bias region of a Sn-I-Pb sample characteristic at 1.2°K. In addition to the current at zero bias, there are several, rather well-defined, steps in the characteristic at regular voltage intervals. This is evidence of the Josephson AC effect. What defines the steps? A priori, a continuum of values would be expected. The observed intervals are approximately 17.5 μV in this sample, corresponding to an emitted photon frequency of 8.5 Gc/s. An attempt was made to detect background radiation of this frequency in the laboratory but with negative results. Such radiation, it was felt, might be responsible for producing the observed steps.

Next, microwave power, at 9.5 Gc/s was shone on the sample from a horn outside the cryostat in an attempt to produce different voltage steps. None was observed. Such an experiment has since been successfully carried out by Shapiro[77] under conditions of better sample-radiation coupling.

At this stage of the experiments it was clear that external radiation was not responsible for the observations. It was difficult, on the other hand, to understand how the radiation frequency could be determined by the sample. The wavelength would be 3.55 cm and all the dimensions of the junction were much less than this.

FIGURE (4-18)

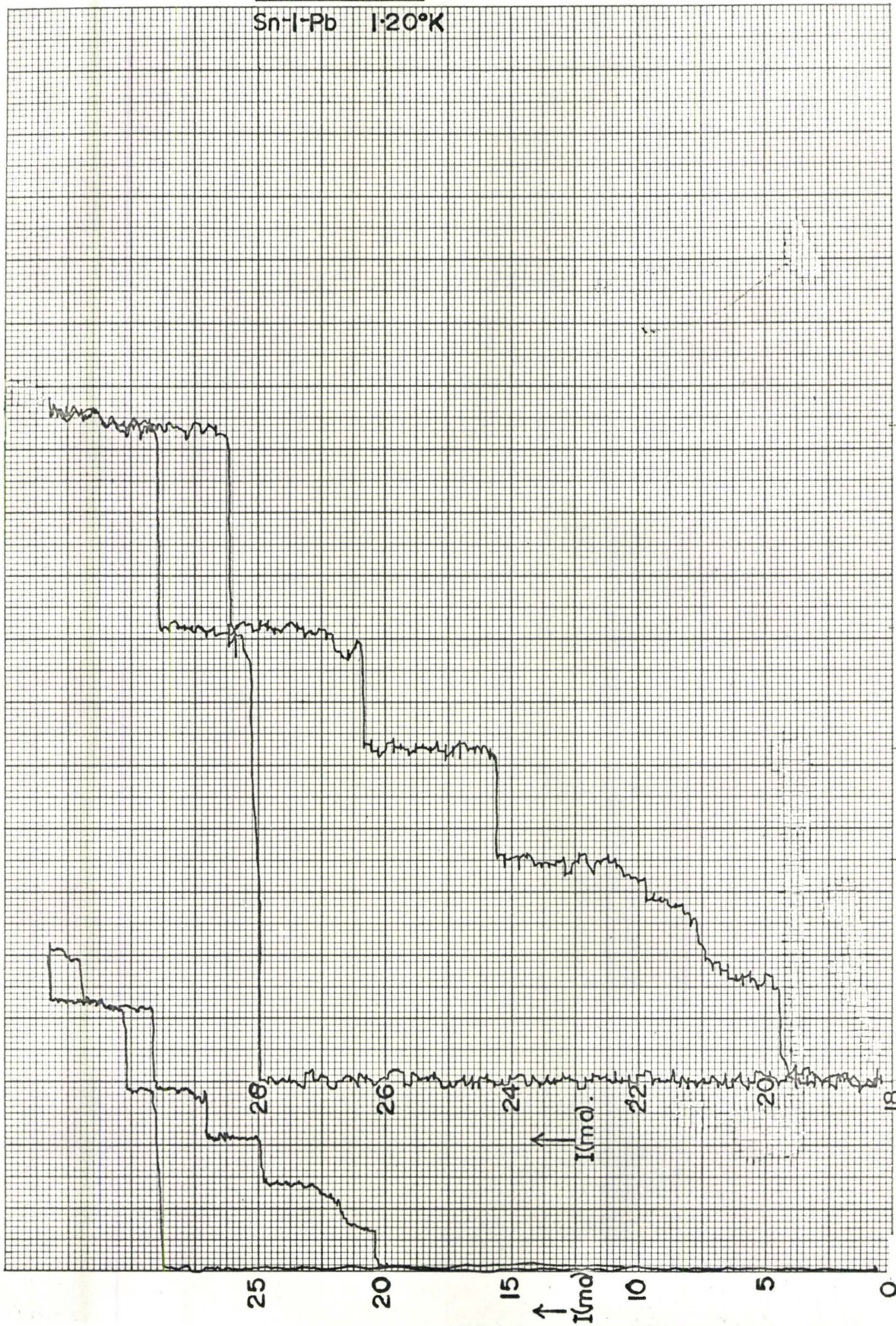
Sn-I-Pb 1·20°K
V(20μv/inch)
V(50μv/inch)
I(ma)
I(ma)
28
26
24
22
20
18
25
20
15
10
5
0

Fiske[78,35] has recently pointed out that a correction must be applied for inductive loading in the junction which effectively reduces the wavelength of the radiation to about sample dimensions. Then the explanation of the observed steps is clear. The region between the films is acting as a resonant cavity and its natural modes, which are determined by its geometry, dictate the voltage step intervals. Our observations check out numerically against this interpretation.

4.3. TUNNELLING BETWEEN THICK SUPERCONDUCTING FILMS

(a) Thick Films, Anisotropy, and Dirty Superconductors

The reason for carrying out experiments on thick films has been to explore whether or not anisotropy effects can be revealed with the tunnelling technique. First, let us consider why thick films might show such effects.

Lead, tin, and indium anneal rapidly at room temperature; they therefore recrystallize and grain growth is to be expected. Aluminium, if very pure, behaves similarly, but significant grain growth only occurs at somewhat higher temperatures. It is likely that thick films of lead, tin, or indium will develop fairly large crystallites if left at room temperature for some minutes after preparation. Fairly large in this context may be of the order of one micron (10^4 Å), if the film thickness is as much as this. Growth may even continue until platelets, with surface dimensions greater than their film-thickness-limited depth, are formed.

We assume that, in samples involving annealed thick films, there will be tunnel current contributions from a relatively small number of large crystallites, as compared with the situation for thin films, in

which the crystallites are small. (Only in rare circumstances, which do not prevail here, will crystallites extend laterally over large areas while the film is still thin.) If the films are thicker than the coherence distance of the metal being examined, then anisotropy prevails in the individual crystallites (see below), and this may be reflected in the tunnelling results.

Anderson[63] has discussed the difference between pure single crystal superconductors in which the electrons enjoy long-lived occupation of Bloch states, and "dirty" superconductors in which the mean-free-path of the electrons is seriously reduced by scattering. Such scattering may arise from small amounts of nonmagnetic impurity, say a few atomic percent, or from intercrystallite boundaries in polycrystalline samples. Thin films represent a situation in which the "dirty" condition prevails. Thick films, on the other hand, if annealed, may develop sufficiently large crystallites that the pure superconductor domain is approached within each crystallite.

Anderson points out that in the presence of strong scattering it is necessary to redetermine the electron wave functions and couple them in time-reversed pairs. This reduces to the BCS opposite-momentum pairing in the limit of weak scattering. The new wave functions are constituted by taking normalized linear combinations of Bloch states from all over the Fermi surface of the superconductor. There is then an averaging-out of properties and the material is isotropic with a unique energy gap.

In pure single crystals, where the BCS opposite-momentum pairing is appropriate, there are expected to be multiple energy gaps because the gap is a sensitive function of electron momentum vector, and the Fermi surface is not exactly spherical in any known superconductor. In

addition, anisotropy of the phonon spectral distribution and the electron-phonon coupling contribute to the non-uniqueness of the gap in pure single crystals. Unfortunately it does not seem possible to acquire much information on the phonons, which are mediating the electron-electron interaction, since only the final state of the tunnelling electron can be determined with any certainty. Even this determination relies on the assumption that only electrons with total momentum vector nearly perpendicular to the barrier have high tunnelling probability, and it also requires a knowledge of the crystal orientation. (It is therefore not readily applicable to thick films.)

It is important to note in this connection that if the energy gap is non-zero at some region of the Fermi surface then, according to Cooper[79], the gap must be non-zero at all parts of the surface, except perhaps at isolated points or lines. Hence all gaps will begin to open up at the same critical temperature and their separation will increase as the temperature is reduced. This condition is a consequence of mixing of states in the presence of scattering[80]. In an ideally perfect crystal each gap would open up at a different critical temperature. Ideally perfect crystals do not exist; they are thermodynamically unstable. A plot of densities-of-states for an anisotropic superconductor, with very slight scattering, is shown in Figure (4-19) (after Hohenberg[80]).

The threshold is seen to be the same for all gaps but the behaviour of most of the density-of-states curves is rather different from the simple pattern in a one-gap superconductor. With more scattering present the separate density-of-states peaks would "condense" into a single peak. This trend to "dirty" superconductivity should occur[81] when

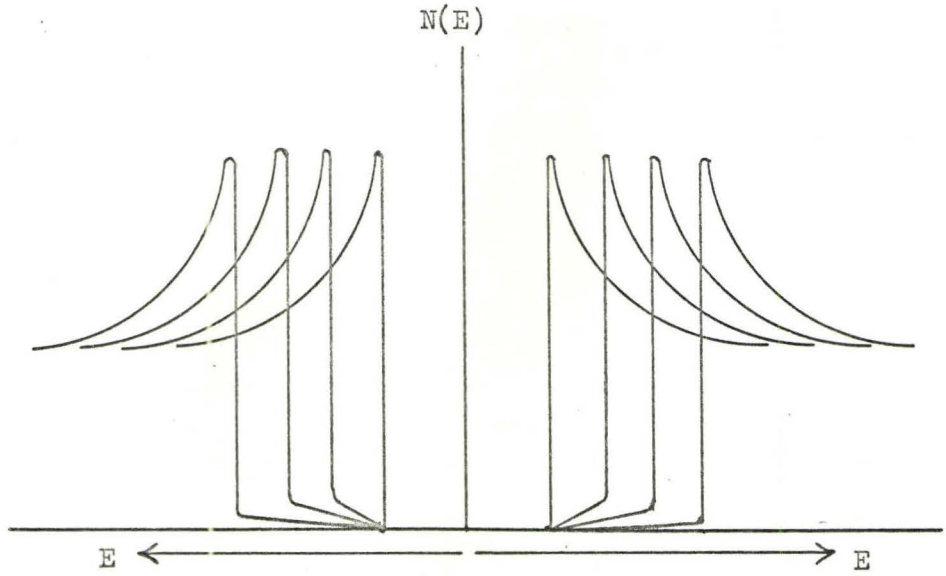

FIGURE (4-19)

the electron mean-free-path becomes comparable with the coherence distance, ξ_o, of the pure superconductor. The values for ξ_o for aluminium, indium, tin, and lead are 16000, 4400, 2300, and 830 Ångstroms respectively. In Section 2.2.(a) the spatial extension of the wave-functions for Cooper pairs was discussed; this is the coherence distance of the pure superconductor. (Coherence as discussed in Section 2.3.(c) refers to matrix element coherence and is not related to the present use of the term.)

If a continuum of gap values is to be found over the various faces of a given crystallite in a thick film, and if the crystallites are randomly oriented on the substrate, then not much information would be obtained beyond that available in thin film samples. The tunnel junction conductance would have a structureless, wide peak at the gap edge. The width of the peak would give an indication of the extent of the anisotropy. (A reversal of this argument suggests that thinner films should give sharper features in the I-V curves and their derivatives.)

With these considerations in mind, it is now convenient to consider the results of tunnelling measurements on thick films.

(b) First-Derivative Results on Al-I-M^x Samples

Figures (4-20a), (4-20b) and (4-20c) show dI/dV results obtained from Al-I-In^x samples. (The affix "x" is used to denote thick films.) There is more structure present than when indium thin films are examined (cf Figure (4-13)). In each of these three curves there are four well-defined peaks which may be grouped in pairs and interpreted as arising from the existence of two gaps in indium and one in aluminium. Table (4-2) records the positions of the peaks in the three samples; the designation of each peak in terms of Δ_{Al} and different Δ_{In} values (Δ^1_{In}, Δ^2_{In}, ... etc.) is that which seems most reasonable to the author.

TABLE (4-2)

Peak	Figure (4-20a)	Figure (4-20b)	Figure (4-20c)
$\Delta^1_{In} - \Delta_{Al}$	0.30 meV	0.32 meV	0.32 meV
$\Delta^2_{In} - \Delta_{Al}$	0.49 meV	0.49 meV	0.50 meV
$\Delta^1_{In} + \Delta_{Al}$	0.68 meV	0.69 meV	0.70 meV
$\Delta^2_{In} + \Delta_{Al}$	0.85 meV	0.84 meV	0.85 meV
$2\Delta^1_{In}$	0.98 meV	1.01 meV	1.02 meV
$2\Delta^2_{In}$	1.34 meV	1.33 meV	1.35 meV
$2\Delta_{Al}$	0.38, 0.36 meV	0.37, 0.35 meV	0.38, 0.35 meV

Over thirty Al-I-In^x samples have been examined. The peak positions vary from sample to sample and it is not always possible to group the peaks in pairs as has been done for the curves in Figures (4-20a), (4-20b) and (4-20c). Figure (4-20d) is an example of the latter problem. Sometimes too, a peak is seen to be almost completely absorbed on the

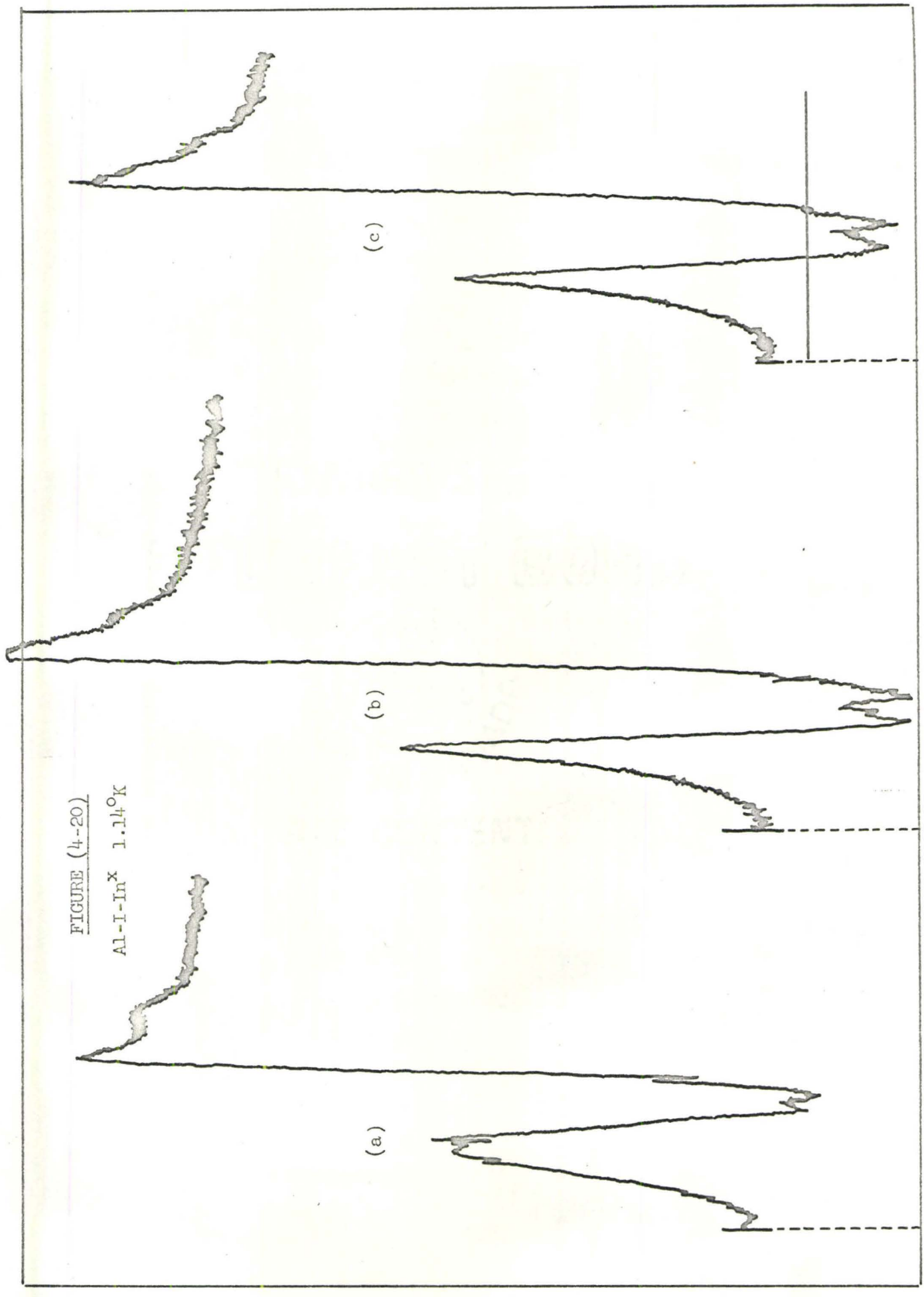

FIGURE (4-20)

Al-I-In^{x} 1.14°K

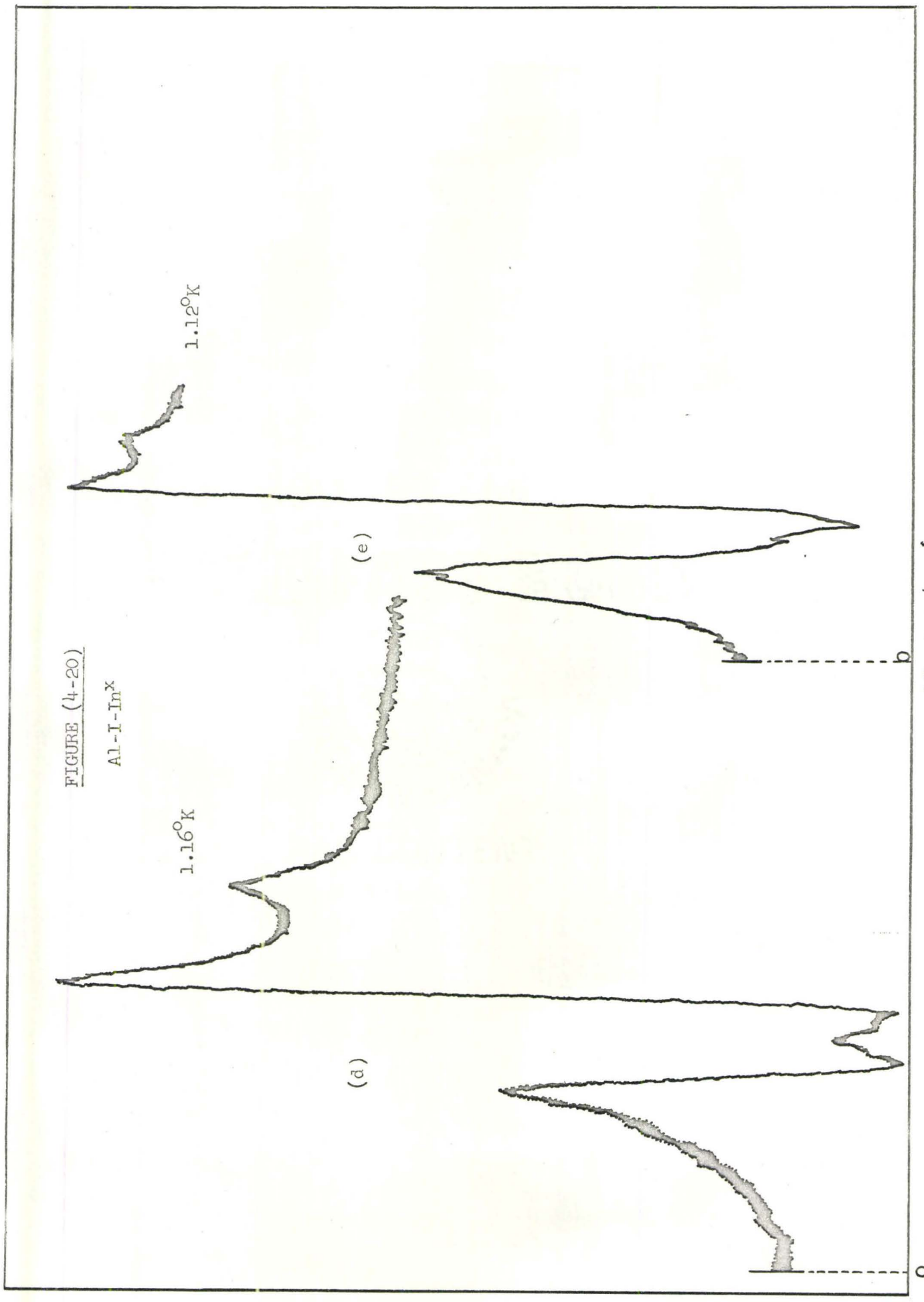
FIGURE (4-20)
Al-I-In^x
1.16°K
1.12°K
(a)
(e)
b
0
V(0.5 mV/inch)
dI/dV

side of another peak as shown in Figure (4-20e). Such a condition probably exists in more extreme form in Figure (4-20f) where only three peaks are present. The opposite situation is evidenced by Figure (4-20g) where a rather impressive amount of detail shows up.

The multiple peaks are not of instrumental origin. Two factors support this view. Firstly, thin films give simple curves and secondly, the I-V characteristics of thick films have a structure obviously compatible with the conductance measurements (see Figure (4-20h)).

Comparable behaviour has been found in Al-I-Sn^x samples though not so many have been examined. Figure (4-21) is the result from one such investigation. Four peaks are present in (a) though one is not well defined. Values of $2\Delta^1_{Sn}$ = 1.23 meV, $2\Delta^2_{Sn}$ = 1.56 meV and $2\Delta_{Al}$ = 0.27 to 0.30 meV account for the behaviour. The rather dramatic change that occurs when the temperature is raised so that aluminium goes normal is well illustrated by (b). Resolution of separate peaks is then not possible.

Finally, the results on an Al-I-Pb^x sample are shown in Figure (4-22). Two humps appear, one on either side of the main peak at $(\Delta_{Pb} + \Delta_{Al})/e$. If we presume that there are corresponding small humps on the sides of the lesser peak at $(\Delta_{Pb} - \Delta_{Al})/e$, and assume a constant value of $2\Delta_{Al}$ = 0.45 meV in the probing film, then gaps in lead may be derived with the values $2\Delta^1_{Pb}$ = 2.46 meV, $2\Delta^2_{Pb}$ = 2.82 meV, $2\Delta^3_{Pb}$ = 3.07 meV.

A comparison experiment involving a common base film of aluminium with four cross-strips, one each of aluminium, indium, tin, and lead, gave results in agreement with those described above. No structure appeared in the Al-I-Al junction conductance. It therefore seems reasonable to exclude aluminium as the source of the multiple peaks.

FIGURE (4-20)

Al-I-In^{x}

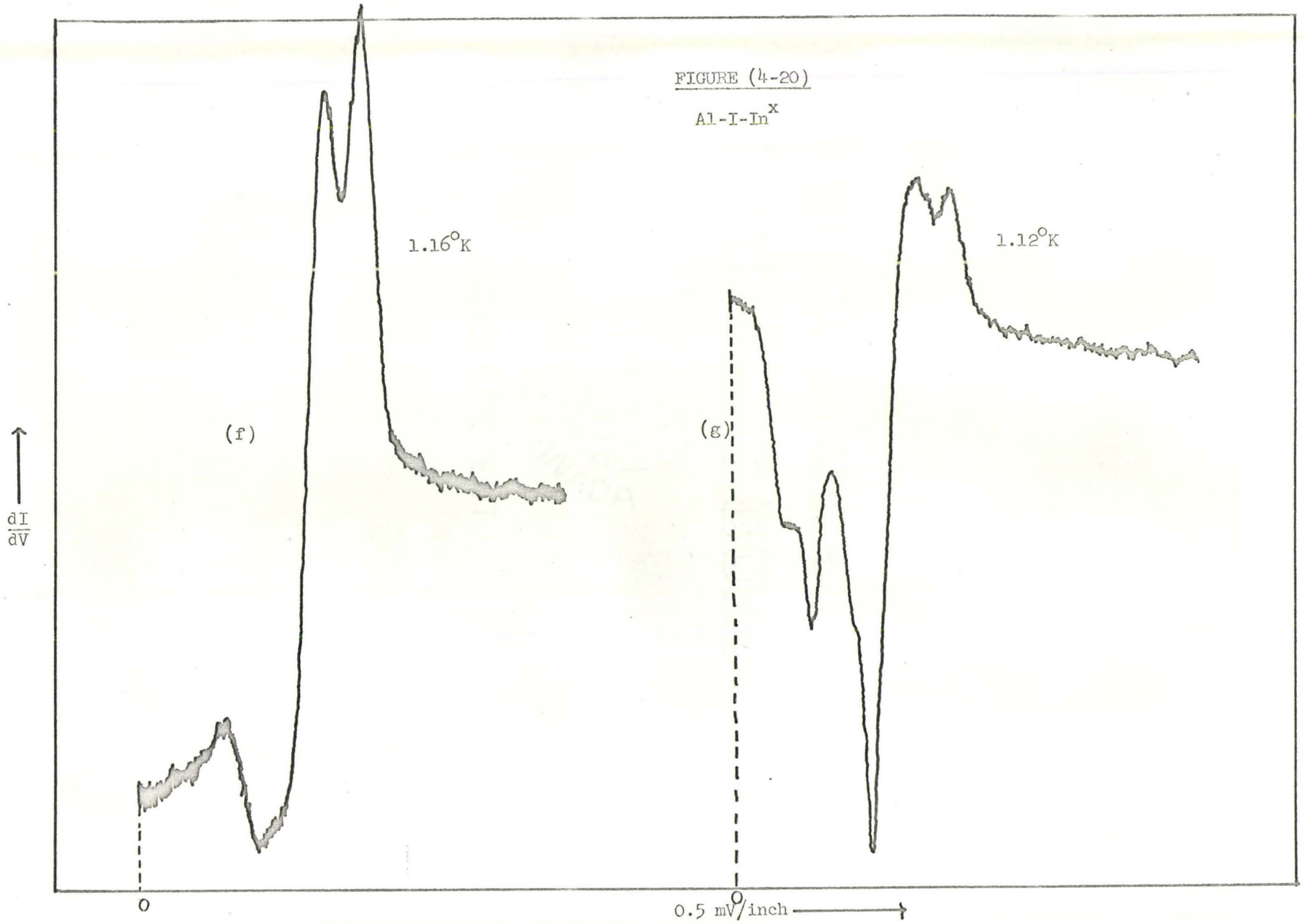

FIGURE (4-20)

Al-I-In^{x} 1.12°K

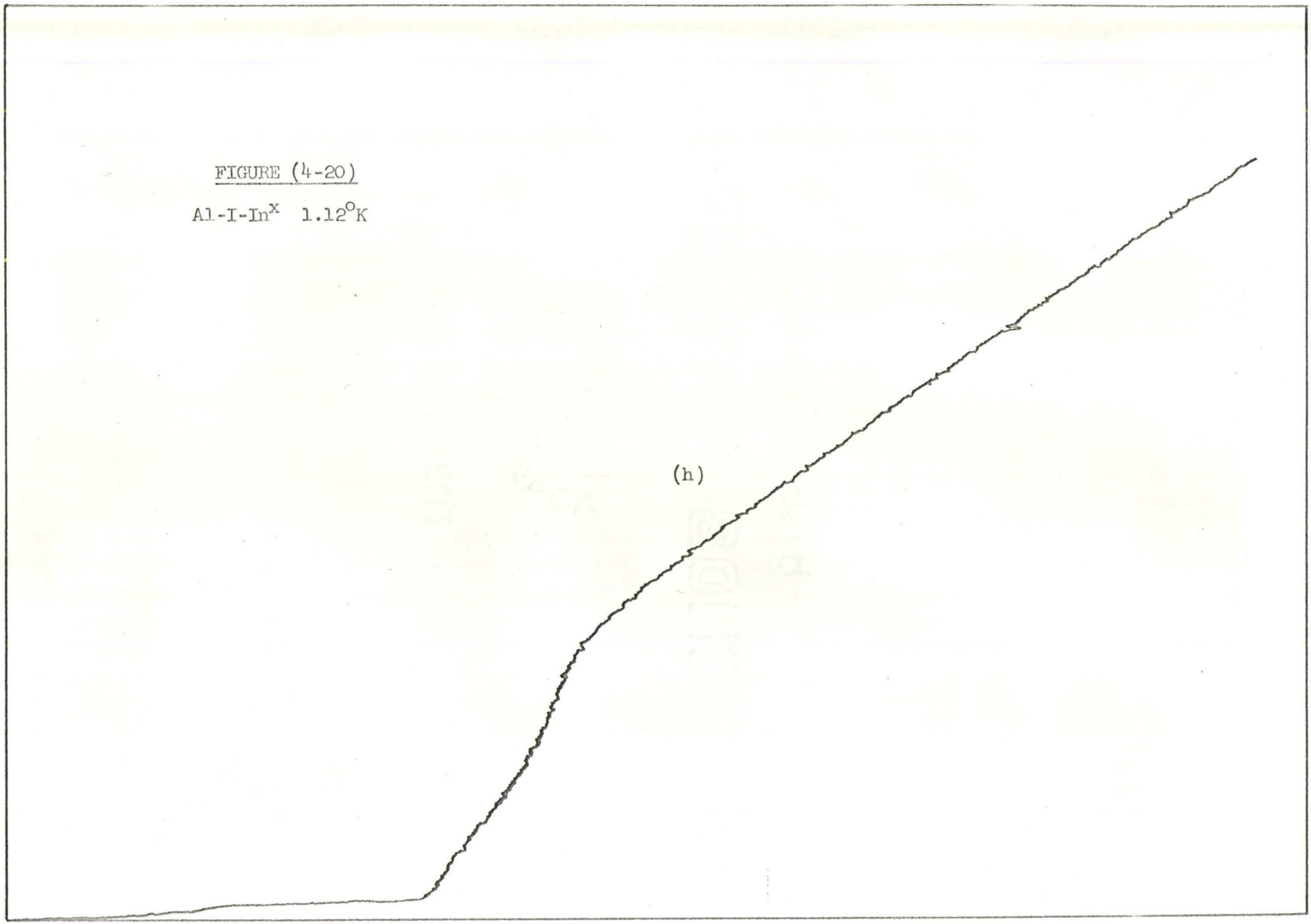

FIGURE (4-21)

Al-I-Sn^x

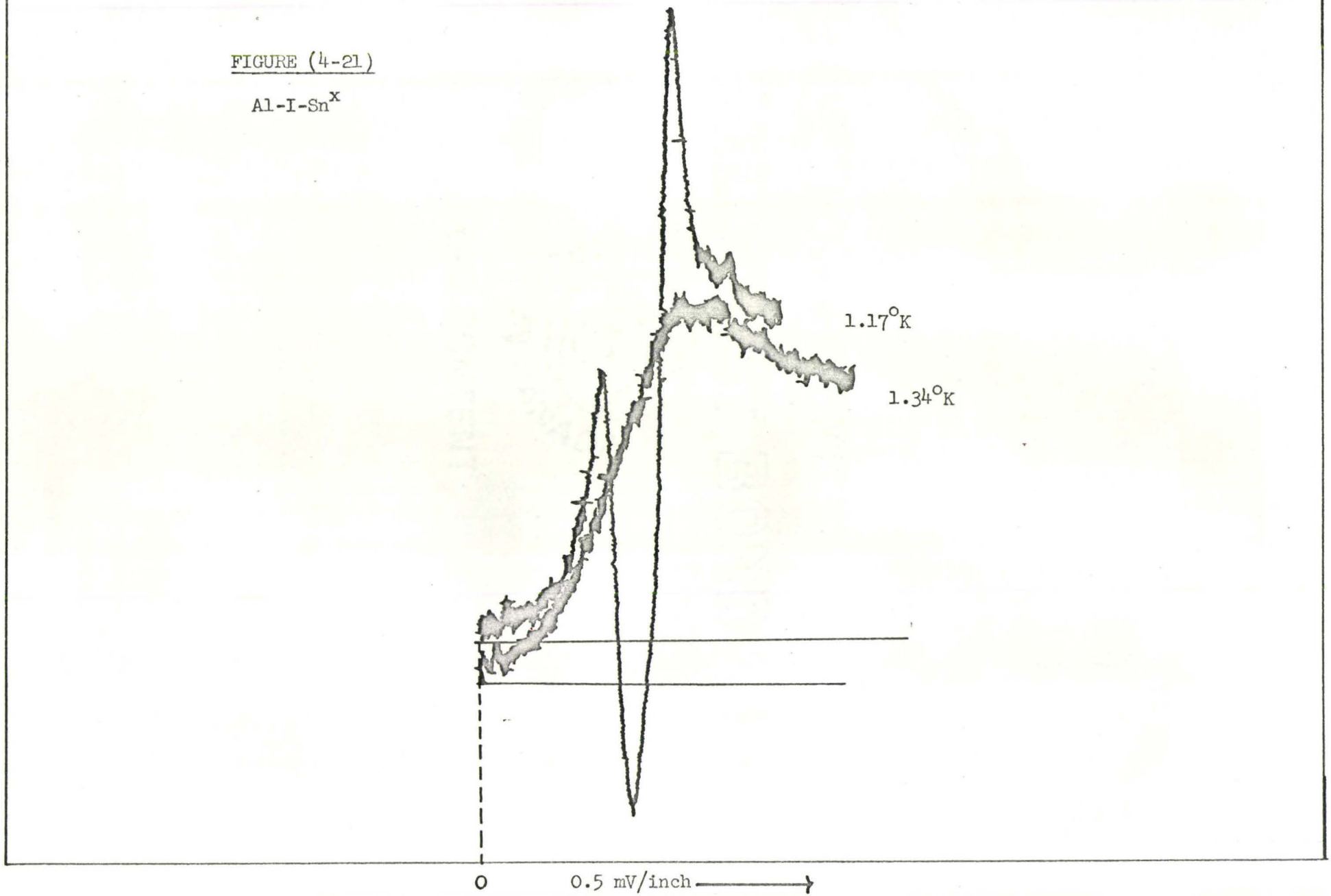

FIGURE (4-22)

Al-I-Pb^{x} 1.20°K

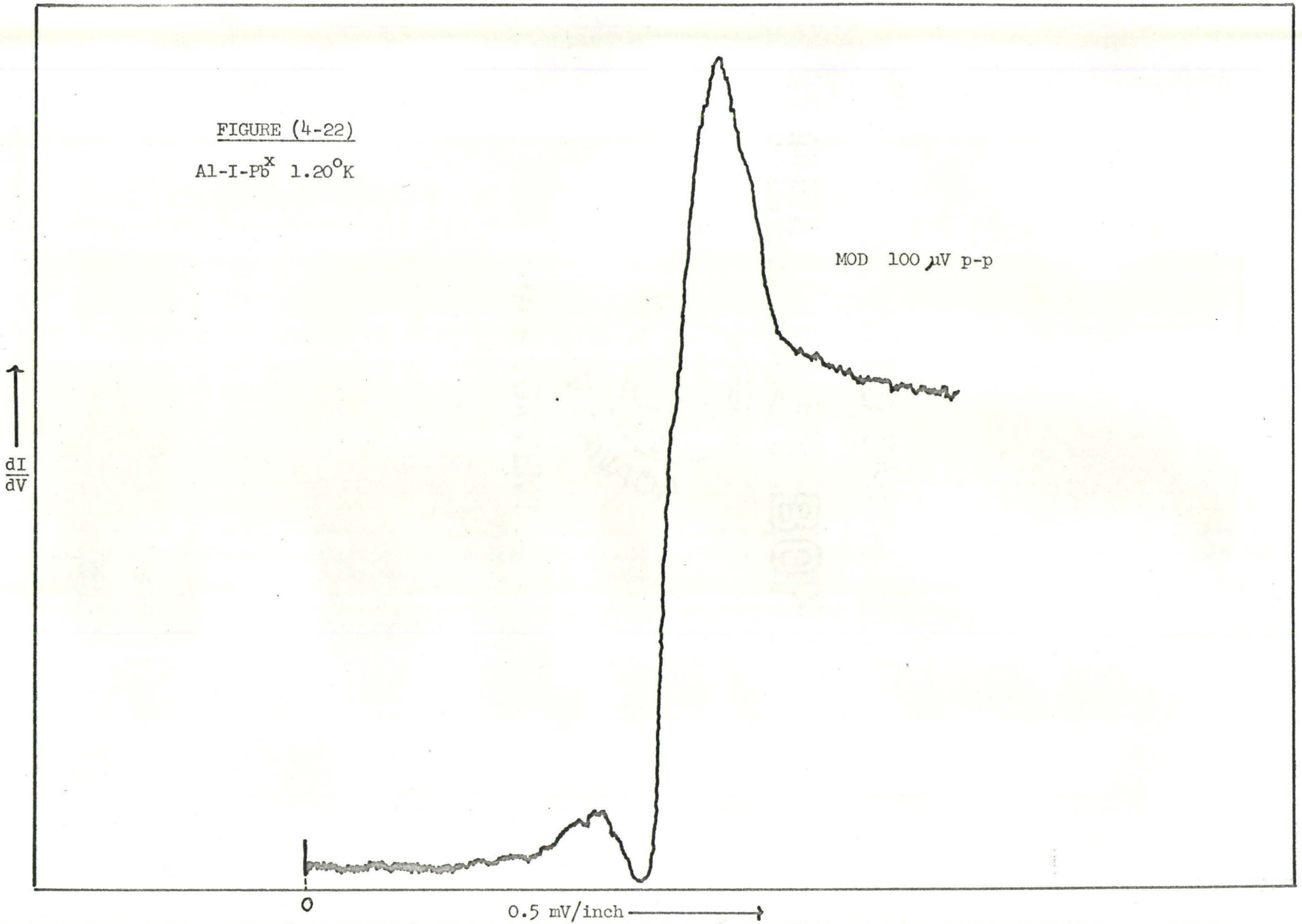

(c) Discussion of First-Derivative Results on Al-I-M^x Samples

Anisotropy seems to be the most likely cause of multiple peaks. In Table (4-2) two values for the indium gaps recur. It would be decidedly wrong to infer from this that only two values of the energy gap are to be found in indium. More probably, a range of values exists and these two are very common. The width of each peak is a measure of the range of gaps found close to the main one. The fact that there is structure in the curves at all suggests that either the energy gaps do not form a continuum or else that some degree of epitaxy exists in the thick films. A further reason for exercising caution in the interpretation of data such as that in Table (4-2) is that it represents results only from curves with well-separated peaks. Other, less well resolved, peaks would no doubt extend the range of gaps that should be included if a suitable method could be found to interpret them uniquely. Extension of equation (2-49) to include the possibility of multiple gaps in one metal, and the second metal having a unique gap, might be such a method. If fits were obtained over a significant temperature range with one set of parameters considerable confidence could be placed in the results. In view of the complications in such a scheme implied by Figure (4-19) the difficulties might be prohibitive. A single crystal experiment would be a neater solution to the problem if experimental difficulties could be overcome.

Similar comments are valid for the lead and tin results. The present thick film results on tin are compatible with the measurements of Zavaritskii[51] and they were performed as a cross-check on the method and interpretation. Zavaritskii's measurements were performed on single crystals and are therefore much more useful.

It is rather interesting that the lead thick films gave energy gaps at three well separated values. A similar observation has been made by Rochlin and Douglass[82] though their values are not exactly in agreement with those reported here. Townsend and Sutton[64] have seen two lead gaps in a Ta-I-Pb^{x} sample, again a little different in exact value and by an amount probably beyond measurement error limits (see Table (4-3)).

TABLE (4-3)

	$2\Delta^{1}_{Pb}$	$2\Delta^{2}_{Pb}$	$2\Delta^{3}_{Pb}$
This Work	2.46 meV	2.82 meV	3.07 meV
Rochlin, Douglass	2.44 meV	2.71 meV	2.99 meV
Townsend, Sutton	not observed	2.67 meV	2.90 meV

Disagreement on the exact values is not disquieting since variations occur from one sample to another. The fact that there are three groups in lead is suggestive of the influence of the face-centred cubic lattice structure. It had been hoped to carry out measurements on a lead single crystal to learn more about any such relationship but technical problems have made this impossible so far. The Fermi surface in lead is simple[83] and its influence might show up rather clearly. Since lead is a strong-coupling superconductor even single crystal experiments may not give as well-resolved data as tin because of state mixing.

(d) Second-Derivative Results on Thick Lead Film Samples and Discussion

Figure (4-23) shows two d^2I/dV^2 traces for a Pb-I-Pb^x sample. The second film was evaporated from two filaments, in quick succession, to give a thick deposit. Resistance measurements showed the thickness to be 3200 Å. It had been hoped that anisotropy effects might show up sufficiently to give a splitting of the phonon peaks. This did not occur but a new peak appeared at a bias of 5.40 ± 0.02 mV.

No corresponding Van Hove singularities are to be expected at this energy on the basis of the neutron scattering data on lead[72] (the equivalent frequency is 6.53×10^{11} c/s). It is noteworthy that this peak occurs very close to $4\Delta_{Pb}/e$ which would correspond to the bias appropriate for the onset of simultaneous tunnelling of two separate quasi-particles. Such a process might occur at a thin point in the tunnel barrier. Then the I, dI/dV, and d^2I/dV^2 curve would take the following form for this behaviour:

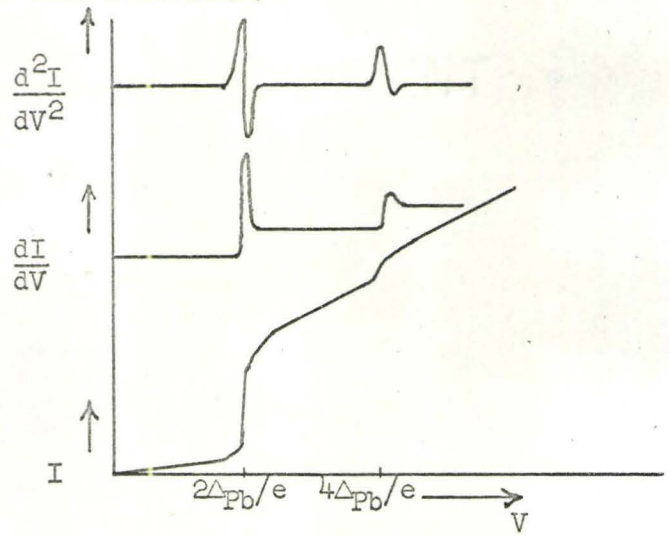

This source for the peak seems more likely than a phonon effect since neither this nor any other new peak showed up in some later samples. It is hoped to find the effect again and check its temperature dependence. A phonon effect would vary as $2\Delta(T)$ and a two-quasi-particle effect as $4\Delta(T)$.

FIGURE (4-23d)

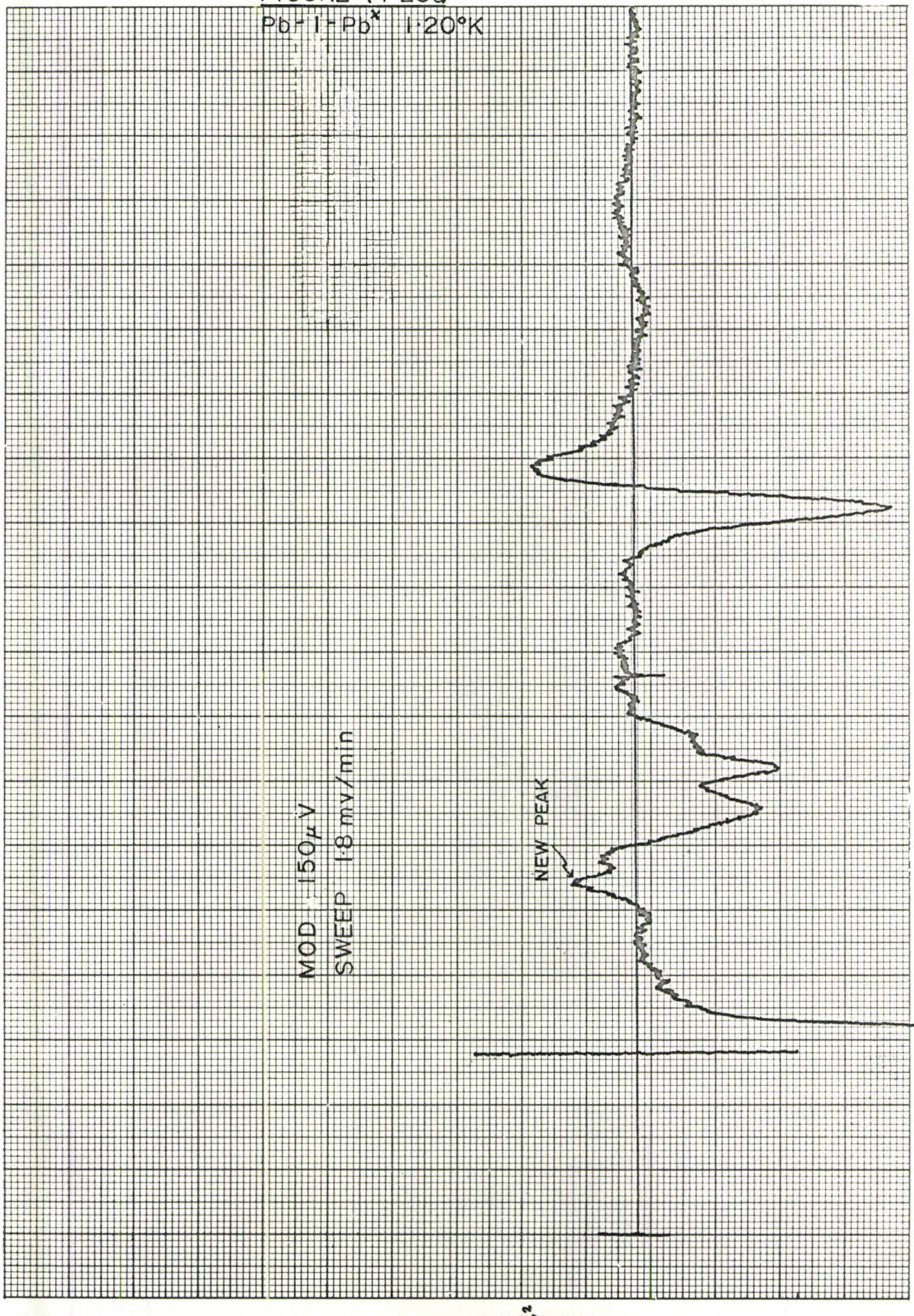
Pb-I-Pb* 1·20°K
MOD 150μV
SWEEP 1·8 mv/min
NEW PEAK
0
2
4
6
8
10
12
14
16
18
V(mv)
$\frac{d^2I}{dV^2}$

FIGURE (4-23b)

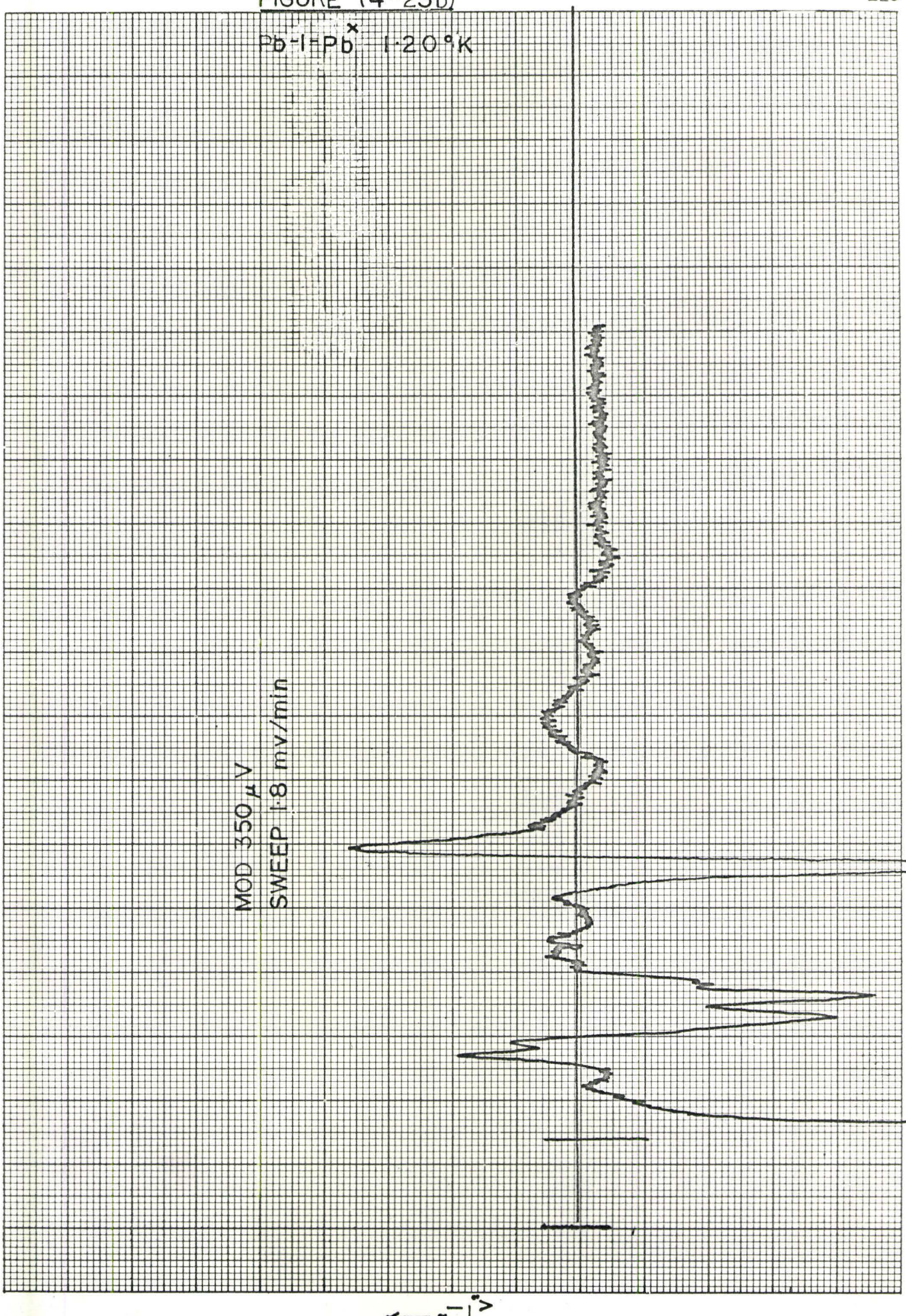
Pb-I-Pb* 1·20°K
MOD 350 μV
SWEEP 1·8 mV/min
0
4
8
12
16
20
24
28
V(mv)
$\frac{d^2I}{dV^2}$

Figure (4-24) shows results for d^2I/dV^2 for an Al-I-Pb^x sample. Barrier damage does not occur often in the preparation of these samples with the result that very thick films may be examined. The lead film in the sample shown in Figure (4-24) was 15000 Å thick as determined resistively.

Compared with Figure (4-17) obtained from a thin film sample there is no significant change. This is not surprising when we consider how little structure showed up in the first derivative at the gap edge in the same sample (Figure (4-22)). The lack of resolution of structure may be partly a problem of strong coupling in lead and partly a lack of definition in the aluminium gap. It is possible to improve the latter condition by use of very thin aluminium films but the strong-coupling complications are inherent in the metal. Since, in general, tin and indium resolve better than lead in first-derivative measurements it seems probable that coupling strength is relevant.

FIGURE (4-24a)

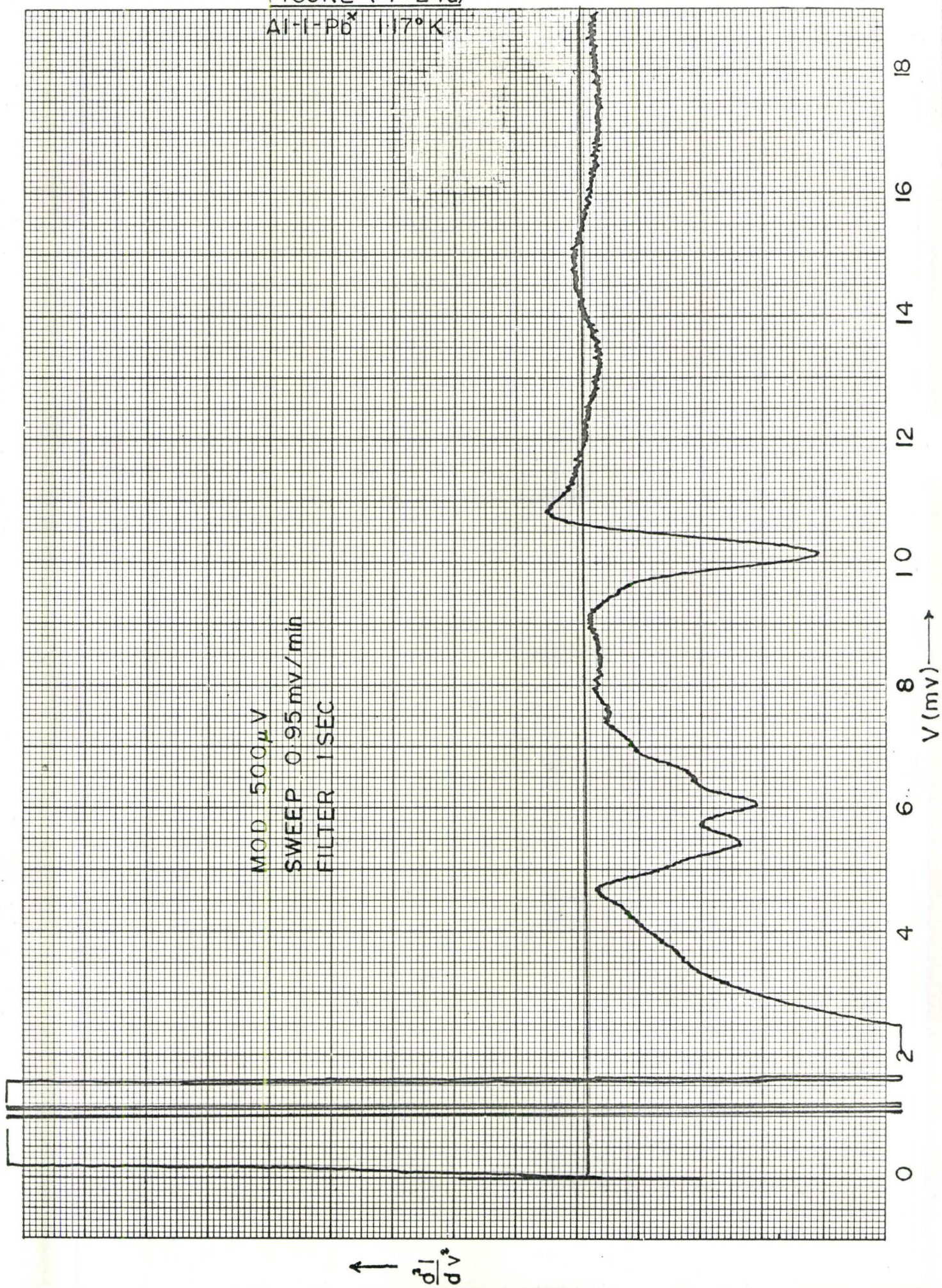
Al-I-Pb* 1.17°K
MOD 500μV
SWEEP 0.95mV/min
FILTER 1SEC
0
2
4
6
8
10
12
14
16
18
V(mV)
$\frac{d^2I}{dV^2}$

FIGURE (4-24b)

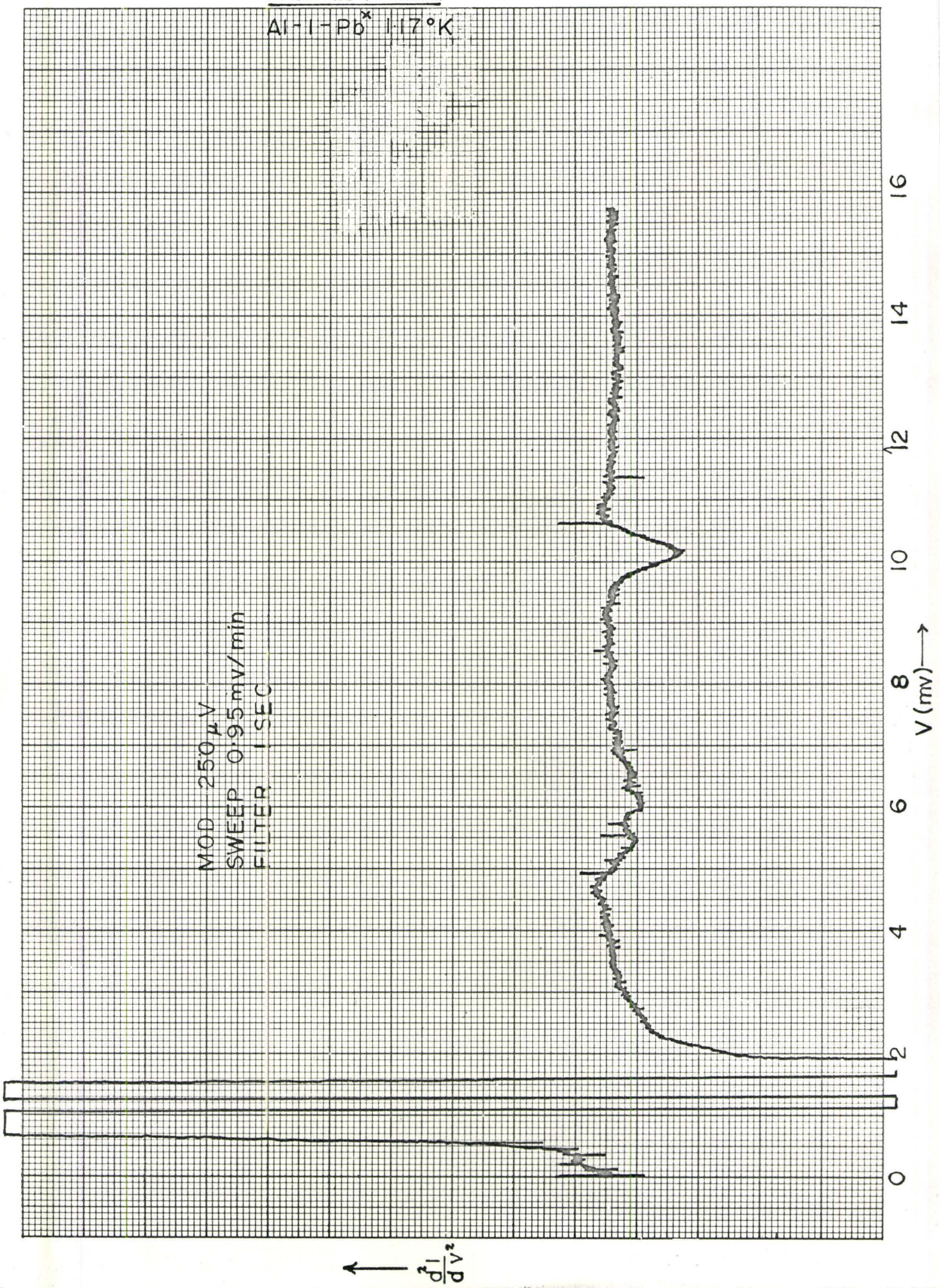
Al-I-Pb^x 1.17°K
MOD 250 μV
SWEEP 0.95 mV/min
FILTER 1 SEC
0
2
4
6
8
10
12
14
16
V (mv) ⟶
⟵ d²I/dV²

CHAPTER 5. CONCLUSIONS

The method of quantum-mechanical tunnelling between superconductors has been applied to the study of aluminium, indium, tin, and lead vapour-deposited films between $4.24^{\circ}K$ and approximately $1.20^{\circ}K$.

Techniques have been developed for the growth of insulating tunnel barriers, in the form of natural oxides, on the metals tin and lead. These allow more flexibility to the type of experiment that may be performed than was previously possible, when aluminium oxide was the only reliable barrier material known, because tin and lead have transition temperatures well above that available to a pumped He^4 cryostat. The current literature suggests that similar advances have been made independently in other laboratories. Attempts to prepare a lead single crystal with a tunnel barrier have been unsuccessful so far.

A cryostat with temperature measurement and control facilities has been constructed and appropriate circuitry for continuous plotting of current-voltage characteristics of the tunnel junctions has been assembled. In addition, a circuit has been available for direct continuous plotting of the first and second derivatives, dI/dV and d^2I/dV^2, of the characteristics. Temperature measurement accuracy, and control, decrease with the vapour pressure of the liquid helium. At $4.2^{\circ}K$ a temperature may be produced and measured to an accuracy of $\pm$ 1 millidegree while at $1.4^{\circ}K$ this has deteriorated to a figure of $\pm$ 40 millidegrees. Temperatures below $1.4^{\circ}K$ have been measured on a McLeod gauge and should be accurate to 1

millidegree though the possibility of a calibration error (not greater than 10 millidegrees) can not be entirely eliminated. Voltage measurements from which energy gap values are determined are good to better than 2 percent.

The generally accepted interpretation of tunnelling characteristics in terms of energy gaps has been critically considered and an attempt has been made to clarify the relationship between the theoretical formalism of current superconductivity theory and the observations made in tunnelling experiments. The semiconductor gap analogy often used in the literature has been avoided since it can be a source of gross misunderstanding.

Considerable advance has been made, it is felt, in following up the consequences of superconducting energy-gap anisotropy which is known to exist in real superconductors. It is considered to be responsible for smearing of features in the current-voltage characteristics at temperatures well below the transition temperature. Experimental results obtained bear out this hypothesis.

A detailed fit has been obtained for the temperature dependence of the energy gap in tin to the BCS theoretical predictions where the latter have been scaled with the parameters $2\Delta_{Sn}(0) = 1.22$ meV and $T_c = 3.85^{\circ}K$. This corresponds to a relation $2\Delta_{Sn}(0) = 3.68\ k_B T_c$ as opposed to the BCS ideal value $2\Delta(0) = 3.52\ k_B T$ given in equation (2-40). It is comforting to note the agreement between this limiting value for the energy gap in tin and that determined by Giaever et al.[58] at $0.30^{\circ}K$. All other tin tunnelling curves in the literature known to this author show rather ill-defined features when compared with Figures (4-7b) and (4-9)

of this thesis. The tin films used were quite thin. Under such conditions anisotropy smearing is minimized. Therefore we conclude isotropic tin exhibits an energy gap given by $2\Delta_{Sn}(0) = 1.22 \pm 0.02$ meV as $T = 0^{\circ}K$ is approached.

The energy gap in lead has been observed to deviate at $4.2^{\circ}K$ by almost 3 percent above the value predicted by a BCS temperature dependence. This is seemingly compatible with the treatment of lead within the strongly-coupled-superconductor theory of Swihart et al.[65]. There is no question of the reality of the effect because even though voltage measurements are only claimed to be accurate in absolute magnitude to within 2 percent much greater sensitivity to changes than 2 percent of the total value is available.

Very thin aluminium films have yielded tunnelling characteristics with sharp features even at high reduced temperatures — a fact which may be interpreted as further evidence that anisotropy smearing causes lack of definition in thicker films. The temperature range available in the present cryostat has not been sufficient to permit temperature dependence measurements on the gap in aluminium.

Agglomeration makes impossible the preparation of very thin films of indium, tin, and lead on room temperature substrates. Some attempts at preparing very thin Al-I-M samples on liquid-air-cooled substrates encountered technical difficulties associated with too-thick aluminium oxide barriers. The method is in process of improvement.

Thick films give ill-defined results if simple gap information is required but they do provide a wealth of data on anisotropy of the energy gap. Its interpretation is non-trivial. Detail is best seen in

the conductance curves, that is, in the first derivatives of the characteristics. Values of $2\Delta_{Pb}$ of 2.46, 2.82 and 3.07 meV have been tentatively identified in lead, in fair agreement with observations by other workers[64,83]. Values of $2\Delta_{In}$ of 1.34 and 1.00 meV have been seen in indium where no other data has yet been reported, while 1.23 and 1.56 meV values for $2\Delta_{Sn}$ explain well the results on some tin samples. Undoubtedly a great many other gaps are present but are not being observed. The ideal experimental arrangement in investigating anisotropy is to use a single crystal as a member of the sample. Zavaritskii[51] has already accomplished this for tin and found a vast number of gaps which show some correlation to the Fermi surface of tin. Lead is an obvious candidate for extension of this work.

The two extremes of thin films showing sharp features in their characteristics and thick films exhibiting multiple gaps are readily understood in terms of "dirty" and pure superconductors respectively as discussed by Anderson[63].

Second derivatives of the current-voltage characteristics have been plotted for Al-I-Pb and Pb-I-Pb samples beyond the energy gap edge. The reflection of the phonon spectrum is present with about the same resolution as obtained by Rowell and Kopf[67]. This is a little remarkable since the two circuits used are somewhat different. (Rowell and Kopf seem to measure $\frac{d^2V}{dI^2} = -\left(\frac{dV}{dI}\right)^{+3} \cdot \frac{d^2I}{dV^2}$ whereas the circuit used in this work measures d^2I/dV^2 independently of the value of dI/dV.) It seems reasonable to conclude that this resolution is typical of lead under these conditions and is not the limit of the circuit. Reduction of modulation amplitude from 300 μV peak-to-peak to 120 μV peak-to-peak reveals no further detail. It might be argued that thermal smearing has an associated

energy of 100 μeV at 1.2°K and therefore below 300 μV peak-to-peak (that is 110 μV r.m.s.) modulation level no further detail would be expected. The existence of the gap however reduces the smearing to be expected in the excited quasi-particles and therefore it will be (considerably) less than k_BT. Rowell and Kopf indeed find resolution at less than k_BT in tin and other weakly-coupled superconductors.

Any attempt to improve the lead resolution will have to bear in mind the following considerations.

When impurities are introduced to a pure material they give a sharpening of the gap edge (see Figure (4-8c)); they do not however give a corresponding improvement in the resolution of phonon detail. Quite the contrary in fact. Dynes[52] has established that when a few percent bismuth is added to lead there is a broadening of the details in the phonon spectrum reflected in the second derivative in accordance with a rather drastic shift in the phonon frequency distribution.

In very thin films there is strong scattering which causes gap edge sharpening. Provided the film purity is high there will not be any broadening of the peaks from phonon frequency spectrum changes. Also the sharp edge should provide a better-defined reference point for the positioning of the various contributions to the phonon peaks. Closer superposition of contributions and hence better resolution would result. One the debit side, severe scattering may cause phonon lifetime broadening which might more than cancel out any gain from gap edge sharpening.

Further experiments are planned to measure the second derivatives of very thin lead films and, if possible, also a single crystal to learn more about the situation.

An observed peak in the d^2I/dV^2 trace from a Pb-I-Pb^x sample at a bias of $4\Delta_{Pb}/e$ is attributed to two particle tunnelling. Such events have been used to explain details in current-voltage curves below the main current edge but there are no reports in the literature of such an event beyond this region. The effect would not be readily apparent without the second-derivative measurements.

Finally, the DC and AC Josephson effects have been observed in many samples. The AC effect was observed before it was first reported in the literature but quantitative anomalies cast doubt on the interpretation of the results. Subsequent theoretical developments by other workers have enabled a reconciliation between the results obtained, and the proper theory, to be effected.

In the light of the investigation described in this thesis it is now possible to make some suggestions on the matter of what projects might be pursued with profit in this field.

First and foremost would be a set of gap determinations made on the thinnest, electrically continuous films that can be prepared (perhaps less than 100 Å thick). These would give a set of "isotropic metal" results which could be unambiguously interpreted and checked against theoretical predictions such as gap temperature dependence. An "isotropic metal" bears little more relation to reality than does jellium or nuclear matter but it gives clear-cut results in a domain where present superconductivity theory is expected to be most reliable.

It would be interesting, too, to examine simultaneously the behaviour of second-derivative curves, in the limit of extreme film thinness, in the region where they reflect the phonon spectrum. Very small

crystallites should reduce the phonon mean-free-paths sufficiently to cause lifetime broadening as Rowell and Kopf[67] suggest is present in their observations on indium. Also, the gap edge might experience further sharpening in this " very dirty'' superconductor.

Single crystals represent the other extreme — pure superconductors. Lead should be quite feasible. Aluminium would require He^3 temperatures but sample fabrication would not seem to pose problems. Thallium, gallium and mercury may represent a challenge. Since mercury is the only other strongly-coupled superconductor, apart from lead, its study in single crystal form would prove useful in reaching conclusions on the relative properties of strongly- and weakly-coupled superconductors.

Thick films serve to define the range of gaps present but not much more. A probe metal with a gap larger than that in aluminium at $1.1^{o}K$ is necessary for good determinations.

BIBLIOGRAPHY

1. H. K. Onnes, Commun. Phys. Lab. Univ. Leiden, No. 119b (1911).

2. See e.g. B. T. Matthias, T. H. Geballe and V. B. Compton, Revs. Mod. Phys. 35, 1 (1963).

3. J. F. Schooley, W. R. Hosler, E. Ambler, J. H. Becker, M. L. Cohen and C. S. Koonce, Phys. Rev. Letters 14, 305 (1965).

4. N. B. Hannay, T. H. Geballe, B. T. Matthias, K. Andres, P. Schmidt and D. MacNair, Phys. Rev. Letters 14, 225 (1965).

5. W. Meissner and R. Ochsenfeld, Naturwissenschaften 21, 787 (1933).

6. C. J. Gorter and H. B. G. Casimir, Phys. Z. 35, 963 (1934); Z. techn. Phys. 15, 539 (1934).

7. H. London and F. London, Proc. Roy. Soc. (London) A149, 71 (1935); Physica 2, 341 (1935).

8. E. Maxwell, Phys. Rev. 78, 477 (1950).

9. C. A. Reynolds, B. Serin and L. B. Nesbitt, Phys. Rev. 84, 691 (1951).

10. See e.g. A. Brown, M. W. Zemansky and H. A. Boorse, Phys. Rev. 92, 52 (1953).

11. L. N. Cooper, Phys. Rev. 104, 1189 (1956).

12. J. Bardeen, L. N. Cooper and J. R. Schrieffer, Phys. Rev. 108, 1175 (1957).

13. H. Fröhlich, Phys. Rev. 79, 845 (1950).

14. L. D. Landau, Zhur. Eksp. i Teoret. Fiz. 30, 1058 (1956) (English Translation, Soviet Phys. - JETP 3, 920 (1957)).

15. L. D. Landau, Zhur. Eksp. i Teoret. Fiz. 35, 97 (1958)(English Translation, Soviet Phys. - JETP 8, 70 (1959)).

16. D. Pines, The Many Body Problem (W. A. Benjamin Inc., New York, 1961).

17. I. Giaever, Phys. Rev. Letters 5, 147 (1960).

18. J. R. Schrieffer, D. J. Scalapino and J. W. Wilkins, Phys. Rev. Letters 10, 336 (1963).

19. M. R. Schafroth, S. T. Butler and J. M. Blatt, Helv. Phys. Acta 30, 93 (1957).

20. See e.g. E. A. Lynton, Superconductivity (Methuen and Co. Ltd., London, 1961), Page 113.

21. See e.g. P. M. Morse, Thermal Physics (W. A. Benjamin Inc., New York, 1962), Page 207.

22. B. Mühlschlegel, Z. Physik 155, 313 (1959).

23. P.-O. Löwdin, Revs. Mod. Phys. 35, 724 (1963).

24. See e.g. C. A. Mead, J. Appl. Phys. 32, 646 (1961).

25. See e.g. L. I. Schiff, Quantum Mechanics (McGraw-Hill Book Company Inc., New York, 1955), Page 199.

26. J. Nicol, S. Shapiro and P. H. Smith, Phys. Rev. Letters 5, 461 (1960).

27. S. Shapiro, P. H. Smith, J. Nicol, J. L. Miles and P. F. Strong, IBM J. Research Develop. 6, 34 (1962).

28. S. Bermon and D. M. Ginsberg, Phys. Rev. 135, A306 (1964).

29. J. R. Schrieffer, Revs. Mod. Phys. 36, 200 (1964).

30. B. D. Josephson, Phys. Letters 1, 251 (1962).

31. J. Bardeen, Phys. Rev. Letters 6, 57 (1961).

32. M. H. Cohen, L. M. Falicov and J. C. Phillips, Phys. Rev. Letters 8, 316 (1962).

33. J. M. Rowell, Revs. Mod. Phys. 36, 199 (1964).

34. S. Shapiro, A. R. Janus and S. Holly, Revs. Mod. Phys. 36, 223 (1964).

35. D. D. Coon and M. D. Fiske, Phys. Rev. 138, A744 (1965).

36. I. Giaever, Phys. Rev. Letters 14, 904 (1965).

37. D. N. Langenberg, D. J. Scalapino, B. N. Taylor and R. E. Eck, Phys. Rev. Letters 15, 294 (1965).

38. B. D. Josephson, Revs. Mod. Phys. 36, 216 (1964).

39. P. W. Anderson, Lectures on the Many-Body Problem, Vol. 2 (Ed. E. R. Caianiello, Academic Press, New York, 1964).

40. L. Holland, Vacuum Deposition of Thin Films (John Wiley & Sons, Inc., New York, 1956).

41. N. Cabrera and N. F. Mott, Reports on Progr. in Phys. 12, 163 (1949).

42. R. M. Handy, Phys. Rev. 126, 1968 (1962).

43. G. Haas, J. Opt. Soc. Am. 39, 532 (1949).

44. J. A. Davies, J. Friesen and J. D. McIntyre, Can. J. Chem. 38, 1526 (1960).

45. See e.g. J. Strong, H. V. Neher, A. E. Whitford, C. H. Cartwright and R. Hayward, Procedures in Experimental Physics (Prentice-Hall, Inc., New York, 1938).

46. N. V. Zavaritskii, Zhur. Eksp. i Teoret. Fiz. 41, 657 (1961) (English Translation, Soviet Phys. - JETP 14, 470 (1962)).

47. C. J. Adkins, Phil. Mag. 8, 1051 (1963).

48. D. H. Douglass, Jr. (private communication).

49. W. J. McG. Tegart, The Electrolytic and Chemical Polishing of Metals (Pergamon Press Ltd., London, 1956).

50. I. Dietrich, Z. Naturforsch. 17A, 94 (1962).

51. N. V. Zavaritskii, Zhur. Eksp. i Teoret. Fiz. 45, 1839 (1963) (English Translation, Soviet Phys. - JETP 18, 1260 (1964)).

52. R. C. Dynes, M.Sc. Thesis, McMaster University (1965).

53. F. G. Brickwedde, H. van Dijk, M. Durieux, J. R. Clement and J. K. Logan, National Bureau of Standards, Washington, Monograph 10 (1960).

54. T. R. Roberts and S. G. Sydoriak, Phys. Rev. 102, 304 (1956).

55. P. R. Emtage and W. Tantraporn, Phys. Rev. Letters 8, 267 (1962).

56. R. Holm, Electric Contacts Handbook (Springer-Verlag, Göttingen, 1958), see Appendix III.

57. I. Giaever and K. Megerle, Phys. Rev. 122, 1101 (1961).

58. I. Giaever, H. R. Hart and K. Megerle, Phys. Rev. 126, 941 (1962).

59. D. H. Douglass, Jr. and R. Meservey, Phys. Rev. 135, A19 (1964).

60. M. Strongin, A. Paskin, O. F. Kammerer and M. Garber, Phys. Rev. Letters 14, 362 (1965).

61. M. Strongin, O. F. Kammerer and A. Paskin, Phys. Rev. Letters 14, 949 (1965).

62. J. G. Adler, Ph.D. Thesis, University of Alberta, Edmonton (1963).

63. P. W. Anderson, J. Phys. Chem. Solids 11, 26 (1959).

64. P. Townsend and J. Sutton, Phys. Rev. 128, 591 (1962).

65. J. C. Swihart, D. J. Scalapino and Y. Wada, Phys. Rev. Letters 14, 106 (1965).

66. See e.g. J. A. Stratton, Electromagnetic Theory (McGraw-Hill Book Company Inc., New York, 1941).

67. J. M. Rowell and L. Kopf, Phys. Rev. 137, A907 (1965).

68. J. M. Rowell, P. W. Anderson and D. E. Thomas, Phys. Rev. Letters 10, 334 (1963).

69. D. J. Scalapino and P. W. Anderson, Phys. Rev. 133, A921 (1964).

70. L. Van Hove, Phys. Rev. 89, 1189 (1953).

71. J. C. Phillips, Phys. Rev. 104, 1263 (1956).

72. B. N. Brockhouse, T. Arase, G. Caglioti, K. R. Rao and A. D. B. Woods, Phys. Rev. 128, 1099 (1962).

73. W. L. McMillan and J. M. Rowell, Phys. Rev. Letters 14, 108 (1965).

74. J. M. Rowell, Phys. Rev. Letters 11, 200 (1963).

75. V. Ambegaokar and A. Baratoff, Phys. Rev. Letters 10, 486 (1963); ibid 11, 104 (1963).

76. R. A. Ferrell and R. E. Prange, Phys. Rev. Letters 10, 479 (1963).

77. S. Shapiro, Phys. Rev. Letters 11, 80 (1963).

78. M. D. Fiske, Proceedings of the Ninth International Conference on Low Temperature Physics, Columbus, Ohio, 1964 (to be published).

79. L. N. Cooper, Superconductivity Conference, Cambridge, 1959. Quoted in D. H. Douglass, Jr. and L. M. Falicov, Progress in Low Temperature Physics, Vol. IV (North Holland Publishing Company, Amsterdam, 1964), Page 113.

80. P. Hohenberg, Zhur. Eksp. i Teoret. Fiz. 45, 1208 (1963) (English Translation, Soviet Phys. - JETP 18, 834 (1964)).

81. See e.g. M. Tinkham, Low Temperature Physics (Edited by C. De Witt, B. Dreyfus and P. G. de Gennes, Gordon and Breach, New York, 1962), Page 203.

82. G. I. Rochlin and D. H. Douglass, Jr., Bull. Am. Phys. Soc., Ser. II, 10, 46 (1965).

83. J. R. Anderson and A. V. Gold, Phys. Rev. 139, A1459 (1965).